ADVANCES IN INORGANIC CHEMISTRY, VOL. 39

STRUCTURES OF COMPLEXES IN SOLUTION DERIVED FROM X-RAY DIFFRACTION MEASUREMENTS

GEORG JOHANSSON

Department of Inorganic Chemistry, Royal Institute of Technology,
S-10044 Stockholm, Sweden

I. Experimental Data
II. Separation of Interactions
III. Model Calculations
IV. Illustrative Examples of Structure Derivations
V. Gold(III) Halide Solutions
VI. Tetrachloroplatinate(II) and -palladate(II) Complexes in Aqueous Solution
VII. Techniques Used for Structure Derivations
VIII. Aqua Ions
IX. Anion Hydration
X. Complexes with Halide Ions
XI. Polyatomic Ligands
XII. Nonaqueous Solutions
XIII. Polynuclear Complexes
XIV. Concluding Remarks
References

Few methods are available for the direct determination of coordination geometry, bond lengths, and bond angles for complexes in solution, although such information is important, for example, for the interpretation of thermodynamic and dynamic data. Complexes, which can be found also in crystals where their structures can be easily determined by diffraction methods, are usually assumed to have the same structure in solution, although the different environment can be expected to influence bond lengths and coordination geometry. But many complexes, which are stable in solution, do not occur in the solid state, where structures with infinite rather than discrete complexes may be preferred. Direct determinations of structures in solution are, therefore, needed and methods that can provide such information are all based on diffraction.

X-ray diffraction, neutron diffraction, and EXAFS all give similar types of structural information that can be used to calculate a radial distribution function (RDF) that directly shows interatomic distances in the solution.

Neutron diffraction has been successfully used for structure determinations of aqua complexes of some metal ions, which have isotopes with sufficient differences in scattering lengths to be used for isotopic substitution methods. Not only bond lengths but also coordination numbers and the orientation of the water molecules in the first coordination sphere can then be determined. Several review articles have summarized these results (*1–6*).

EXAFS has the advantage of giving information on the distribution around a specific atomic species, but is limited to the immediate surrounding of an atom and gives no information on longer distances. It also seems to give less precise information, in particular on coordination numbers, and its use for determining structures of complexes in solution has been limited (*7*).

X-ray diffraction, which can be more generally applied, has also been used for determining structures of aqua complexes of metal ions in aqueous solution. Since hydrogen atoms are weak scatterers of X-rays, their positions and, therefore, the orientation of the water molecules in the hydration sphere, cannot be determined, but bond lengths and to some extent coordination numbers can be obtained. Several review articles have appeared, the most extensive one being that by Magini *et al.* (*7–11*).

Other types of complexes in aqueous as well as in nonaqueous solutions can also be successfully studied by means of X-ray diffraction and their structures can often be derived, completely or in part (*7, 12–15*). Structural changes in the coordination sphere of a metal ion, caused by the stepwise replacement of solvent molecules on addition of a ligand, can be followed. Under favorable conditions structures can be derived for the whole series of complexes formed, from the solvated noncomplexed metal ion to the complex in which all solvent molecules have been replaced. Structural changes beyond the first coordination sphere can sometimes be determined, making it possible to differentiate between inner- and outer-sphere complexes. Even when the information that can be obtained from X-ray diffraction measurements is not sufficient for an unambiguous determination of a structure, it may still give significant structural features, which, in combination with information from other sources, can lead to the complete structure.

The information given by an X-ray diffraction curve for a solution is one dimensional only. By a Fourier inversion it can be transformed into

an RDF, which gives the distribution of interatomic distances in the solution. A solution of chemical interest consists of several different atomic species and several partial distribution functions, each giving the time and space averaged distribution of one of the atomic species around each of the others, are needed for a full description of its structure. From an X-ray diffraction experiment, however, only the total distribution function, which contains contributions from each of the partial functions, can usually be obtained, and this is the major obstacle for an unambiguous structure determination. To derive the structure of a specific complex in a solution its intramolecular contributions to the total scattering has to be separated from those of other complexes, which may be simultaneously present, and from the contributions from all intermolecular distances. This can seldom be done without approximations and a careful analysis of the results are needed in order to make an unambiguous structure determination and to avoid systematic errors in the derived parameter values.

In the following, a survey will be given of structures of complexes derived from solution diffraction data. The methods used and the approximations involved will be discussed. The basic theory of diffraction in solutions has been covered in several previous reviews (*5, 7, 8*) and will not be given here. Structure determinations of aqua complexes of metal ions in aqueous solutions have also been extensively reviewed (*7–11*) and will be discussed here only when they are of interest for the structures of complexes containing other ligands.

I. Experimental Data

A commonly used instrument for measuring the large-angle X-ray scattering from a solution is the θ–θ goniometer (Fig. 1). The Bragg–Brentano parafocusing geometry is used in which the incoming X-ray beam and the measured diffracted beam form the same angle, θ, with the horizontal surface of the liquid sample. The intensity scattered from the free surface of the solution is measured as a function of θ, where 2θ is the scattering angle. Usually, a focusing single crystal monochromator of graphite or, preferably, lithium fluoride is used to reflect the diffracted beam before it reaches the scintillation counter, which is equipped with a pulse height discriminator.

A typical diffraction curve is shown in Fig. 2. It gives the measured intensity from a solution as a function of the scattering vector

$$s = 4\pi \frac{\sin \theta}{\lambda}$$

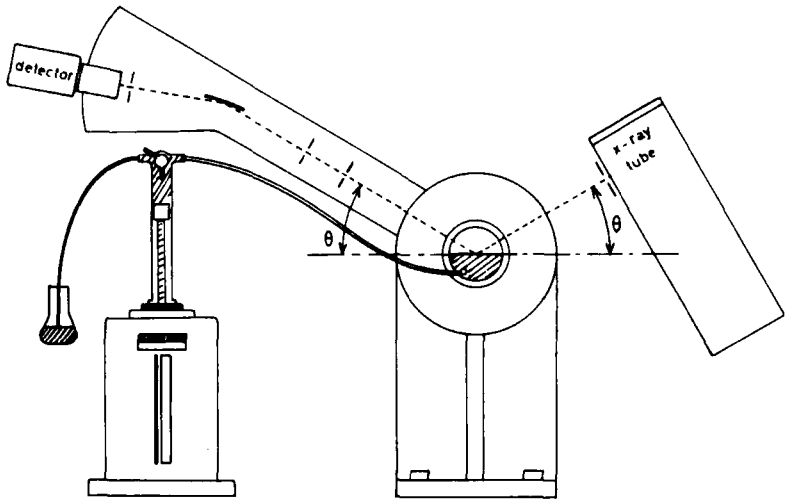

FIG. 1. Theta–theta diffractometer for solution X-ray diffraction measurements.

where λ is the wavelength. MoKα-radiation (λ = 0.7107 Å) is generally used but can be replaced by, for example, AgKα-radiation (λ = 0.5608 Å) in order to avoid fluorescence radiation or to extend the experimentally available s region to larger values. CuKα-radiation, which has a longer wave length (λ = 1.5418 Å), does not cover a sufficiently large s region to be useful for structure determinations of complexes, since the high-angle part of a diffraction curve is of crucial importance for an analysis of intramolecular interactions.

With the use of standard procedures (*16, 17*) the measured intensity values are corrected for polarization in the sample and in the monochromator, and for absorption, multiple scattering, and incoherent scattering. Contributions to the scattering curve can be separated into a part which depends on the structure of the sample, and a structure independent part, the independent coherent scattering, that can be calculated from tabulated values for the scattering factors, $f_i(s)$, for the atomic species making up the sample. For a chosen stoichiometric unit of volume, V, which contains n_i atoms of the species i, the independent coherent scattering is given by $\sum n_i f^2(s)$. The structure-dependent part of the scattering is centered around this curve, as illustrated in Fig. 2, and the amplitude of its variation decreases with increasing s values. In the high-angle part the measured intensity values approach the curve representing the independent coherent scattering, which can be used to put the experimental data on an absolute scale. Different procedures have been used for this normalization and for the correction

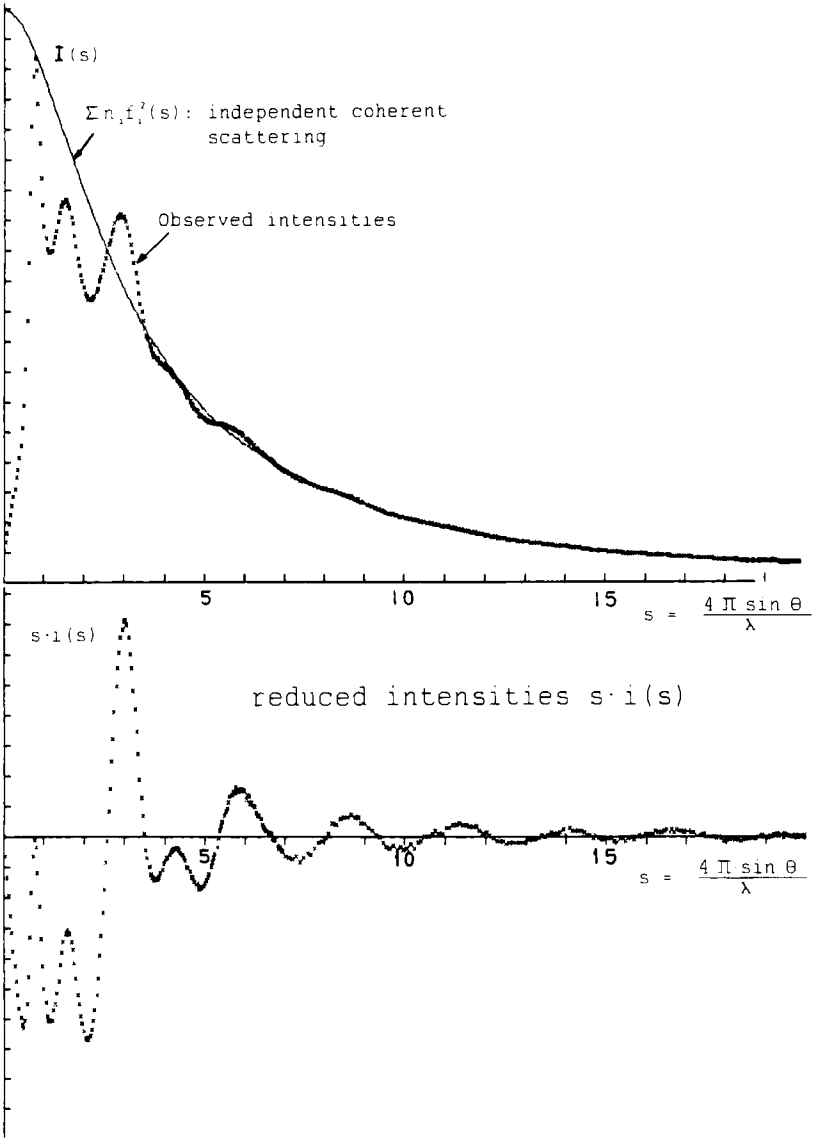

FIG. 2. Experimental intensities (crosses) measured with AgKα-radiation for a concentrated erbium(III) chloride solution. The values have been normalized with the use of calculated values for the independent coherent scattering (solid line). The lower part shows the reduced intensities, $s \cdot i(s)$, where $i(s)$ is obtained by subtracting the independent coherent scattering from the observed intensity values.

of the experimental intensity curve for low-frequency variations, which have no physical meaning in terms of interatomic distances.

The structure-dependent part of the diffraction curve, the reduced intensity function, $i(s)$, is obtained by subtracting the independent coherent scattering from the normalized experimental values (Fig. 2):

$$i(s) = I_{obs} - \sum_i n_i f_i(s)^2$$

The reduced function intensity, $i(s)$, can be transformed into a radial distribution function, $D(r)$, by means of a Fourier inversion

$$D(r) = 4\pi r^2 \rho_0 + \frac{2r}{\pi} \int_0^{s_{max}} s \times i(s) \times M(s) \frac{\sin(rs)}{rs} ds$$

Here ρ_0 is the average scattering density, defined by the expression $\sum_i (n_i Z_i)^2 / V$, with n_i the number of atoms i with atomic number Z_i in the stoichiometric unit of volume V. A modification function, $M(s)$, is included in order to give an appropriate weight to $i(s)$ values in different s regions. A commonly used function consists of a sharpening factor, for example $[f_i(0)/f_i(s)]^2$, which compensates for the decrease in $f(s)$ values with increasing s, and a damping factor, $\exp(-bs^2)$, where b is chosen to reduce the cutoff effects in the Fourier inversion resulting from the upper s limit, s_{max} not being infinity.

The radial distribution function gives direct information on the short-range order in the solution (Fig. 3) and prominent interatomic distances will appear as distinct peaks in the RDF. The position of a peak gives the interatomic distance for the corresponding interaction. The size of the peak is proportional to the number of such distances in the stoichiometric unit chosen and the shape of the peak gives information on the variation of the distance around its average. For values of r smaller than possible interatomic distances the RDF will be zero. For large values of r it will approach the average distribution, $4\pi r^2 \rho_0$, because of the lack of a long-range order in a solution. It is often convenient to use the reduced RDF, $D(r) - 4\pi r^2 \rho_0$, which shows the variation of the RDF around its average (Fig. 3).

II. Separation of Interactions

In a solution containing n atomic species, p, q, etc., the number of different pair interactions is $n(n + 1)/2$. The pair correlation function, $g_{pq}(r)$, measures the probability of finding an atom q at a distance r

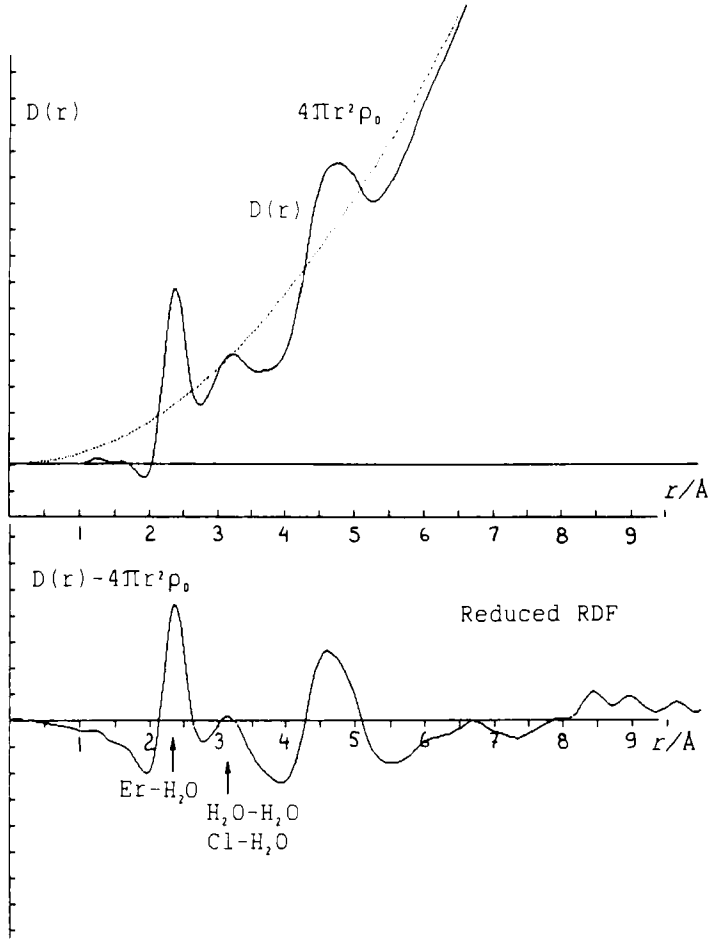

FIG. 3. The radial distribution function, $D(r)$, calculated from the intensity values in Fig. 2. The lower part shows the reduced RDF, $D(r) - 4\pi r^2\rho_0$.

from an atom p (Fig. 4). The number of q atoms between two spherical shells surrounding p is obtained by an integration

$$n_q V^{-1} 4\pi \int_{r_1}^{r_2} r^2 g_{pq}(r)\, dr$$

where n_q is the number of atoms q in the stoichiometric volume V. The partial structure factor $S_{pq}(s)$ is related to $g_{pq}(r)$ by a Fourier transformation and the total structure function for a solution can be written as a sum over the different partial structure functions $S_{pq}(s)$.

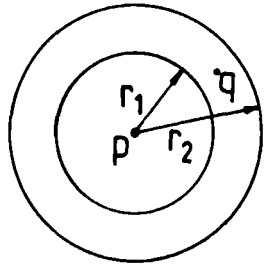

FIG. 4. The number of atoms q between two spherical shells with radii r_1 and r_2 is obtained by an integration over the partial correlation function $g_{pq}(r)$.

The reduced intensity observed in an X-ray diffraction experiment corresponds to the sum over the different partial structure functions, each weighted by the product of the scattering factors for the two atomic species involved. In an aqueous solution of a salt MX, which contains four atomic species M, X, O, and H, the number of different pair interactions is ten and the reduced intensity function can be written:

$$\begin{aligned} i(s) = {} & K_1 f_M(s) f_X(s) [S_{MX}(s) - 1] + K_2 f_M(s) f_O(s) [S_{MO}(s) - 1] \\ & + K_3 f_M(s) f_H(s) [S_{MH}(s) - 1] + K_4 f_M^2(s) [S_{MM}(s) - 1] \\ & + K_5 f_X(s) f_O(s) [S_{XO}(s) - 1] + K_6 f_X(s) f_H(s) [S_{XH}(s) - 1] \\ & + K_7 f_X^2(s) [S_{XX}(s) - 1] + K_8 f_O(s) f_H(s) [S_{OH}(s) - 1] \\ & + K_9 f_O^2(s) [S_{OO}(s) - 1] + K_{10} f_H^2(s) [S_{HH}(s) - 1] \end{aligned}$$

where K are constants determined by the composition of the solution. By a Fourier transformation the corresponding partial distribution functions can be obtained, each of which measures the probability of finding an atom q at a distance r from an atom p (Fig. 4).

For a complete description of the structure of a solution each of the partial functions should be known, but experimentally only the total function, that is the weighted combination of the partial functions, can be determined. Since the scattering factor of an atom is roughly proportional to its number of electrons, and the contribution from a specific interaction to the total function is weighted by the product of the scattering factors for the two atoms involved, partial functions involving heavy atoms will contribute more to the total function than those involving only light atoms. Therefore, complexes containing heavy atoms will give more dominant contributions to a diffraction curve and will be more favorable for a structure determination.

If two metal ions, M and M′, form isostructural solutions, interactions, which do not involve the metal ions, are identical and are eliminated in the difference function $\Delta i(s)$:

$$\begin{aligned}\Delta i(s) &= i_{\mathrm{M}}(s) - i_{\mathrm{M}'}(s)\\ &= K_1 \Delta f_{\mathrm{M}}(s) f_{\mathrm{X}}(s) [S_{\mathrm{MX}}(s) - 1]\\ &\quad + K_2 \Delta f_{\mathrm{M}}(s) f_{\mathrm{O}}(s) [S_{\mathrm{MO}}(s) - 1]\\ &\quad + K_3 \Delta f_{\mathrm{M}}(s) f_{\mathrm{H}}(s) [S_{\mathrm{MH}}(s) - 1]\\ &\quad + K_4 [f_{\mathrm{M}}{}^2(s) - f_{\mathrm{M}'}{}^2(s)] [S_{\mathrm{MM}'}(s) - 1]\end{aligned}$$

where

$$\Delta f_{\mathrm{M}}(s) = f_{\mathrm{M}}(s) - f_{\mathrm{M}'}(s)$$

This reduces the ten partial functions to four and of these the last two terms are small and can usually be neglected.

A Fourier transformation of $\Delta i(s)$ using the convolution function $f_{\mathrm{M}}(s)/\Delta f_{\mathrm{M}}(s)$:

$$D^{\mathrm{M}}(r) = 4\pi r^2 \rho_{\mathrm{O}}{}^{\mathrm{M}} \frac{2r}{\pi_{\mathrm{O}}}$$

$$\times \int_0^{S_{\max}} s \Delta i(s) \mathbf{M}(s) \frac{f_{\mathrm{M}}(s)}{f_{\mathrm{M}}(s) - f_{\mathrm{M}'}(s)} \sin(rs)\, ds$$

gives a distribution function to which only interactions involving the metal ion, M, contribute and it shows the coordination around the exchanged atom unobscured by other types of interactions.

For an unambiguous structure determination of a specific complex in a solution a separation of interactions becomes extremely useful. For two solutions to be isostructural, however, requires that one of the atomic species in the solution can be replaced by another one, having a sufficiently large difference in scattering factor, without causing a change in the structure of the solution. In neutron diffraction it can be achieved by using isotopic substitution, which is much less likely to affect the structure, but isostructural solutions, that can be used for X-ray diffraction, can also be prepared, although they are rare.

III. Model Calculations

An analysis of diffraction data can be done either in s space, by a comparison of observed intensities with theoretical values for an as-

sumed model for the solution, or in r space, by a comparison of the RDF with calculated peaks for assumed interactions.

Two atoms, p and q, bonded together at a distance r_{pq} give a contribution, $i_{pq}(s)$, to the diffraction curve, which can be calculated according to the Debye expression

$$i_{pq}(s) = f_p(s) f_q(s) \frac{\sin(r_{pq}s)}{r_{pq}s} e^{-(l_{pq}^2 s^2)/2}$$

If the distance r_{pq} has a Gaussian distribution around its average its contribution to the intensity is modified by the exponential factor, in which l_{pq} is the root mean square variation of the distance.

The corresponding contribution to the radial distribution function can be obtained by means of a Fourier inversion analogous to the one for the experimental data using the same modification function and upper integration limit.

The total contribution from a specific complex can be calculated by summing over all of its intramolecular distances. In order to make a complete structural model of the solution all other contributions would also have to be included. Distances from the complex to surrounding atoms are often approximated by assuming it to occupy a spherical hole in an evenly distributed electron density. Other interactions can also be approximated by a combination of discrete interactions for short distances and a continuous atomic distribution for long distances.

The parameters needed to describe such a model are, for each discrete interaction, the distance, its rms variation and the frequency, and corresponding parameters for describing the emergence of the continuum. The parameter values can be refined either in s space by a least squares procedure minimizing

$$\sum w[i_{obs}(s) - i_{theor}(s)]^2$$

where w is a weighting factor, or in r space by a comparison of a theoretical RDF with the experimental one.

The approximate nature of a model of this kind, the large number of parameters needed for its description, and the likely occurrence of many overlapping interactions, can make the results ambiguous and lead to systematic errors in the refined parameter values. Usually, therefore, diffraction data for a single solution are not sufficient for a complete and unbiased derivation of the structure of a specific complex. If isostructural substitution can be used to eliminate some of the pair interactions, then much more precise and detailed information about the

structure can be obtained but pairs of isostructural solutions are rare and this method can seldom be used. Often, however, approximate separations of interactions can be made by comparing diffraction curves for solutions of different compositions, in which the concentrations of complexes are known.

A separation of intramolecular interactions is often possible since they correspond to sharp, well-defined interatomic distances which give distinct contributions to a diffraction curve in the high-angle region, where intermolecular interactions, which have their largest contributions in the low-angle part, are usually very weak. From an analysis of the high-angle part of an intensity curve, therefore, intramolecular distances can often be unambiguously and precisely determined, especially for heavy atoms which dominate the scattering in this region. Coordination numbers, on the other hand, are more difficult to determine accurately, being more sensitive to systematic errors.

The calculations needed for corrections and normalization of solution X-ray diffraction data, for calculation of radial distribution functions, for model calculations, and for least-squares refinements (*16*) can conveniently be done on a personal computer for which integrated program systems are available (*17*).

IV. Illustrative Examples of Structure Derivations

Two straightforward structure derivations can be used to illustrate the analysis of a diffraction curve and the structural information that can be extracted when conditions are favorable.

One example is the square-planar tetrachloro- and tetrabromo-complexes formed by gold(III) in aqueous solution, which can be uniquely and precisely structure determined from a single diffraction curve (*18*). The heavy atoms in the complexes and the highly concentrated solutions, that can be prepared, result in dominant contributions from the complexes to the scattering curve.

The other example is the chloro complexes of platinum(II) and palladium(II), which also have square-planar structures (*13*). The $PtCl_4^{2-}$ and the $PdCl_4^{2-}$ complexes have identical structures, with the same bond lengths, and form isostructural solutions. By using the difference between their normalized diffraction curves contributions from interactions not involving the metal atoms can be eliminated and precise structures can be derived, not only for the complex but also for the structure beyond the first coordination sphere of the metal ion.

V. Gold(III) Halide Solutions

The reduced intensity curves for 2.7 M aqueous solutions of tetrachloro- and tetrabromo-aurate(III) solutions ($HAuCl_4$ and $HAuBr_4$) are shown in Fig. 5. The corresponding RDFs are given in Fig. 6. For a square-planar complex three peaks are expected: the gold–halide bonding distance and the halide–halide intramolecular distances along the edges and along the diagonals of the square. They are all present in the RDFs, and can be best seen in the reduced RDFs, $D(r) - 4\pi r^2\rho_0$ (Fig. 7). The ratio between the peak positions is found to correspond closely to that expected for the distances in a square-planar complex, which is $1 : \sqrt{2} : 2$. This uniquely defines the structure of the complexes in the solutions. The intramolecular contribution to the intensity curves for a square-planar model can be calculated as the sum over the three different distances. Each interaction is described by three parameters: the distance, the number of distances in the stoichiometric unit chosen,

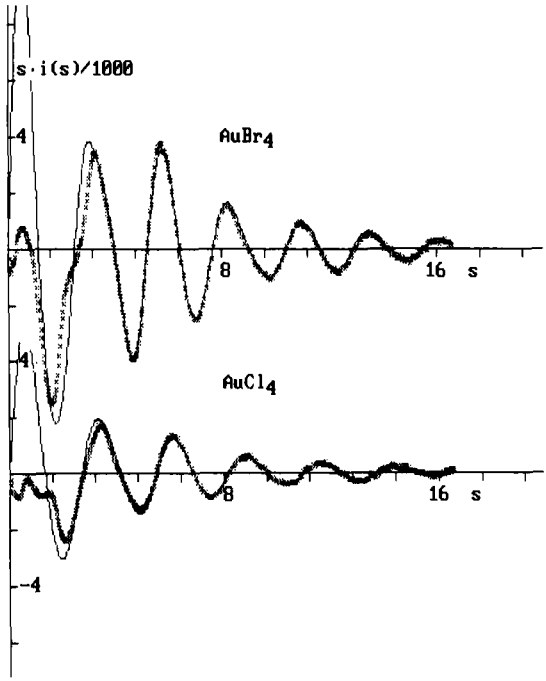

FIG. 5. Experimental $s \cdot i(s)$ values (crosses) for gold(III) halide solutions compared with theoretical values (solid lines) calculated for square-planar AuX_4^- complexes.

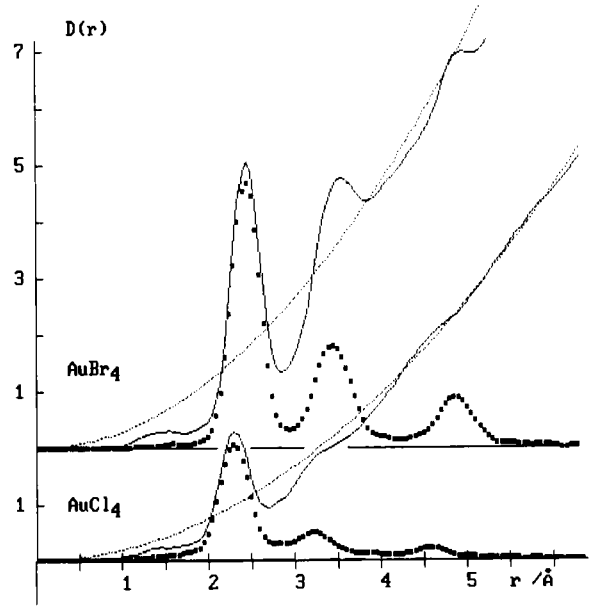

FIG. 6. Radial distribution functions, $D(r)$, for the gold(III) halide solutions (solid lines), compared with calculated peaks (dots) for a square-planar AuX_4^- complex. The $4\pi r^2\rho_0$ functions are shown by dotted lines.

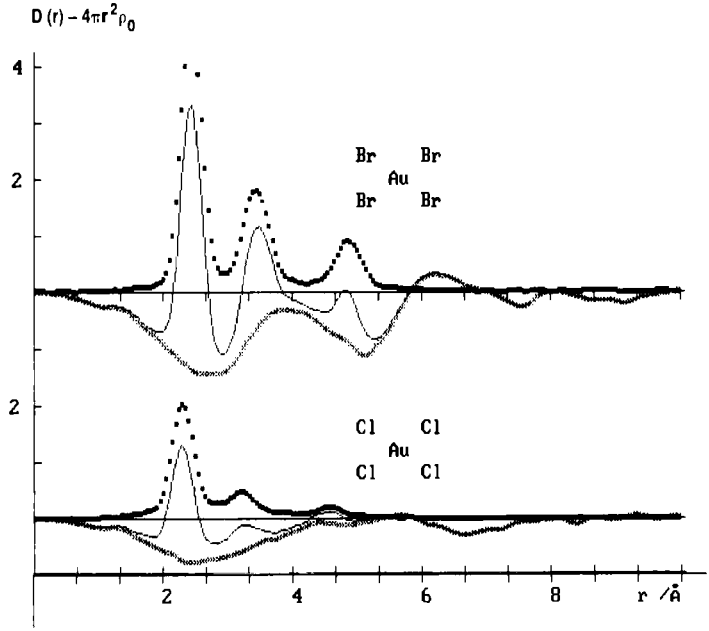

FIG. 7. $D(r)$-$4\pi r^2\rho_0$ functions for gold(III) halide solutions (solid lines), calculated peaks for a square-planar AuX_4^- complex (dots) and difference curves (crosses).

and the rms variation of the distance, assuming the distribution to be Gaussian. By means of a least-squares procedure values of these parameters, giving the best agreement between observed and calculated intensities, can then be obtained (Fig. 5). Although all other structural features in the solutions have been neglected the calculated intensity values reproduce closely those observed, except for the low-angle part of the curves.

From the theoretical intensity values the corresponding peaks in the RDFs can be calculated (Figs. 6 and 7). If these theoretical peaks are subtracted from the experimental RDF the resulting curve shows the remaining structure of the solution (Fig. 7). The main features in this difference curve include diffuse peaks in the region around 3 Å, primarily corresponding to H_2O–H_2O and Cl–H_2O hydrogen bond distances and to distances from the complex to surrounding atoms. Since these interactions correspond to nondistinct distances and involve light atoms, their contributions to the intensity curves will be limited to the low-angle region. In the high-angle region the contributions from the intramolecular distances in the gold(III) complexes will by far be the dominant ones, as shown by the comparison between observed and calculated values in Fig. 5. It would be possible to include intermolecular interactions in the model to get agreement between observed and calculated intensities also in the low-angle region of the intensity curve. However, the many overlapping interactions would make such a model nonunique and its physical significance would be doubtful. A considerable improvement in the low-angle intensity range can be obtained by merely assuming the complexes to occupy a spherical hole in an evenly distributed electron density.

Since intensity contributions other than those from the complexes are limited to the low-angle region, this part of the intensity curve can be excluded from the least-squares refinement, minimizing its influence on the parameters derived for the intramolecular interactions. The final parameter values, obtained in this way, are given in Table I, together with the estimated standard deviations. The values illustrate that bond lengths can be determined with an accuracy, which is as good as, or better, than can be obtained in a crystal structure determination. This is because intensity values are measured up to high s values, where the Au–X contributions are solely dominant.

The coordination numbers can be less precisely determined primarily because of the correlation between the frequency, n, and the rms variation, l. An increase in the value of n and a decrease in l will have similar effects and will both increase the calculated intensity values in the

TABLE I

RESULTS FROM LEAST-SQUARES REFINEMENTS OF X-RAY DIFFRACTION DATA FOR GOLD(III) HALIDE SOLUTIONS

	Au—X			X—X		
Solution	r/Å	n	l/Å	r/Å	n	l/Å
$AuCl_4^-$	2.291(3)	3.6(2)	0.06(6)	—	—	0.08(6)
$AuBr_4^-$	2.431(3)	3.9(1)	0.05(2)	3.44(1)	4.1(2)	0.08(4)

high-angle region. They can be resolved, and each of them can be accurately determined in the least squares procedure, only if the corresponding interaction is dominant over a sufficiently large s region. This is often not the case, although for the gold(III) halide solutions, where the intramolecular interactions dominate down to rather low s values, a separation is possible.

The separate contributions to the intensity curve from the three different types of intramolecular interactions in the AuX_4^- complexes are shown in Fig. 8. The lower atomic numbers for the halide atoms and, in particular, for chlorine, will reduce the X–X contributions to the i(s) curve relative to those from the Au–X interactions. They will be further reduced in the high-angle region because of larger values for the rms variations in the corresponding distances, either because of larger thermal vibrations or because of irregularities in the structures. This is reflected in the standard deviations obtained for the n and b values (Table I). For the $AuCl_4^-$ complex the contribution from the Cl–Cl distances is too small to allow an independent refinement, and the square-planar symmetry has to be used as a restraint. For the bromide solution, however, an independent refinement is possible because of the larger relative contributions from the heavier bromide ions (Table I).

Alternatively, the structural parameters for the complexes can be determined in r space by fitting calculated peaks for different d, l, and n values to observed peaks in the RDFs. Since the background curve, which is determined by the remaining structure in the solution, is not known, this method also leads to uncertainties in the determination of l and n values, especially for the long X–X distances, which occur in regions where a large number of interactions other than those in the complexes contribute to the $D(r)$ curve (Figs. 6 and 7).

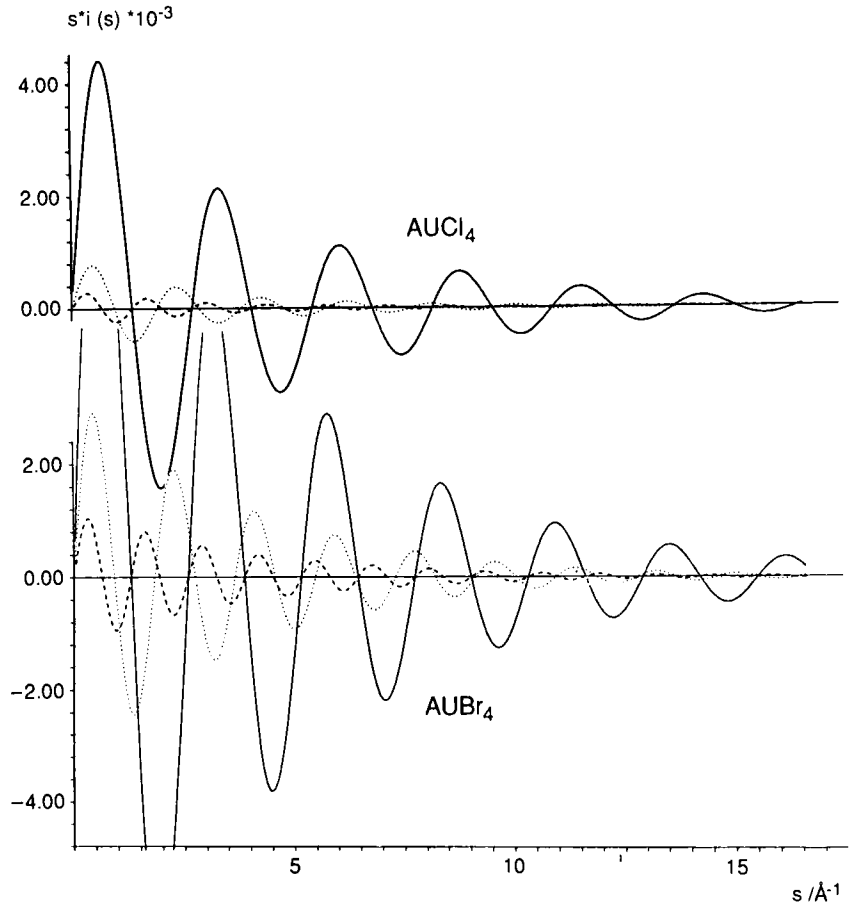

FIG. 8. Intramolecular contributions to the intensity curve from the square-planar AuX_4^- complexes, separated into contributions from Au–X (solid line), X–X along the edge of the square (dotted line), and X–X along the diagonal (broken line).

VI. Tetrachloroplatinate(II) and -palladate(II) Complexes in Aqueous Solution

The $PtCl_4^{2-}$ and $PdCl_4^{2-}$ complexes have the same square-planar structure as the gold(III) halide complexes and concentrated solutions of each of them can be prepared. In crystal structures the Pt—Cl and the Pd—Cl bond lengths in these complexes do not differ significantly and their solution diffraction curves show this to be true also in solution. They can, therefore, be expected to form isostructural solutions and the difference between the normalized diffraction curves for a platinate(II)

and a palladate(II) solution of equal compositions will contain contributions only from interactions involving the metal atoms. This allows the original RDFs to be separated into a part containing contributions only from interactions involving the metal atoms and another part with only nonmetal interactions.

In the total RDF for the tetrachloroplatinate(II) solution (Fig. 9), the peak at 2.3 Å, corresponding to the Pt—Cl bonding distances, is not fully resolved from longer interactions, and this overlap is more severe for the solution containing the lighter Pd atom. After separation, however, using the isostructural palladate(II) solution the Pt–Cl bonding interactions form a fully resolved peak, which is in perfect agreement with a Gaussian peak calculated for four Pt—Cl bonds of 2.31 Å, with a rms variation of 0.06 Å (Fig. 10) (*13*). All nonmetal interactions, including the intramolecular Cl—Cl distances, which are clearly indicated in the original RDF (Fig. 9), have been eliminated. The result shows that there is no distinct structure beyond the first coordination sphere of the metal atom. In particular it shows no preferred occupation of the two empty octahedral sites of the complex.

The part of the distribution function that includes the nonmetal interactions only, is the dominant part, as shown by the comparison in Fig. 10, but has much less distinct features than the part involving the metal atom interactions. It shows diffuse peaks in the region around 3.0 Å, which can be related to H_2O—H_2O, Cl—H_2O, and Cl—Cl dis-

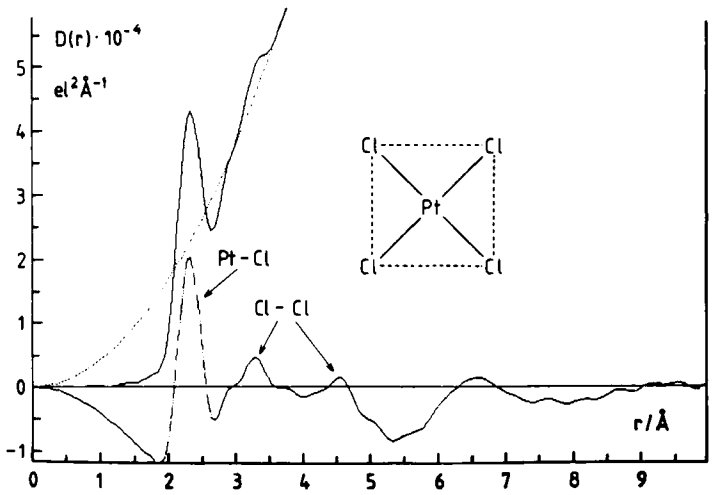

FIG. 9. The $D(r)$ and the $D(r)$-$4\pi r^2\rho_0$ functions for an aqueous 1 M ammoniumtetrachloroplatinate(II) solution containing square-planar $PtCl_4^{2-}$ complexes.

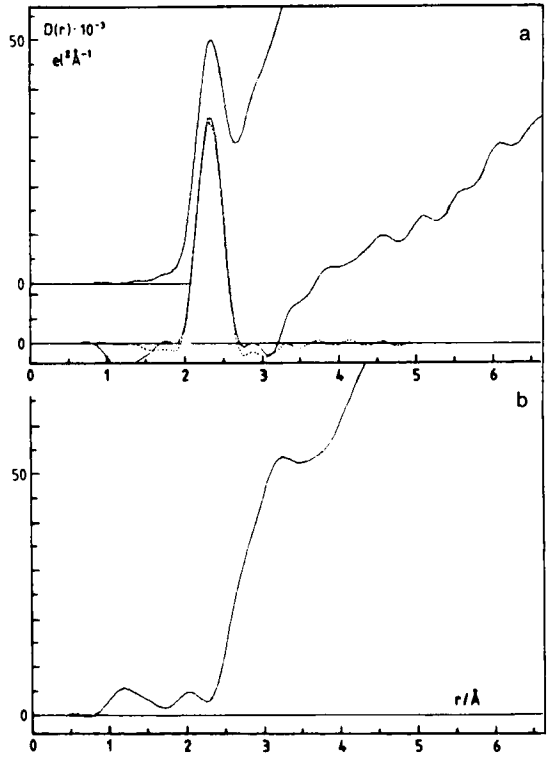

FIG. 10. (a) Upper curve shows the RDF for a 1 *M* tetrachloroplatinate(II) solution before separation of interactions. Lower curve shows the RDF after elimination of nonplatinum interactions. It is compared with a theoretical curve calculated for four Pt—Cl bonds. (b) The part of the RDF involving only nonplatinum interactions.

tances in the solution. In the original RDF they partly overlap the metal–chloride bonding distances and will effectively prevent the identification of possible longer distances involving the metal atoms. The use of a difference method thus results in a much more detailed information on the coordination around the metal atom than can be obtained by an analysis of the individual data sets.

VII. Techniques Used for Structure Derivations

The strategy for analyzing solution X-ray diffraction data for structures of complexes will depend on the characteristics of each specific

system, and the method that can be chosen will determine if a unique and unambiguous structure determination is possible.

The number of pairs of isostructural solutions is limited. It requires the replacement of one atomic species in a solution for another, with a sufficiently large difference in scattering power, without changing the structure of the solution. It requires not only that the bonding characteristics of the two atoms, but also the bond lengths, will be the same. When available, however, it makes it possible to derive a precise and detailed structure for the coordination around the exchanged atom, since the corresponding interactions will not be obscured by contributions from other types of interactions. Even when truly isostructural solutions cannot be obtained, however, difference curves can still be useful. Contributions from a specific interaction can be brought out by comparing diffraction data for solutions containing different concentrations of one of the atoms involved, keeping concentrations of other atoms approximately constant, or by observing changes in a diffraction curve, when a complex forming anion is replaced by a similar ion, which does not form bonds to the metal ion.

The results obtained for the tetrahalogenoaurate(III) solutions illustrate that, when conditions are favorable, a limited number of discrete interactions can be separated and quantitatively analyzed, either in s space or in r space, even when only a single diffraction curve is available. A least-squares procedure can then be used to determine not only the distances but also the frequency and the rms variation of each of these distances. For lower concentrations and for complexes containing lighter atoms the intramolecular interactions will no longer be dominant or will dominate over a more restricted range of the diffraction curve. Although the distances can probably still be accurately determined, their frequencies and rms variations cannot. If the angular range that can be used for the refinement of the intramolecular interactions becomes too restricted the correlation between the frequency and the rms variation for an interaction will increase and it may no longer be possible to resolve them in a least-squares procedure.

X-ray diffraction measurements on aqueous metal salt solutions with no complex-forming anions, have been extensively used for determining structures of hydrated metal ions. A commonly used method for analyzing the data has been to refine the parameters in an assumed model, consisting of a number of discrete interactions, approximating longer distances by assuming an evenly distributed electron density surrounding an atom beyond a sphere of radius R. The intensity values over the whole s range are then used for the refinement and the result is usually

an excellent agreement between observed and theoretical intensities and RDFs.

The number of discrete interactions in the model then includes the first and usually a second coordination sphere of water molecules around the metal ion. The intramolecular interactions of the anion and a hydration sphere surrounding it can also be included. The contribution from the water structure is taken into account by a H_2O–H_2O interaction at about 3 Å or by assuming it to be unchanged from that in pure water. Other interactions are approximated by an evenly distributed electron density around each complex or each atomic species. A Gaussian distribution is assumed for all of the interactions, even for H_2O—H_2O distances and second coordination spheres, where this is probably a poor approximation. The number of parameters even for this very simplified model becomes rather large and extensive correlation between them are likely to occur. Since they cannot always be resolved in a least-squares procedure, restraints, based on preconceived assumptions about the structures, have to be introduced. The physical significance of many of the parameter values obtained is difficult to judge even when the refinement leads to a final good agreement between observed and calculated values. Although the bonding distance between the metal ion and the H_2O molecules in its first coordination sphere is probably not affected by the approximations involved, values obtained for coordination numbers, n_{pq}, and rms variations in the distances, l_{pq}, probably are. For longer and less distinct interactions the physical significance of the values obtained becomes uncertain. The accuracy in the derived parameter values is difficult to estimate and a careful testing of the results is needed by using different weighting schemes and different s regions for the least squares refinement, and by using the agreement between observed and calculated values in r space as an additional criterion.

In the presence of a complex-forming anion the number of interactions is increased, and in order to get information beyond a simple determination of average bond lengths, this method cannot be used. Comparisons between diffraction curves for solutions of different compositions are then needed in order to separate and analyze specific interactions.

VIII. Aqua Ions

Diffraction data for concentrated aqueous metal salt solutions containing noncomplex-forming anions have been used to derive structures

for a large number of metal aqua ions. Anions have been ClO_4^-, which does not usually form innersphere complexes, and Cl^-, which has no intramolecular distances and, at least in some cases, cannot compete with H_2O for positions within the first coordination sphere of the metal ion.

The most detailed structures have been obtained from neutron diffraction data, when isotopic substitution methods have been possible to use. Neutrons are strongly scattered by hydrogen atoms, making it possible to determine not only bond lengths and coordination number of the metal ion, but also the orientation of the water molecules in its first coordination sphere. A summary of results is given in Table II (*19–31*).

TABLE II

STRUCTURES OF AQUA COMPLEXES IN AQUEOUS SOLUTIONS DERIVED FROM NEUTRON DIFFRACTION DATA IN COMBINATION WITH ISOTOPIC SUBSTITUTION[a]

Cation	Conc.	Anion	Coord.	M—O	M—D	Tilt	Ref.
Ag(I)	3.7 *M*	ClO_4^-	4.1(3)	2.41(2)	2.97(4)	45(4)	*19*
Ca(II)	4.5 m	Cl^-	5.5(3)	2.40(3)	2.93(5)	51(15)	*20*
Ca(II)	4.5 m	Cl^-	6.4(3)	2.41(3)	3.04(3)	34(9)	*21*
	2.8 m	Cl^-	7.2(2)	2.39(2)	3.02(3)	34(9)	
	1 m	Cl^-	10.0(6)	2.46(3)	3.07(3)	38(9)	
Cu,Ni(II)	3.0 *M*	ClO_4^-	6(1)	1.97(2)	2.60(2)	39(10)	*22*
Cu(II)	4.3 m	Cl^-	2.3(3)	2.05(3)	2.56(10)	58(10)	*23*
Dy(III)	2.4 m	Cl^-	7.4(5)	2.370(3)	3.042(3)	17(3)	*24*
Dy(III)	1.0 m	Cl^-	7.87	2.386	3.037		*25*
	1.0 m	ClO_4^-	7.99	2.386	3.032		
	0.3 m	ClO_4^-	7.96	2.399	3.032		
Mn,Ni(II)	4.3 *M*	Cl^-	5(1)	2.09(2)	2.69(2)	43(10)	*22*
	2.6 *M*	SO_4^{2-}	5(1)	2.05(2)	2.75(2)	20(15)	
Nd(III)	2.9 m	Cl^-	8.4(2)	2.48(2)	3.13(2)	24(4)	*26, 27*
Ni(II)	4.4 m	Cl^-	5.8(2)	2.05	2.65	30	*28*
Ni(II)	4.4 m	Cl^-	5.8(2)	2.07(2)	2.67(2)	40(10)	*29, 3*
	3.1 m	Cl^-	5.8(2)	2.07(2)	2.67(2)	40(10)	
	1.5 m	Cl^-	5.8(3)	2.07(2)	2.67(2)	40(10)	
	0.9 m	Cl^-	6.6(5)	2.09(2)	2.76(2)	27(10)	
	0.4 m	Cl^-	6.8(8)	2.10(2)	2.80(2)	17(10)	
	0.1 m	Cl^-	6.8(8)	2.07(3)	2.80(3)	0(20)	
Ni(II)	3.8 m	ClO_4^-	5.8(2)	2.07(2)	2.67(2)	42(8)	*30*
Ni(II)	4.4 m	Cl^-	5.8(2)	2.07(2)	2.67(2)	40(10)	*31*
Yb(III)	1.0 m	ClO_4^-	7.84	2.328	2.981		*25*

[a] Estimated errors are given within parentheses. The derived metal–oxygen, M—O, and metal–deuterium, M—D, distances are given in angstroms. The tilt angle is defined as the angle between the M—O bond and the plane of the water molecule.

Unlike neutron data, X-ray data do not show the positions of hydrogen atoms, and the orientation of the water molecules cannot be directly determined, which, on the other hand, can be an advantage for the derivation of the structure beyond the first coordination sphere, since the absence of hydrogen contributions will reduce the number of overlapping peaks in the RDFs. A summary of structure determinations of aqua ions from X-ray diffraction measurements on solutions is given in Table III (*41–143*). Results reported for the alkali metal ions, Cs^+ (*73–75*), Li^+ (*100*), and Na^+ (*109–111*), which have less distinct hydration spheres, have not been included in the table.

TABLE III

STRUCTURES OF AQUA AND HALIDE COMPLEXES IN AQUEOUS SOLUTIONS DERIVED FROM X-RAY DIFFRACTION DATA[a]

Cation	[C]	Anion	[A]/[C]	Bond	*d*/Å	Complex	*l*/Å	Ref.
Ag(I)	4.2 *M*	ClO_4^-	1.0	–O	2.410(4)	1.99(3)	0.09	*41*
	3.5 *M*	NO_3^-	1.0	–O	2.450(8)	2.45(7)	0.09	
$Ag(NH_3)_2^+$	4.0 *M*	NO_3^-	1.0	–N	2.22(2)	2.0(5)	0.06	*41*
Ag(I)	3 *M*	ClO_4^-	1.0	–O	2.38(1)	4	0.16	*42*
	9 *M*	ClO_4^-	1.0	–O	2.43(1)	4	0.16	
Ag(I)	< 3.7 *M*	I^-	3–6	–I	2.9	AgI_4		*43*
Al(III)	9.2 *N*	Cl^-	3	–O	1.90	6.0(5)		*44*
Al(III)	0.5 *M*	NO_3^-	3	–O	1.90	6		*45*
Al(III)	1 *M*	Cl^-	3	–O	1.902(4)	6	0.04	*46*
	2 *M*	Cl^-	3	–O	1.888(3)	6	0.10	
Al(III)	2.5 *M*	NO_3^-	3	–O	1.87	6	0.15	*47*
Au(III)	2.8 *M*	Br^-	4.6	–Br	2.432(3)	$AuBr_4$	0.05	*18*
	3.1 *M*	Cl^-	4.4	–Cl	2.291(3)	$AuCl_4$	0.07	*18*
Be(II)	5.3 m	Cl^-	2	–O	1.67	4	0.04	*48*
Ca(II)	1.0 *M*	Cl^-	2	–O	2.416	6	0.14	*49*
	2.0 *M*	Cl^-	2	–O	2.411(3)	6	0.15	
	4.0 *M*	Cl^-	2	–O	2.422(3)	6	0.13	
Ca,Mg(II)	2 *M*	Cl^-	2	–O	2.428(7)	6	0.14	*50*
				–O	2.044(5)	6	0.06	
Ca(II)	6.3 *M*	Cl^-	2	–O	2.355(3)	3	0.09	*51*
				–O	2.698(7)	6	0.29	
Ca(II)	5.2 m	Cl^-	2	–O	2.4	8.0		*52*
	3.3 m	Cl^-	2	–O	2.4	8.2		
Ca(II)	1.2 *N*	Br^-	2	–O	2.40	6–8	0.12	*53*
	2.0 *N*	Br^-	2	–O	2.44–9	6–8	0.15	
Ca(II)	1.1 m	Cl^-	2	–O	2.39(1)	6.9(5)	0.14	*54*
Ca(II)	18.7 *M*	Cl^-	800°C	–Cl	2.76	5.4		*55*
	8.4 *M*	Cl^-	120°C	–O	2.46	3.9		
				–Cl	2.80	2.1		
	7.5 *M*	Cl^-	72°C	–O	2.45	4.8		
				–Cl	2.75	1.7		
	6.9 *M*	Cl^-	80°C	–O	2.45	5.6		
				–Cl	2.74	1.0		

TABLE III *Continued*

Cation	[C]	Anion	[A]/[C]	Bond	*d*/Å	Complex	*l*/Å	Ref.
	6.8 *M*	Cl^-	33°C	–O	2.44	5.9		
				–Cl	2.75	0.9		
	6.7 *M*	Cl^-	15°C	–O	2.45	5.3		
				–Cl	2.74	1.4		
	5.3 *M*	Cl^-	25°C	–O	2.44	6.0		
Cd(II)	1.3 *M*	NH_3	9.9	–N	2.37(3)	$Cd(NH_3)_6$		*56*
Cd(II)	1.0 *M*	ClO_4^-	3.08	–O	2.292(5)	$Cd(H_2O)_6$		*57*
Cd(II)	0.9 *M*	Cl^-	2	–Cl	2.569(4)	2	0.15	*51*
				–O	2.366(6)	4	0.17	
	1.3 *M*	Cl^-	2	–Cl	2.570(3)	2	0.14	*51*
				–O	2.373(5)	4	0.13	
Cd(II)	1 *M*	NO_3^-	2	–O	2.289(13)	5.8(2)		*32*
Cd(II)	2.9 *M*	ClO_4^-	2.2	–O	2.31(2)	6	0.06	*58*
	2.2 *M*	I^-	5.1	–I	2.79(1)	CdI_4	0.09	
Cd(II)	1.3 *M*	NO_3^-	2	–O	2.18	4		*59*
	2.0 *M*	NO_3^-	2	–O	2.35	6		
Cd(II)	1.3 *M*	I^-	0.72	–O	2.30(5)	$CdI(H_2O)_5$		*60*
				–I	2.80(5)		0.08	
Cd(II)	1.3 m	Cl^-	2.0	–O	2.359(2)	4.4(2)	0.08	*61*
				–Cl	2.576(2)	1.75(8)	0.08	
Co(II)	3.8 m	Cl^-	2	–O	2.1	6		*62*
CO(II)	1 *M*	NO_3^-	2	–O	2.091(15)	5.9(2)		*32*
Co(II)	2.7 *M*	ClO_4^-	2	–O	2.08	6		*63*
Co(II)	2.9 *M*	ClO_4^-	2	–O	2.096(1)	6	0.12	*64*
Co(II)	3.0 *M*	Cl^-	2.0	–O	2.104(2)	$COCl(H_2O)_5$	0.10	*65*
				–Cl	2.47(1)		0.10	
Co(II)	0.5 *M*	Cl^-	21.1	–Cl	2.290(2)	$CoCl_4$	0.08	*66*
	0.6 M	Cl^-	22.1	–Cl	2.29(1)	$CoCl_4$	0.06	
	2.1 *M*	Cl^-	3.4	–O	2.135(5)	5.0(1)	0.11	
				–Cl	2.353(9)	1.03(3)	0.11	
Co(II)	1.8 *M*	Cl^-	4.2	–O	2.104(4)	5	0.13	*67*
				–Cl	2.49(1)	1	0.16	
Co(II)	0.9 *M*	Cl^-	4.15	–O	2.088(3)	6.2(2)	0.10	*68*
	1.0 *M*	Cl^-	6.09	–O	2.082(2)	5.7(1)	0.10	
				–Cl	2.36(4)	0.22(8)	0.18	
	1.0 *M*	Cl^-	7.18	–O	2.074(3)	5.6(1)	0.12	
				–Cl	2.391(6)	1.13(5)	0.14	
Co(II)	2.8 *M*	Br^-	2	–O	2.101	5.96	0.09	*69*
				–Br	2.577	0.28	0.13	
	4.3 *M*	Br^-	2	–O	2.086	5.26	0.09	
				–Br	2.587	0.60	0.12	
Cr(III)	0.5 *M*	NO_3^-	3	–O	1.98	6		*45*
Cr(III)	1 *M*	NO_3^-	3	–O	2.034(2)	6	0.08	*70*
	2 *M*	NO_3^-	3	–O	2.024(3)	6	0.09	
Cr(III)	1 *M*	Cl^-	3.6	–O	1.995(3)	6	0.07	*71*
Cr(III)	1.9–2.8	Cl^-	3–5	–O	1.97(1)	5.3–4.5	0.07	*72*
				–Cl	2.31(2)	0.7–1.5	0.09	
Cu(II)	1.4 *M*	SO_4^{2-}	1	–O	1.94	4	0.06	*63*
				–O	2.38	2	0.09	
Cu(II)	3.6 *M*	ClO_4^-	2.1	–O	1.94(2)	4	0.06	*76*
				–O	2.43(3)	2	0.10	

(*continued*)

TABLE III *Continued*

Cation	[C]	Anion	[A]/[C]	Bond	*d*/Å	Complex	*l*/Å	Ref.
Cu(II)	2.1 *M*	NH_3	4.9	–N	2.03(2)	4		*77*
		Cl^-	2	–O	2.33(3)	2		
	1.5 *M*	NH_3	11.2	–N	1.93(2)	4		
		Cl^-	2	–N	2.30(3)	2		
Cu(II)	1.9 *M*	ClO_4^-	2.0	–O	1.976(1)	4	0.05	*78*
				–O	2.339(4)	2	0.10	
	2.9 *M*	ClO_4^-	2.0	–O	1.979(1)	4	0.07	
				–O	2.392(5)	2	0.12	
Cu(II)	1.4 *M*	SO_4^{2-}	1	–O	2.006(4)	4	0.09	*79*
				–O	2.33(2)	2	0.23	
Cu(II)	3.2 *M*	Cl^-	2	–O	1.93(3)	2.7 p.n.		*80*
				–Cl	2.43(1)	3.3		
	4.4 *M*	Cl^-	2	–O	1.93(3)	2.4 p.n.		
				–Cl	2.43(1)	3.6		
Cu(II)	3.7 *M*	Cl^-	2.5	–O	1.95	2 p.n.		*81*
				–Cl	2.27	2		
				–Cl	2.6	2		
Cu(II)	3.0 *M*	Cl^-	2.0	–O	1.954(2)	2.8	0.08	*65*
				–Cl	2.250(2)	1.19(5)	0.10	
				–O	2.626(8)	2	0.17	
Cu(II)	1.0 *M*	Br^-	2.0	–O	1.96	3.67		*82*
				–Br	2.42	0.33		
				–O	2.50	2		
Cu(II)	2.0 *M*	Br^-	2.0	–O	1.99	3.32		
				–Br	2.43	0.60		
				–O	2.51	2		
Cu(II)	3.3 *M*	Br^-	2.0	–O	1.96	2.73		
				–Br	2.44	1.10		
				–O	2.41	2		
Cu(II)	4.4 *M*	Br^-	2.0	–O	1.97	2.52		
				–Br	2.46	1.31		
				–O	2.37	2		
Cu(II)	2.1 *M*	Br^-	3.97	–O	1.93	1.10		
				–Br	2.42	2.91		
				–O	2.42	2		
Cu(II)	1.5 *M*	Br^-	6.7	–Br	2.41	3.85		
Fe(II)	2.7 *M*	Br^-	2	–O	2.120	5.51	0.09	*69*
				–Br	2.605	0.33	0.12	
Fe(II)	4.5 *M*	Br^-	2	–O	2.124	5.07	0.08	
				–Br	2.621	0.75	0.12	
Fe(II)	2.2 *M*	ClO_4^-	2	–O	2.12	6		*63*
Fe(III)	1.5–4.9 *M*	NO_3^-	3–4	–O	2.03	5.8	0.06	*83*
Fe(III)	1.5–2.2 *M*	ClO_4^-	3.5–4.4		2.00(1)	6	0.09	*84*
Fe(III)	1.8–5.1 m	Cl^-	3.0	–O	2.3	$FeCl_6$, Fe_2Cl_6		*85*
Fe(III)	5.0 *M*	Cl^-	3–4.2	–Cl	2.3	$FeCl_4(H_2O)_2$ p.n.		*86*
Fe(III)	2.2–5.9 *M*	Cl^-	3–4.7	–O	1.94–2.08	$Fe(Cl, H_2O)_6$		*87*
				–Cl	2.30–2.37			
				–Cl	2.24–2.26	$FeCl_4$		
Fe(III)	10–15 m	Cl^-	3	–O	2.04	6		*88*
	4.9 m	Cl^-	3	–O		0.5		
				–Cl	2.28	3.5		
	5.7 m	Cl^-	3	–Cl	2.28	4.0		

TABLE III *Continued*

Cation	[C]	Anion	[A]/[C]	Bond	*d*/Å	Complex	*l*/Å	Ref.
Fe(III)	2.2 *M*	Cl^-	5.2	–Cl	2.26	$FeCl_4$		*89*
Fe(III)	3.6 *M*	Cl^-	4.0	–O	2.010(5)	$FeCl_3(H_2O)_3$		*90*
+ H^+				–Cl	2.358(2)			
				–Cl	2.213(2)	$FeCl_4$	0.05	
Fe(III)	3.6 *M*	Cl^-	4.0	–O	2.034(4)	$FeCl_3(H_2O)_3$		*90*
+ Li^+				–Cl	2.348(1)			
				–Cl	2.237(2)	$FeCl_4$	0.06	
Hg(II)		I^-	4	–I	2.78	HgI_4		*91*
Hg(II)		Cl^-	4	–Cl	2.51	$HgCl_4$		*91*
Hg(II)	2.7–3.5 *M*	I^-	3.5–4.5	–I	2.785(3)	HgI_4	0.10	*92*
				–I	2.76	HgI_3	0.10	
Hg(II)	1.6–3.6 *M*	Br^-	3.4–4.5	–Br	2.610(5)	$HgBr_4$	0.11	*92*
				–Br	2.58	$HgBr_3$	0.11	
Hg(II)	1–5 *M*	Cl^-	3–6	–Cl	2.47(1)	$HgCl_4$	0.11	*93*
Hg(II)	1.2 *M*	OH^-		–C	2.04(3)	CH_3HgOH	0.06	*94*
				–O	2.06(2)		0.06	
Hg(II)	3.5 *M*	ClO_4^-	2.2	–O	2.42(1)	5.7(3)	0.19	*95*
Hg(II)	3.5 *M*	ClO_4^-	2.2	–O	2.41(1)	$Hg(H_2O)_6$	0.23	*96*
In(III)	15 *N*			–O	2.35	6		*44*
In(III)	3.0 *M*	ClO_4^-	3.1	–O	2.15(3)	$In(H_2O)_6$	0.09	*97*
In(III)	4.0 *M*	NO_3^-	3.2	–O	2.17	6.0	0.11	*98*
In(III)	2.5 *M*	Cl^-	6	–Cl	2.52	$InCl_6$		*99*
Er(III)	1–3 m	Cl^-	3	–O	2.3	6.5–6.3		*101*
	1.3 m	I^-	3	–O	2.3	6.3		
La(III)	1.5–2.7 m	Cl^-	3–6	–O	2.48	8.0(2)		*102*
Gd(III)	2.7 m	Cl^-	3	–O	2.37(2)	$Gd(H_2O)_8$		*103*
	1.6 m	Cl^-	6	–O	2.37(2)	$GdCl_2(H_2O)_6$		
				–Cl	2.8			
La(III)	2.7–3.0 m	Br^-	3–5	–O	2.48	8.0(2)		*104*
Nd(III)	1.7 m	Cl^-	3.0	–O	2.41	$Nd(H_2O)_8$		*105*
	1.5 m	Cl^-	6.0	–O	2.41	$NdCl(H_2O)_7$		
				–Cl	2.78			
Lu(III)	3.6 m	Cl^-	3	–O	2.338	7.97		*38*
Tm(III)	3.6 m	Cl^-	3	–O	2.358	8.12		*38*
Er(III)	3.5 m	Cl^-	3	–O	2.369	8.19		*38*
Dy(III)	3.3 m	Cl^-	3	–O	2.396	7.93		*38*
Tb(III)	3.5 m	Cl^-	3	–O	2.409	8.18		*38*
Eu(III)	3.2 m	Cl^-	3	–O	2.450	8.34		*39*
Sm(III)	3.2 m	Cl^-	3	–O	2.474	8.80		*39*
Nd(III)	3.4 m	Cl^-	3	–O	2.513	8.90		*40*
Pr(III)	3.8 m	Cl^-	3	–O	2.539	9.22		*40*
La(III)	3.8 m	Cl^-	3	–O	2.580	9.13		*40*
Y(III)	1.1 *M*	ClO_4^-	4.8	–O	2.370	8.0(3)	0.06	*34*
	2.9 *M*	ClO_4^-	3.0	–O	2.365	8.0(3)	0.08	
Tb(III)	1.1 *M*	ClO_4^-	4.9	–O	2.400	8.0(3)	0.08	*34*
	2.7 *M*	ClO_4^-	3.3	–O	2.400	8.0(3)	0.10	
Er(III)	3.0 *M*	ClO_4^-	3.1	–O	2.360	8.0(3)	0.10	*34*
Sm(III)	2.5 *M*	ClO_4^-	3.2	–O	2.455	8.0(3)	0.09	*34*
La(III)	2.9 *M*	ClO_4^-	3.2	–O	2.570	8.0(3)	0.09	*34*
Er(III)	1.0 *M*	ClO_4^-	3.3	–O	2.35(1)	8.0(3)	0.09	*35*
	1.0 *M*	ClO_4^-	9.5	–O	2.36(2)	8.0(3)	0.09	
	2.9 *M*	ClO_4^-	3.2	–O	2.36(2)	7.9(3)	0.09	

(*continued*)

TABLE III *Continued*

Cation	[C]	Anion	[A]/[C]	Bond	*d*/Å	Complex	*l*/Å	Ref.
Er(III)	1.0 *M*	Cl^-	3.2	–O	2.35(1)	8.0(3)	0.10	*35*
	0.8 *M*	Cl^-	10.3	–O	2.35(1)	7.8(8)	0.08	
				–Cl	2.67(7)	0.8(3)	0.11	
	2.4 *M*	Cl^-	3.1	–O	2.33(2)	7.8(3)	0.08	
				–Cl	2.65(10)	0.3(2)	0.10	
Er(III)	1.0 *M*	Br^-	3.2	–O	2.35(1)	8.1(3)	0.10	*35*
	0.8 *M*	Br^-	10.4	–O	2.35(1)	7.9(3)	0.07	
				–Br	2.87(2)	0.3(1)	0.11	
Mg(II)	9.9 N	Cl^-	2	–O	2.05	6.0(5)		*44*
Mg(II)	2.6 *M*	SO_4^{2-}	1	–O	2.094(4)	6	0.12	*106*
Mg(II)	1.1 m	Cl^-	2	–O	2.12(1)	6	0.04	*107*
Mg(II)	5.6–4.3 m	Cl^-	2	–O	2.1	8.1–7.9		*52*
Mn(II)	2.6 *M*	ClO_4^-	2.2	–O	2.20	6		*63*
Mn(II)	2.1–5.7 *M*	Br^-	2	–Br	2.62	1.1–1.2		*108*
	2.7–4.7 *M*	Cl^-	2	–Cl	2.49	1.3–1.5		
Ni(II)	2.0 *M*	Cl^-	2	–O	2.063(2)	6	0.12	*51*
	3.9 *M*	Cl^-	2	–O	2.068(3)	6	0.13	
Ni(II)	1 *M*	NO_3^-	2	–O	2.07(2)	5.7(2)		*32*
Ni(II)	2.5 *M*	ClO_4^-	2	–O	2.04	6		*63*
Ni(II)	2.9 *M*	ClO_4^-	2	–O	2.050(1)	6	0.10	*64*
Ni(II)	2 *M*	Cl^-	2	–O	2.052(3)	6	0.10	*112*
	4 *M*	Cl^-	2	–O	2.062(2)	6	0.13	
Ni(II)	2.0 *M*	Br^-	2	–O	2.065(3)	5.15	0.11	*113*
				–Br	2.62(1)	0.85	0.09	
Ni(II)	2.1 *M*	Br^-	2	–O	2.066(2)	5.71	0.08	*114*
				–Br	2.610(9)	0.29(3)	0.13	
	4.1 *M*	Br^-	2	–O	2.079(3)	5.56	0.10	
				–Br	2.615(9)	0.44(6)	0.13	
Ni(II)	4.8 *M*	Br^-	2	–O	2.04	5.40	0.08	*115*
				–Br	2.52	0.68	0.12	
	4.1 *M*	Br^-	2	–O	2.05	5.46	0.09	
				–Br	2.53	0.47	0.13	
	2.0 *M*	Br^-	2	–O	2.04	5.73	0.09	
				–Br	2.58	0.18	0.13	
Ni(II)	3.0 *M*	Cl^-	2	–O	2.069(1)	5.51	0.09	*65*
				–Cl	2.44(1)	0.49(2)	0.10	
Ni(II)	2.0 *M*	Cl^-	4.0	–O	2.056(1)	5.08	0.09	*116*
+ Li^+				–Cl	2.468(4)	0.92	0.15	
Ni(II)	2.0 *M*	Cl^-	4.0	–O	2.064(1)	4.84	0.09	*116*
+ H^+				–Cl	2.431(2)	1.16	0.14	
Ni(II)	2.0 *M*	Cl^-	5.0	–O	2.072(1)	4.57	0.09	*116*
+ Li^+				–Cl	2.444(2)	1.43	0.13	
Ni(II)	2 *M*	SO_4^{2-}	1	–O	2.063(3)	6	0.14	*117*
	1 *M*	SO_4^{3-}	3.9	–O	2.126(5)	6	0.12	
Ni(II)	2 *M*	SO_4^{2-}	1	–O	2.059(3)	6	0.14	*118*
	1.5 *M*	SO_4^{2-}	2	–O	2.059(3)	6	0.11	
Pt(IV)	2.7 *M*	Br^-	6.2	–Br	2.47(1)	$PtBr_6$	0.08	*119*
Pt(IV)	2.9 *M*	Cl^-	6.4	–Cl	2.33(1)	$PtCl_6$	0.06	*119*
Pt(II)	1 *M*	Cl^-	4.0	–Cl	2.31	$PtCl_4$	0.06	*13*
Rh(III)	0.3 *M*	ClO_4^-	5.8	–O	2.04(1)	6	0.10	*120*

TABLE III *Continued*

Cation	[C]	Anion	[A]/[C]	Bond	*d*/Å	Complex	*l*/Å	Ref.
Rh(III)	0.2 *M*	Cl^-	10.7	–O	2.062(4)	6	0.08	*121*
	0.4 *M*	Cl^-	4.9	–O	2.09(1)	3	0.13	
				–Cl	2.33(1)	3	0.05	
Sn(II)	3.3 *M*	ClO_4^-	2.1	–O	2.33(1)	2.3(4)	0.04	*122*
Sn(II)	3.3 *M*	ClO_4	2.1	–O	2.34(2)	3.4(3)	0.06	*123*
Sr(II)	1.5 *M*	Cl^-	2	–O	2.636(2)	8	0.14	*124*
	2.0 *M*	Cl^-	2	–O	2.644(2)	8	0.12	
Te(VI)	1.5 *M*	OH^-	6	–O	1.935(3)	$Te(OH)_6$	0.08	*125*
Th(IV)	1.0 *M*	ClO_4^-	5.0	–O	2.486(4)	8.1(3)	0.08	*126*
	1.0 *M*	ClO_4^-	11.1	–O	2.486(4)	7.9(3)	0.07	
	2.5 *M*	ClO_4^-	4.4	–O	2.484(4)	8.0(3)	0.08	
Tl(III)	1.0–2.1 *M*	ClO_4^-	5.7–7.3	–O	2.236(5)	5(1)	0.09	*127, 128*
	1.0–2.7 *M*	Br^-	2–12	–Br	2.481(2)	$TlBr_2$	0.06	
				–Br	2.512(2)	$TlBr_3$	0.06	
				–Br	2.564(2)	$TlBr_4$	0.07	
Tl(III)	0.9–2.7 *M*	Cl^-	4–13	–Cl	2.43(1)	$TlCl_4$	0.10	*127, 129*
				–Cl	2.59(1)	$TlCl_6$	0.09	
U(IV)	2.1 *M*	ClO_4^-	4.4–4.1	–O	2.44(1)	8.2(4)	0.06	*130*
UO_2^{2+}	1.0 *M*	ClO_4^-	2	–O	2.421(5)	5	0.04	*131*
Zn(II)	4.7 *M*	NO_3^-	2	–O	2.17(4)	6.6(5)	0.28	*132*
Zn(II)	1 *M*	NO_3^-	2	–O	2.09(2)	6.2(2)		*32*
Zn(II)	2.9 *M*	ClO_4^-	2.1	–O	2.081(4)	6	0.09	*63*
Zn(II)	2.8 *M*	SO_4^{2-}	1	–O	2.08	6	0.09	*63*
Zn(II)	0.6–3.1 *M*	SO_4^{2-}	1	–O	2.115–2.144	6	0.09–0.11	*133*
Zn(II)	2 *M*	SO_4^{2-}	1	–O	2.115(2)	6	0.10	*134*
	2 *M*	SO_4^{2-}	1	–O	2.099(2)	6	0.11	
Zn(II)	3–23 m	Br^-	2.0–4.3	–Br	2.40	2–4		*135*
Zn(II)	1.6 *M*	Br^-	3.1	–O	2.21	2.42	0.09	*136*
				–Br	2.42	2.26	0.12	
Zn(II)	3.0 *M*	ClO_4^-	2	–O	2.10(1)	6	0.17	*137, 143*
	1.0–7.6 *M*	Br^-	0.5–5.0	–Br	2.406(4)	$ZnBr_4$	0.08	*137*
				–Br	2.386	$ZnBr_3$	0.08	
				–Br	2.386	$ZnBr_2$	0.08	
Zn(II)	5–27 m	Cl^-	2.0	–O	2.05			*138*
				–Cl	2.28			
Zn(II)	2.2–2.6 *M*	Cl^-	6.1–6.5	–Cl	2.30(1)	$ZnCl_4$		*139*
Zn(II)	2.3 *M*	Cl^-	2–6	–Cl	2.30	2–4		*140*
				–O	2.05			
Zn(II)	2.2–2.7 *M*	NH_3	3.8–6.6	–N	2.03(2)	$Zn(NH_3)_4$		*141*
		Cl^-	2	–N	2.00(3)	$ZnCl(NH_3)_3$		
				–Cl	2.30(3)			
Zn(II)	1 m	Cl^-	2	–O	2.068(5)	5.3(1)	0.16	*61*
				–Cl	2.240(5)	1.06(4)	0.11	
Zn(II)	7–19 *M*	Cl^-	2	–O	2.05			*142*
				–Cl	2.3	2.4–4		
Zn(II)	1.1–4.6 *M*	I^-	0.5–8.1	–I	2.635(4)	ZnI_4	0.11	*143*
				–I	2.592(6)	ZnI_3H_2O	0.10	
				–I	2.592(6)	$ZnI_2(H_2O)_2$	0.07	
				–I	2.90(1)	$ZnI(H_2O)_5$	0.06	

[a] A = anion, C = cation. For bond lengths *d* and for coordination numbers, listed in the column "complex," estimated errors are given within parentheses. Charges on complexes formed are not given. p.n. = polynuclear.

In some instances it has been possible to use isostructural substitution for the analysis of X-ray diffraction data. The method was first applied by Bol *et al.* (*32*) for an investigation of the coordination around Co(II), Ni(II), Zn(II), and Cd(II) in aqueous chloride solutions. The pairs $Co(NO_3)_2$–$Mg(NO_3)_2$, $Ni(NO_3)_2$–$Mg(NO_2)_2$, $Zn(NO_3)_2$–$Mg(NO_3)_2$, and $Cd(NO_3)_2$–$Co(NO_3)_2$ were assumed to form isostructural solutions, although the ionic radii are slightly different. The calculated difference RDFs showed two pronounced peaks corresponding to a distinct first and a more diffuse second coordination sphere, which could be analyzed by comparison with theoretical curves.

This "isomorphic substitution" technique has also been used for neutron diffraction measurements as an attempt to extend the use of difference methods beyond what can be obtained by isotopic substitution (*22*). The structures of the aqua ions of Mn(II) and Cu(II), using Ni(II) as the isomorph, have been investigated in this way (Table II).

The three-valent ions formed by erbium and yttrium are structurally very similar and have been used for an extensive investigation of their coordination in different solvents for different anions and concentrations (*33–37*). Yttrium(III) is closely related chemically to the lanthanides, having the same outer electron configuration. The additional *f* electrons in the lanthanide ions do not participate in chemical bonding. Because of the lanthanide contraction the ionic radius of yttrium(III) is close to that found in the lanthanide series for the elements around erbium. Yttrium(III) and erbium(III) form isomorphous structures in the solid state, usually with no significant differences between their interatomic distances, and several diffraction measurements on yttrium(III) and erbium(III) solutions have confirmed that they also form isostructural solutions. An illustration of the close similarity is given in Figs. 11 and 12, which compare intensity curves and RDFs for 2.4 *M* yttrium(III) and erbium(III) chloride solutions of equal concentrations. By using the intensity difference curve, or the difference between the $D(r)$ functions for the two solutions, contributions from interactions involving the metal ions can be separated from those of the nonmetal interactions. The results for a 1 *M* chloride solution, where no inner-sphere complexes are expected, are illustrated in Figs. 13 and 14. The peak at 2.36 Å corresponds to the first coordination sphere in the hydrated metal ion. In the original RDF (Fig. 13) it is overlapped by longer interactions, which prevents its precise analysis, but in the RDF calculated from the difference function (Fig. 14) it appears as a fully separated peak. This proves the presence of a well-defined first coordination sphere around the erbium(III) ion, which can be precisely analyzed by comparison with theoretical Er–H_2O peaks, since nonmetal interactions are eliminated. It is found to be in perfect agreement with a

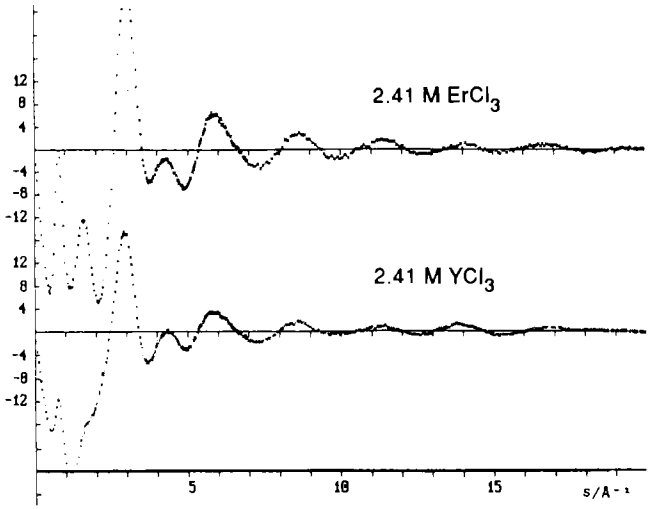

FIG. 11. Reduced intensities, $s \cdot i(s)$, for erbium(III) and yttrium(III) chloride solutions of equal concentration.

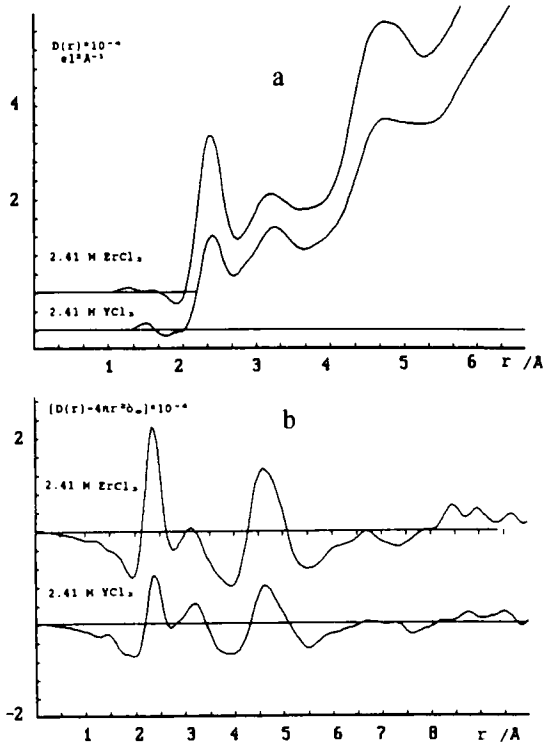

FIG. 12. The RDFs (a) and the reduced RDFs (b) calculated from the intensity values in Fig. 11.

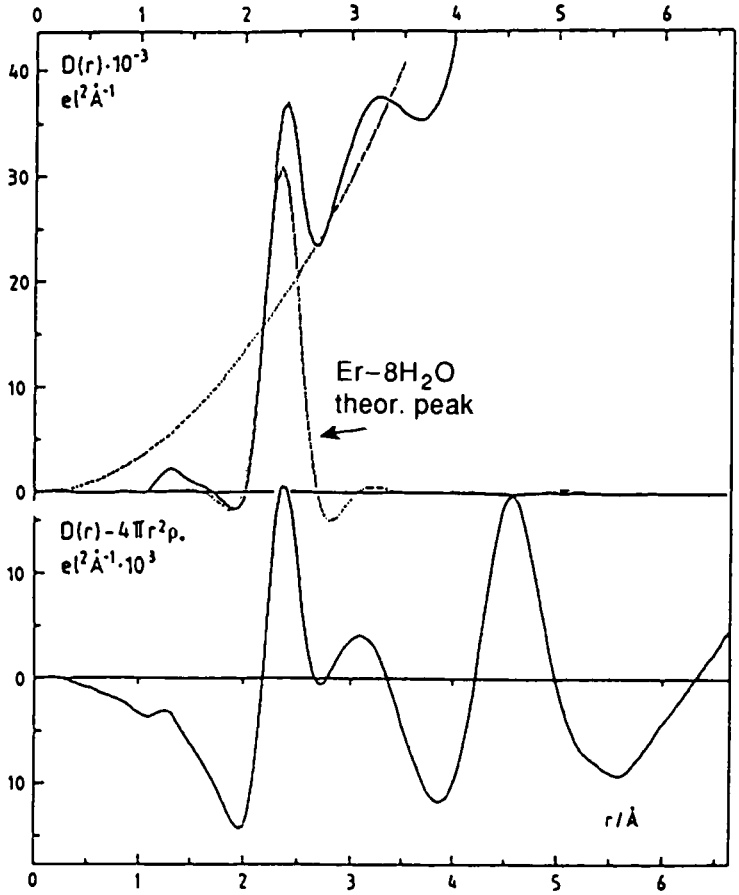

FIG. 13. The RDF (upper curve) and the reduced RDF (lower curve) for a 1 *M* aqueous erbium(III) chloride solution. The peak at 2.36 Å, corresponding to the first coordination sphere of the erbium(III) ion, is compared with a theoretical peak, calculated for a coordination number of eight.

theoretical peak calculated for eight surrounding water molecules with a Gaussian distribution of distances, the rms variation being 0.09 Å.

For perchlorate solutions of different compositions the results show no significant dependence on the concentration of the metal ion (*34, 35*). Values for the coordination number, Er—H_2O bond lengths and their rms variations do not differ significantly between a 1 *M* and a 3 *M* solution (Fig. 15), and are independent of the perchlorate concentration. No inner-sphere complex formation is indicated.

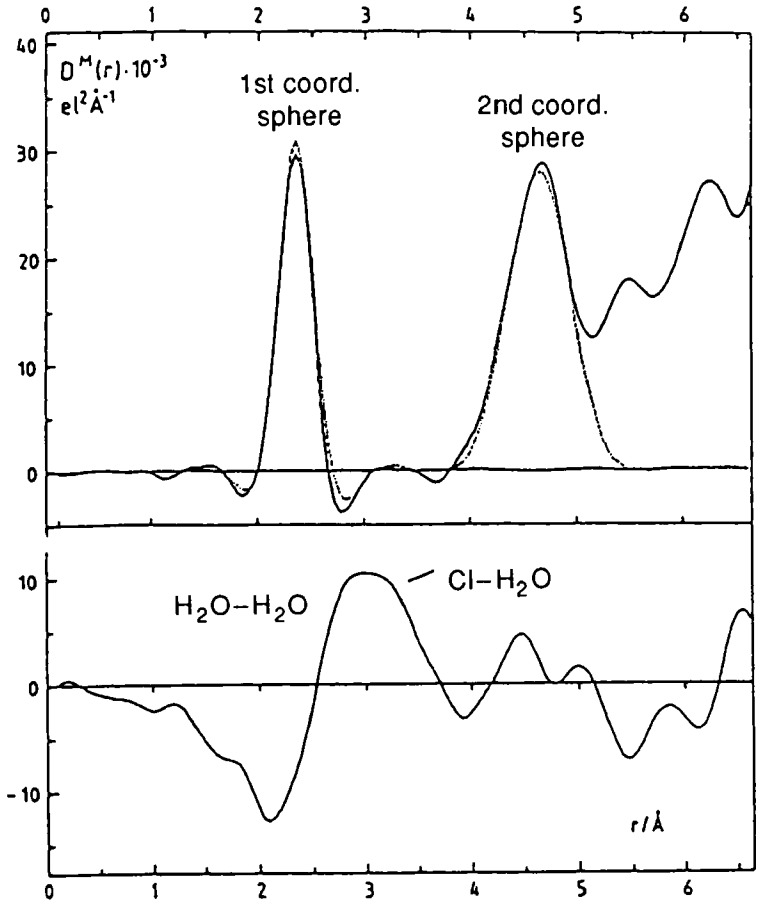

FIG. 14. The separation of the RDF for the 1 *M* erbium(III) chloride solution in Fig. 13 into a RDF involving only the metal ions (upper curve) and a reduced RDF for the remaining nonmetal interactions (lower curve). Theoretical peaks for eight water molecules (1st coordination sphere) and 16 water molecules (2nd coordination sphere) are shown for comparison (upper curve).

In the original RDFs (Figs 12 and 13) the next pronounced peak, beyond that of the first coordination sphere, occurs at about 4.5 Å. It is most clearly seen in the reduced RDFs and it occurs in a region where a second coordination sphere would be expected. The large number of other types of interactions that also occur in this region prevent a quantitative analysis. In the RDFs obtained from the difference curves, however, the nonmetal interactions are eliminated and the structure beyond the first coordination sphere can be analyzed (Figs. 14 and 15).

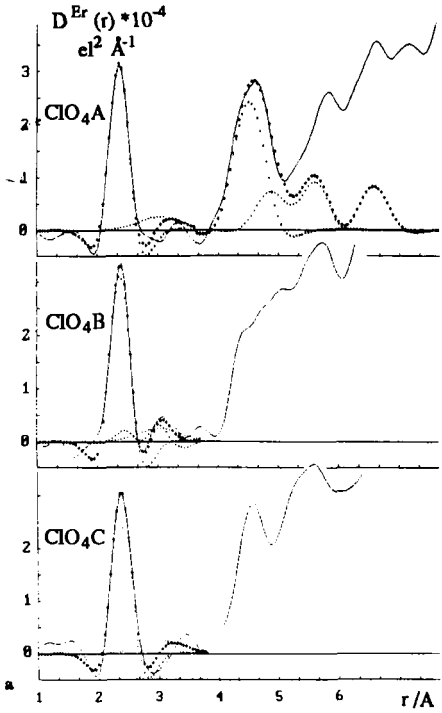

FIG. 15. RDFs for aqueous erbium(III) perchlorate solutions of different compositions after elimination of nonmetal interactions. ClO_4A: 1 *M* $Er(ClO_4)_3$; ClO_4B: 1 *M* $Er(ClO_4)_3$ + 6.5 *M* $HClO_4$; ClO_4C: 2.9 *M* $Er(ClO_4)_3$. Peaks for the first coordination sphere at 2.36 Å are compared with theoretical peaks calculated for 8.0 Er–H_2O interactions with an rms varation of 0.09 Å.

In the 1 *M* solution it shows a distinct and fairly well-separated peak at 4.5 Å, corresponding to about 16 water molecules, which is roughly equal to twice the number of H_2O molecules in the first coordination sphere. In the more concentrated perchlorate solution (Fig. 15) this peak has a more structured appearance, but is not resolved from longer distances, presumably due to the presence of perchlorate ions in the second coordination sphere, apparently bonded as bidentate ligands. The many overlapping interactions, however, prevent an unambiguous analysis.

The use of isostructural solutions in combination with a difference method thus makes it possible to get detailed and precise information on the coordination around the metal ion in solutions of different compositions, not only for the first coordination sphere, but also for the structure beyond and no assumptions about the remaining structure of the solution have to be introduced.

For some of the elements of the lanthanide series isotopes are available which make possible the use of isotopic substitution methods in combination with neutron diffraction (Table II) (*24–27*). Results obtained for the structure of the first coordination sphere of these ions are consistent with those from the X-ray diffraction measurements. The neutron diffraction measurements, however, also give information on the orientation of the water molecules (Table II), which cannot be directly derived from X-ray diffraction data because of the weak scattering power of hydrogen atoms. Neutron diffraction data, on the other hand, have not been used to analyze the structure beyond the first coordination sphere. Although X-ray data do not give direct information on the orientation of the water molecules an estimate of the tilt angle, that is, the angle between the metal–oxygen bond and the plane of the water molecule, can be made from the experimentally determined distances between the metal ion and the water molecules in the first and the second coordination spheres. If reasonable assumptions are made about H_2O—H_2O hydrogen bond distances the results are consistent with those derived from neutron diffraction data (*35*) and indicate an orientation between that for a tetrahedral and a dipolar bonding to the metal ion.

Structures of the lanthanide aqua ions have been derived also from single X-ray diffraction curves, without the use of difference methods, for nearly saturated chloride solutions for each of the elements in the rare earth series (*38–40*). The hydration number was found to be eight for the heavy elements, but seemed to gradually increase to nine for the lighter elements (Table III). The data for each solution were analyzed by fitting Gaussian peaks for specific interactions to the RDF, assuming that complex formation with chloride does not take place. The Ln—H_2O distance in the series increases from 2.34 Å for the last element, Lu, to 2.58 Å for La, the first element in the series (Table III). The Ln—H_2O peak partly overlaps the nonmetal peaks from H_2O–H_2O and Cl–H_2O interactions and this overlap becomes more serious for the lighter elements. Assumptions about the size and the shape of the nonmetal peaks may thus influence the results. There is also evidence that some complex formation with chloride may occur in very concentrated solutions (*35, 103, 105*). However, for the aqua ions of the heavy lanthanides which have been investigated by all three methods, neutron diffraction using isotopic substitution (Table II), X-ray diffraction with isostructural substitution, and analysis of single diffraction curves for very concentrated solutions (Table III), the results show no significant differences.

A correct estimate of the uncertainty in coordination numbers, derived from X-ray diffraction data, is difficult to make unless a separa-

tion of interactions can be made. This is true in particular for ions with large hydration numbers for which several different coordination geometries are possible. For smaller ions the coordination can normally be expected to be octahedral or tetrahedral, and diffraction data are usually sufficient to differentiate between a six and a four coordination. The coordination geometry, however, cannot normally be unambiguously deduced, since the H_2O–H_2O interactions within the coordination sphere are too close to the much larger number of bulk water interactions to be uniquely distinguishable.

In Table III parameter values are given only for the first coordination sphere for which the interactions in the solutions investigated often give dominant contributions. Except for the results discussed above they have all been derived from analyses of single diffraction curves. Coordination geometries are usually assumed, the assumptions being based on the derived value for the coordination number and on the observed M—H_2O distance, which differs for octahedral and tetrahedral coordination. In the usual procedure of a least-squares refinement of the parameter values, using the intensity curves, restraints have often been introduced because of correlations between too many overlapping interactions. This will make the significance of estimated standard deviations uncertain, in particular for less dominant interactions. Estimated errors are those given by the authors and are probably in many cases too low. Often a coordination number has been kept constant at an assumed value during the refinement, in which case an estimated error is not given. Unlike coordination numbers and rms variations bond lengths can usually be determined with high accuracy and the given standard deviations are likely to be more realistic estimates of the errors.

A hydration number of eight for the heavy lanthanide ions seems to be well established by several different investigations (*25, 34, 35, 38*). For the four-valent Th^{4+} ion the hydration number in perchlorate solutions, where no complexes are formed, has also been found to be eight (*126*), although the Th—H_2O distances of 2.49 Å are similar to those of the light rare earth ions for which coordination numbers of nine have been reported (*40*). Other three-valent ions, forming primarily ionic bonds, Al^{3+}, In^{3+}, Tl^{3+}, have all been found to be octahedrally coordinated, as expected from their ionic radii and their crystal structures. Among the lower charged ions in the two first groups of the periodic system those with the higher atomic numbers and, therefore, larger size, seem to have less distinct coordination shells and precise values for the coordination numbers are difficult to determine.

The results obtained for these aqua ions in solution correspond closely

to those of the structures in crystals and usually no significant differences between the metal–water bond lengths in solution and in the solid state seem to occur. An interesting exception has been found for the lanthanide ions, which most often have coordination numbers of eight or nine in the solid state as in solution, but in crystals of $Ln(H_2O)_6(ClO_4)_3$ are octahedrally coordinated by water molecules (*144*).

Among the elements in groups 1B and 2B, which form bonds of a more covalent character, several investigations have been reported for the copper(II) ion, which has the same distorted octahedral coordination as in the solid state (Table III). The silver(I) ion does not form discrete aqua ions in the solid state, but occurs as $Ag(H_2O)_4^+$ in aqueous perchlorate solutions, with Ag—H_2O bond lengths of 2.4 Å, expected for a tetrahedrally coordinated Ag^+ ion (*19, 42*).

Zn^{2+}, Cd^{2+}, and Hg^{2+} are all octahedrally coordinated in aqueous perchlorate solutions. Hg^{2+} has a strong tendency to form two approximately colinear bonds in the solid state, but in the aqua ion it is found to have a regular octahedral coordination both in crystals of $Hg(ClO_4)_2(H_2O)_6$, with Hg—H_2O bond lengths of 2.341(6) Å (*145*), and in solution, with bond lengths of 2.41(1) Å (*95, 96*). In the aqua ion of cadmium(II) the same octahedral coordination is found with Cd—H_2O bond lengths of 2.292(5) Å in solution (*57*) and 2.27(1) Å in crystals of $Cd(ClO_4)_2(H_2O)_6$ (*146*). The greater difference between metal–water bond lengths in crystals and in solution for mercury(II) than for cadmium(II) seems to be significant. The larger value for the rms variation found in solution for the Hg—H_2O bonds, 0.23(1) Å, than that for the Cd—H_2O bonds, 0.06 Å (Table III), also seems to reflect a difference in bond character between these two ions. Similar differences are found for their DMSO solvates in DMSO solutions (*96, 147*).

IX. Anion Hydration

Anions have a much weaker tendency to coordinate water molecules than cations and precise values for hydration numbers are difficult to obtain from X-ray data. Although a hydration sphere around an anion is often included in the least-squares analysis of an intensity curve for a metal salt solution, meaningful values are usually obtained only for the bond lengths. Coordination numbers and rms variations are often kept constant at assumed values. For the halide ions the bond lengths found show no significant deviations from values in crystal structures.

For the chloride ion neutron diffraction in combination with isotopic substitution has been used for extensive investigations of the structure

of the hydration sphere in solutions of different concentrations and in the presence of different cations (*2*). When no complex formation occurs the Cl—H_2O bond length, 3.3 Å, and the coordination number of six, seem to be independent of both concentration and of cation. The water molecules are bonded to the chloride ion with approximately linear hydrogen bonds.

For oxoanions X-ray diffraction data have given evidence for coordinated water molecules, but they are generally not sufficient for a quantitative determination of hydration numbers. For the planar-triangular nitrate ion, where neutron diffraction with isotopic substitution can be used, the results for a 7.8 *M* sodium nitrate solution have been interpreted in terms of a model in which 1.3 water molecules are coordinated axially to the nitrate ion with N—O distances of 2.65 Å and 2.4 water molecules hydrogen bonded to the nitrate oxygens (*148*). A similar investigation of the tetrahedral ClO_4^- ion in a 3.25 *M* $NaClO_4$ solution also shows the presence of a weak hydration shell of four to five hydrogen bonded water molecules (*149*).

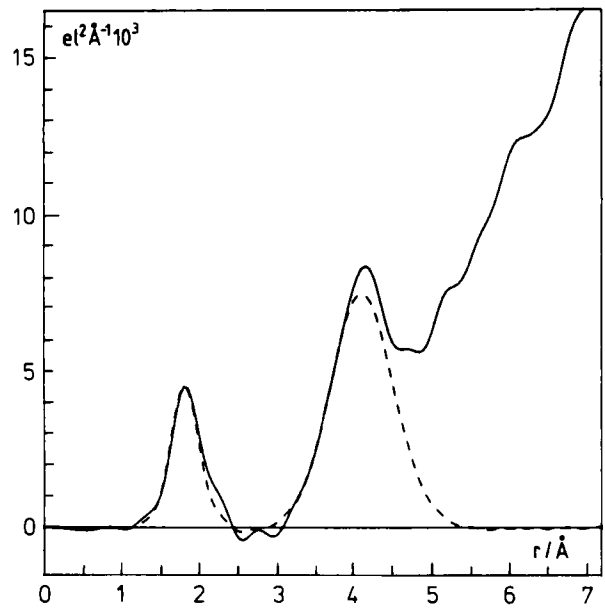

FIG. 16. The difference (solid line) between the $D(r)$ functions for 2 *M* aqueous Na_2WO_4 and Na_2MoO_4 solutions compared with theoretical peaks (dashed lines) calculated for 4.0 (W–Mo)···O interactions (l = 0.08 Å) at 1.786 Å and 12 (W–Mo)···O interactions (l = 0.34 Å) at 4.06 Å.

The tetrahedral molybdate and tungstate ions, MoO_4^{2-} and WO_4^{2-}, have the same metal–oxygen bond lengths and form isostructural solutions. The coordination around the metal ions can, therefore, be derived from X-ray diffraction data, using a difference method (*150*). The RDF calculated from the intensity difference function for 2 *M* Na_2WO_4 and Na_2MoO_4 solutions is shown in Fig. 16. Two distinct peaks appear, the first one at 1.786 Å, which is equal to the M—O bonding distance in the tetrahedral MO_4^{2-} ions in the isomorphous crystals of $Na_2WO_4 \cdot 2H_2O$ (*151*) and $Na_2MoO_4 \cdot 2H_2O$ (*152*). It is in agreement with a theoretical peak calculated for four M—O bonds. The second peak shows the presence of a distinct hydration sphere around the tetrahedral ion with an average M—H_2O distance of 4.06 Å. The theoretical peak in Fig. 16 has been calculated for 12 M—H_2O contacts. The result shows that these tetrahedral ions, which are probably representative for other similar ions like SO_4^{2-}, have a relatively well-defined hydration sphere containing about 12 water molecules probably hydrogen bonded to the anion oxygens.

X. Complexes with Halide Ions

Most structure determinations of complexes in solution using X-ray diffraction have dealt with the monoatomic halide ligands and primarily with chloro complexes. Metal–chloride bond lengths usually fall between metal–water bond lengths and water–water distances in the bulk water. The corresponding peak in the RDF is easily identified and is often only partly overlapped by other peaks. For the heavier halide ions, Br^- and I^-, the corresponding bonds are longer, but their relative contributions to the scattering are larger, and usually they can also be easily distinguished in the RDFs.

A summary of results reported in the literature is given in Table III. Most of these have been derived from analyses of single diffraction curves and only a limited number are based on diffraction data for solutions of different metal ion concentration and halide to metal ratios, which are needed in order to determine structures of individual complexes. The values obtained are, therefore, usually averages over the different complexes, that may be present, and give only limited information on coordination geometry.

For some heavy metal ions, which form strong halide complexes with relatively well-separated regions of existence, diffraction measurements can be done on solutions in each of which one of the complexes is dominant. The complete structures of the individual complexes can

then be derived. The bromide complexes formed by thallium(III) can be used as an illustration (*127, 128*). The addition of bromide ions to a thallium(III) solution leads to a stepwise formation of complexes:

$$Tl^{3+} + n\ Br^- \leftrightarrows TlBr_n^{(3-n)+}$$

Since water molecules also form part of the complexes a more correct formula would be:

$$Tl(H_2O)_m^{3+} + n\ Br^- \leftrightarrows [TlBr_n(H_2O)_{m'}]^{(3-n)+} + (m - m')H_2O$$

not including the water molecules in the weakly hydrated bromide ion. From known stability constants for the formation of these complexes the amount of thallium(III) bonded in each complex can be calculated as a function of the bromide concentration. Since no polynuclear complexes are formed this fraction should be independent of the total thallium(III) concentration, if activity factors do not change.

Literature values for stability constants (*153*) have usually been determined for solutions much less concentrated than those needed for diffraction measurements, and the values for these solutions have to be checked by other methods. For the thallium(III) bromide complexes the stability constants for the concentrated solutions used [1–2.6 *M* in Tl(III)], were derived from Tl-205 NMR shift measurements. The fraction of Tl(III), bonded in each of the complexes calculated from these constants as a function of the chloride concentration (Fig. 17), shows

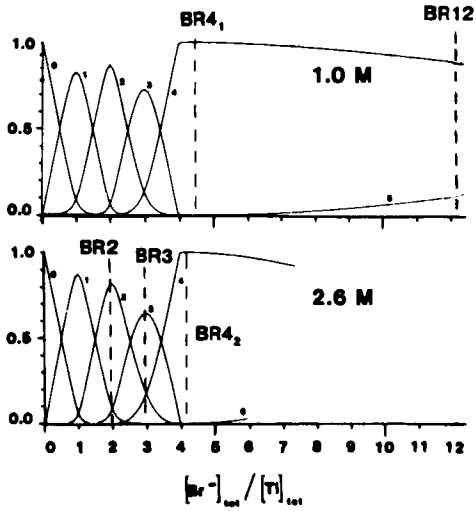

FIG. 17. Fraction of thallium(III) belonging to the different $TlBr_n^{(3-n)+}$ (n = 0–4) complexes at total thallium(III) concentrations of 1.0 and 2.6 *M*, as a function of the Br/Tl ratio. Dashed lines indicate the compositions chosen for X-ray diffraction measurements.

that the regions of dominance of the complexes are well separated. Therefore, solutions can be prepared in each of which one of the complexes predominates. From the known concentrations of the complexes and from the results of an analysis of the dominant Tl–Br and Br–Br intramolecular contributions to the diffraction curves, the structures of all of the complexes formed could be determined with the exception of $TlBr^{2+}$, which is not stable under the conditions used. The structures are illustrated in Fig. 18, which also gives the Tl—Br bond lengths and their estimated standard deviations.

The hydrated thallium(III) ion, $Tl(H_2O)_6^{3+}$, is octahedrally coordinated by water molecules. In the linear complex, $TlBr_2^+$, two of the H_2O molecules are replaced by bromide with no apparent change in the octahedral coordination. $TlBr_3$ is planar trigonal but with two water molecules, one above and one below the plane, forming a trigonal bipyramidal structure. The $TlBr_4^-$ has a regular tetrahedral structure. The positions of the water molecules in the bromide complexes could not be definitely established on the basis of the diffraction data alone, since their contributions in comparison with those from the bromide ions, are small. Support for the derived water positions were obtained from analogies with solid state structures (*127*).

For those of the complexes that appear as discrete units also in crystals, $Tl(H_2O)_6^{3+}$, $TlBr_3(H_2O)_2$, and $TlBr_4^-$, no significant differences in bond lengths were found between the complexes in the solid and the liquid phase (*127, 128*).

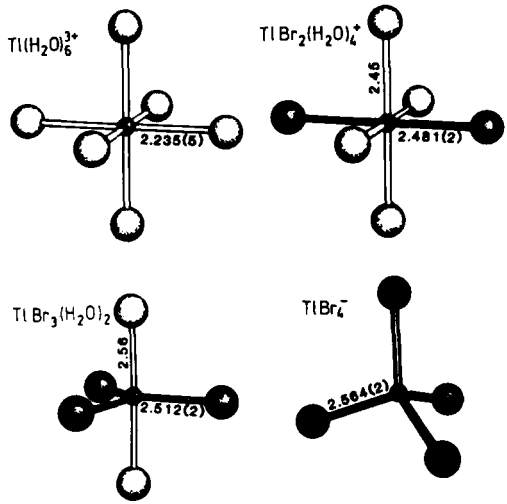

FIG. 18. Derived structures for the $TlBl_n(H_2O)_m^{(3-n)+}$ complexes in aqueous solution. Dark spheres represent Br and light spheres H_2O.

The zinc(II) ion and the complexes it forms with halide ions provide another example in which the structures of all of the complexes in aqueous solution can be derived from X-ray diffraction data (*137, 143*). The concentrations of the complexes can be determined independently from their Raman spectra and although the ranges of existence of the different complexes are more extended than for thallium(III), leading to more extensive overlap, their structures can be derived by using diffraction data for a series of solutions of different concentrations and halide to zinc ratios. The most detailed information is obtained for the zinc–iodide system (*143*), for which structures, including positions for the water molecules, can be derived for all the complexes formed (Fig. 19). The octahedral coordination in the zinc aqua ion is retained in the first complex, $ZnI(H_2O)_5^{3+}$, with a Zn–I bond length of 2.90 Å, but changes into a tetrahedral coordination in the following three complexes (Fig. 19). The approximately tetrahedral $ZnI_3H_2O^-$ units, which occur in crystals of $KZnI_3(H_2O)_2$ (*154*) with average Zn—I bond lengths of 2.57 Å and Zn—H_2O 2.07 Å do not differ significantly from those found in solution: 2.592(6) Å for Zn—I and 2.1 Å for Zn—H_2O. For the tetrahedral ZnI_4^{2-} ions the Zn—I bonds are slightly longer, 2.635(4) Å.

Another heavy metal ion, Hg^{2+}, also forms strong halide complexes

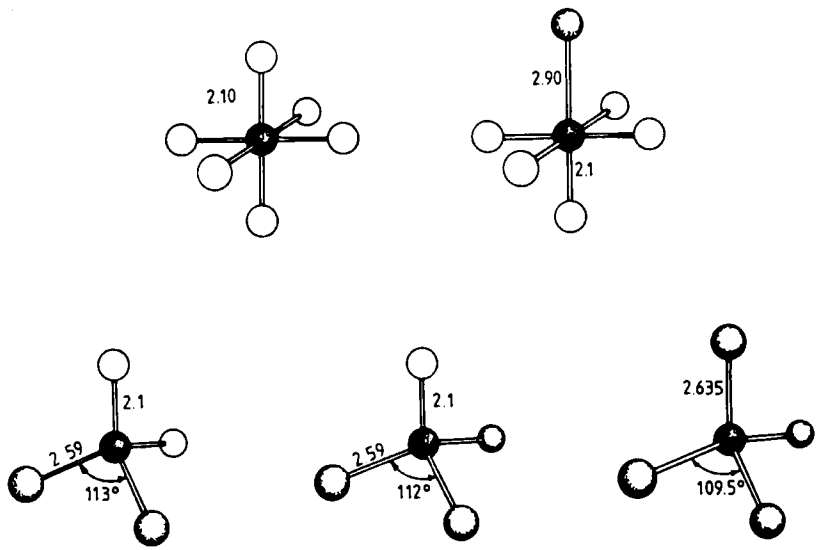

FIG. 19. Derived structures for the zinc(II) iodide complexes formed in aqueous solution: $Zn(H_2O)_6^{2+}$, $ZnI(H_2O)_5^+$, $ZnI_2(H_2O)_2$, $ZnI_3H_2O^-$ and ZnI_4^{2-}. Nonfilled circles indicate water molecules. Bond lengths are in angstroms and bond angles are given.

for which structures have been determined from solution diffraction data (*92, 93*). Of the four complexes formed in aqueous solution only HgX_3^- and HgX_4^{2-} can be obtained in sufficiently high concentrations for diffraction measurements while HgX^+ and HgX_2 are only slightly soluble. HgX_4^{2-} forms a regular tetrahedron with Hg—I 2.785(3) Å and Hg—Br 2.610(5) Å. HgX_3^- is a slightly flattened pyramid, derived from a tetrahedron with H_2O in one of the corners. The Hg—X bonds in HgX_3^- are about 0.03 Å shorter than in the HgX_4^{2-} complexes (*92*).

These examples and some others that are given in Table III show that for selected ions, which form strong complexes, it is possible to make unambiguous structure determinations from solution diffraction data and to obtain direct information on coordination changes that take place during the stepwise formation of complexes. Thermodynamic data provide only indirect information on these structural changes, indicated, for example, by abnormal changes in enthalpy and entropy values or in stability constants for the formation of the complexes.

In the rare cases when difference methods can be used detailed structure determinations can be made also when only weak complexes are formed. Structural changes, caused by changes in composition of the solution, can then be followed not only for the first but also for the second coordination sphere, making it possible to differentiate between inner- and outer-sphere complexes. Inner-sphere complexes are formed by a direct bond between the metal ion and a ligand, usually with a simultaneous release of one or more solvent molecules from the first coordination sphere. Outer-sphere complexes are formed by a bonding of the ligand in the second coordination sphere, and are often described as solvent-separated ion pairs. Metal–ligand interactions for a second coordination sphere are usually indicated in the RDF for a solution, but as they appear at a distance where a large number of other distances will also occur, they cannot be quantitatively analyzed unless a difference method can be used.

The isostructural solutions formed by yttrium(III) and erbium(III) have been used to study the structures of their halide complexes in aqueous solutions at different concentrations (*35*). The RDFs for some erbium(III) bromide and chloride solutions with different metal ion concentration and halide to metal ratios are given in Fig. 20 after elimination of the nonmetal interactions. For comparison those of three perchlorate solutions of similar concentrations are also given. For all of these solutions the peaks at 2.35 Å, which correspond to the inner coordination sphere of the metal ion, are nearly the same and are closely reproduced by a theoretical peak calculated for 8.0 Er–H_2O interactions. This indicates that the anions do not penetrate the first

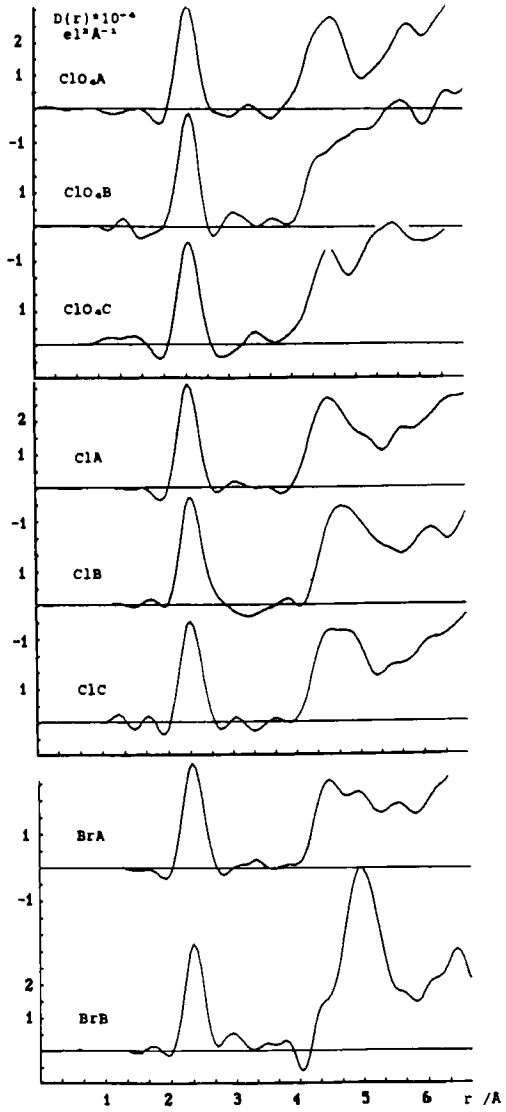

FIG. 20. RDFs for some aqueous perchlorate, chloride, and bromide solutions of erbium(III) after elimination of nonmetal interactions. A and B solutions are 1 *M* in erbium(III), with anion to Er ratios of about three (A) and nine (B). C solutions are about 3 *M* in Er.

coordination sphere to any large extent. Only at very high halide concentrations do inner-sphere complexes appear and then only in small concentrations. The formation of an inner-sphere complex is most clearly indicated for the bromide solution with the highest bromide concentration, where a separate Er—Br peak appears at 2.87 Å (Figs. 20 and 21). For the corresponding chloride solution an Er—Cl peak from an inner-sphere complex, expected at about 2.7 Å, is too close to the Er—H_2O peak to be resolved, but a peak analysis shows a similar but somewhat stronger inner-sphere complex formation in this solution. In the 1 *M* solutions, where halide ions are not in excess, no inner-sphere complexes are indicated. In the more concentrated 2.4 *M* chloride solution a weak inner-sphere complex formation ($< \approx 0.3$ Cl/Er) cannot be excluded.

In contrast to the first coordination sphere the second sphere is strongly dependent on the composition of the solution (Fig. 20). The corresponding peak, which appears at 4.5–5.0 Å, is fairly well resolved from longer distances, with exception for the two concentrated perchlorate solutions. For the halide solutions two overlapping peaks can be distinguished, one of which corresponds to the expected shorter Er–H_2O

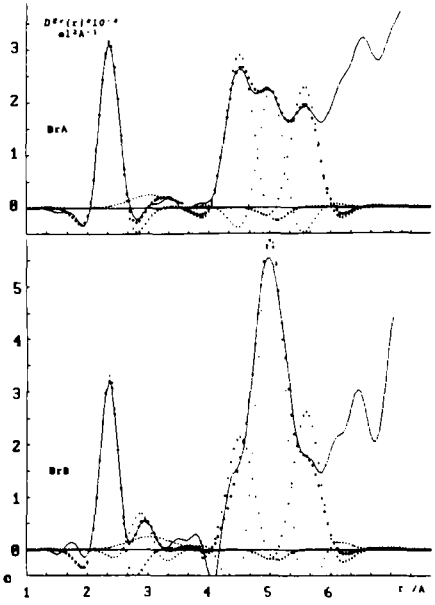

FIG. 21. An analysis of the first and second coordination spheres for 1 *M* erbium(III) bromide solutions with Br/Er ratios of three (BrA) and nine (BrB) by a comparison with theoretical Er–H_2O and Er–Br peaks. Parameter values are given in Tables III and IV.

(≈ 4.5 Å) and the other to the longer Er–X (≈ 5.0 Å) interaction. An analysis in terms of distinct Er–H_2O and Er–X interactions leads to the parameter values given in Table IV. The theoretical peaks, calculated with these values, are illustrated for the two bromide solutions in Fig. 21.

From the results of an analysis of the first (Table III) and the second (Table IV) coordination spheres the distribution of water molecules and halide ions over the different spheres and the remaining solution can be calculated. The values given in Table V clearly show that the halide ions are concentrated to the second coordination sphere, which establishes a preferred formation of outer-sphere complexes.

The distance to the chloride ion in the second coordination sphere, 5.0 Å (Table IV), is similar to corresponding distances found in the crystal structure of $ErCl_3(H_2O)_6$ (*155*), which have an average value of 5.05 Å. The same distance is found in the bromide solution for Er–Br, despite the larger size of the bromide ion. The packing of these two halide ions in the second coordination sphere thus seems to be different, perhaps because of their different tendencies to take part in hydrogen bonding. In iodide solutions the corresponding Er—I distance is 5.25 Å, the increase corresponding to the difference in ionic radii between Br^- and I^- (*35*).

The four-valent Th^{4+} ion, which also forms primarily ionic bonds, has a hydration number of eight in aqueous perchlorate solutions (*126*), which is the same as that of erbium(III), although the Th—H_2O bonds are slightly longer, 2.49 Å, than for erbium(III), 2.35 Å. Diffraction data for an aqueous thorium(IV) chloride solution, with a composition

TABLE IV

THE STRUCTURE OF THE SECOND COORDINATION SPHERE IN SOME ERBIUM(III) CHLORIDE AND BROMIDE SOLUTIONS[a]

Sol.	Comp.		Er—O(H_2O) r/Å	n	l/Å	Er—X r/Å	n	l/Å
ClA	1	3	4.51(4)	13.2(15)	0.24(4)	5.07(8)	2.8(7)	0.24(4)
ClB	1	9	4.60(4)	11.0(10)	0.20(5)	5.06(6)	4.8(5)	0.24(4)
ClC	3	3	4.50(2)	12.8(10)	0.22(4)	4.98(2)	3.5(4)	0.20(3)
BrA	1	3	4.49(1)	12.0(8)	0.20(3)	5.01(1)	1.6(2)	0.20(3)
BrB	1	9	4.5(1)	9(1)	0.2(1)	5.00(2)	5.2(5)	0.25(3)

[a] Compositions of the solutions "comp" are given by the concentration of erbium(III) in mol/l and by the ratio [X]/[Er]. For each interaction the distance, r, the frequency, n, and the rms variation, l, are given.

TABLE V

RELATIVE DISTRIBUTION OF LIGANDS FOR SOME ERBIUM(III) CHLORIDE AND BROMIDE SOLUTIONS[a]

Soln.	Comp.		Stoich	1st	2nd	Bulk
ClA	1	3	0.06	0.0	0.21	0.01
ClB	1	9	0.19	0.10	0.44	0.13
ClC	3	3	0.14	0.03	0.27	—
BrA	1	3	0.06	0.0	0.13	0.05
BrB	1	9	0.20	0.04	0.61	0.14

[a] The ratios between the number of halide ions, X^-, and water molecules in the first and second coordination spheres and in the bulk solution are compared with the value for the total solution "stoich." The solutions are the same as in Table IV.

similar to one of those used for erbium(III), shows similar complex formation and both inner- and outer-sphere complexes are formed (*126*). The inner-sphere complex formation is stronger, however, and can be more precisely analyzed than for the erbium(III) solutions. The results seem to indicate that the complexes are formed by an addition of chloride ions without replacing water molecules in the inner sphere, thus leading to an increased coordination number (*126*).

XI. Polyatomic Ligands

The bonding of a polyatomic ligand to a metal ion increases the number of metal–ligand interactions, but corresponding peaks in the RDFs are usually not well resolved. In nitrate complexes, for example, the metal–nitrogen distance for a bidentately bonded nitrate ion is too close to the metal–oxygen bonds to form a separate peak in the RDF. The M—O(NO_3) and the M—O(H_2O) bonding distances within the first coordination sphere are also too close to be separately determined. The information given by the RDF then becomes mainly indicative of a complex formation and is seldom, depending on the specific characteristics of the system, sufficient for a precise determination of coordination number and conformation of the ligand. A summary of results reported in the literature for polyatomic ligands is given in Table VI (*156–179*).

More precise structural information can be obtained when a separation of interactions can be made. The RDFs for 2.9 *M* solutions of erbium(III) and yttrium(III) nitrate, which are isostructural (*36*), are

TABLE VI

STRUCTURES OF COMPLEXES WITH POLYATOMIC LIGANDS IN AQUEOUS SOLUTION[a]

Ligand	Cation	[C]	[L]/[C]	Coord.	Bonding	Ref.
SO_4^{2-}	Cd(II)	1–3 *M*	1–3	0.8–1.6	Cd-6O 2.28(1) Cd—O—S 134(2)°	*57*
	Cd(II)	2 *M*	1	0.34 (9°C)	Cd-6O 2.32(1) Cd—O—S 133°	*156*
				0.64 (62°C)	Cd-6O 2.30(1) Cd—O—S 133°	
	Cr(III)	1.4 *M*	2.5	0.83(7)	Cr-6O 1.94(1) Cr—O—S 136(1)°	*157*
	Fe(III)	3.4 *M*	1.5	1.20(4)	Fe-6O 2.018(2) Fe—O—S 135.1(3)	*158*
		2.5 *M*	1.5	1.27(10)	Fe-6O 2.016(2) Fe—O—S 133.9(5)	
		1.9 *M*	3.0	0.95(10)	Fe-6O 2.006(3) Fe—O—S 134.7(5)	
	Mn(II)	2.0 *M*	1	0.75(6)	Mn-6O 2.195(3)	*159*
		3.8 *M*	1	0.92(8)	Mn-6O 2.218(3) Mn—O—S 140°	
	Mn(II)	2 *M*	1	0.50(6)	Mn-6O 2.196(2) Mn—S 3.50(2)	*160*
	Ni(II)	2 *M*	1	0.9(1)	Ni-6O 2.068(2) Ni—S 3.49(2)	*160, 161*
	In(III)	1.7 *M*	1.5	0.88(5)	In-6O 2.156(2) In—O—S 134°	*162*
	Zn(II)	3.0 *M*	1	0.4(1)	Zn-5.6O 2.10(1) Zn-SO_4 3.13(5)	*163*
SeO_4^{2-}	Y(III)	0.8 *M*	2.0	0.35	Y-8O 2.330 Y—O—Se 142°	*33, 34*
	Y(III)	0.9 *M*	2.1	0.60	Y-8O 2.325 Y—O—Se 141	*34*
	Er(III)	0.8 *M*	2.0	0.35	Er-8O 2.345 Er—O—Se 140	*33, 34*
	Er(III)	1.0 *M*	2.2	0.60	Er-8O 2.340 Er—O—Se 141°	*34*
	Tb(III)	1.2 *M*	1.6	0.60	Tb-8O 2.380 Tb—O—Se 140°	*34*
	La(III)	0.7 *M*	1.7	0.60	La-8O 2.560 La—O—Se 139°	*34*
NO_3^-	Ag(I)	3.0 *M*	1	1	Ag-4O 2.42(1) Ag—N 3.13	*42*
		8.8 *M*	1	1	Ag-4O 2.43(1) Ag—N 3.13	
	Cd(II)	4.5 *M*	2	0.96(7)	Cd-6O 2.284(5) Cd—N 3.15	*164*

TABLE VI *Continued*

Ligand	Cation	[C]	[L]/[C]	Coord.	Bonding	Ref.
	Ce(IV)	2.1 m	6	6	Ce-11.2 O 2.85 Bidentate	*165*
	Ce(III)	2.0 *M*	3.0	0.9	Ce-8 O 2.555(2) Ce—N 3.44(2)	*166*
	Er(III)	1.0 *M*	3.3	0.9	Er—O 2.35–2.45 Er—N 2.86	*36*
		1.0 *M*	9.5	2.0	Er—O 2.32–2.45 Er—N 2.78	
		2.9 *M*	3.2	2.2	Er—O 2.37–2.45 Er—N 2.86	
	Mn(II)	4.4 *M*	2	0.6	Mn-6O 2.191(2) Mn—O—N 125°	*167*
PO_4^{3-}	Ni(II)	1.0 *M*	4.0	0.75(8)	Ni-6O 2.03(1) Ni—O—P 136(2)°	*168*
	Cd(II)	1.0 *M*	5.0	0.95(6)	Cd-6O 2.30(1) Cd—O—P 130(2)°	*168*
$C_2O_4^{2-}$	Fe(III)	1.1 *M*	3	3	Fe-6O 2.005(1) Fe—6C 2.80	*169*
CH_3COO^-	Mg(II)	1.5 *M*	2	0.8	Mg-6O 2.089(4) Mg—O—C 125(3)°	*170*
		2.9 *M*	2	0.8	Mg-6O 2.098(4) Mg—O—C 125(3)°	
	Co(II)	1.0 *M*	2	0.8	Co-6O 2.140(3) Co—O—C 125(3)°	*170*
	Mn(II)	1.5 *M*	2	0.8	Mn-6O 2.195(3) Mn—O—C 125(3)°	*170*
	Zn(II)	1.4 *M*	2	1.6	Zn-6O 2.075(4) Zn—O—C 125(3)°	*170*
	Cd(II)	1.0 *M*	4.0	1.70	Cd-6O 2.287(5) Cd—O—C 100(2)°	*170*
		2.0 *M*	2	2.50	Cd-6O 2.270(5) Cd—O—C 100(2)°	
SCN^-	Ag(I)				Ag-4 S 2.65	*43*
	Hg(II)	1 *M*	7.0	4	Hg—4S 4.15(4) Hg—S—C 102(2)°	*171*
	Cd(II)	1 *M*	7.0	4	Cd—2N 2.246(6) Cd—2S 2.649(3) Cd—N—C 149(1)° Cd—S—C 106(1)°	*171*
	Zn(II)	1 *M*	7.0	4	Zn—4N 2.041(3) Zn—N—C 145(1)	*171*
en	Zn(II)	1.8 *M*	3.2	3	Zn—6N 2.276(5)	*172*
		1.3 *M*	2.3	2	Zn—4N 2.131(9)	
	Cd(II)	1.9 *M*	3.4	3	Cd—6N 2.371(5)	*173*
		1.8 *M*	2.2	2	Cd—4N 2.339(4)	

(*continued*)

TABLE VI *Continued*

Ligand	Cation	[C]	[L]/[C]	Coord.	Bonding	Ref.
	Ni(II)			2	Ni—2N 2.102(7) Ni—2O 2.10(1)	*174*
	Ni(II)			3	Ni—6N 2.202(4)	
	Cu(II)			$Cu(en)_2(H_2O)_2$	Cu—N 1.93 (eq) —N 2.92(at)	*175*
				$Cu(en)_3$	Cu—N 1.72 (eq) —N 2.22(at)	
tren	Zn(II)	2.2 *M*	1	Zn(tren)Cl	Zn—N 2.09(2) —O 2.37(3)	*176*
gly^-	Ni(II)			$Ni(gly)_3$	Ni—O 2.03 —N 2.14	*177*
	Cu(II)			$Cu(gly)(H_2O)_4$	Cu—O 1.98 (eq) —O 2.27(at) —N 1.99	*178*
				$Cu(gly)_3$	Cu—O 2.02 —N 2.02	
	Zn(II)			$Zn(gly)(H_2O)_4$ $Zn(gly)_3$	Zn—O 2.12 —N 2.12	*179*

[a] [C] = concentration of cation. [L]/[C] = ratio between anion and cation concentration. Coord. = average number of coordinated ligands. "Bonding" gives the type and number of bonded atoms, bond length, and bond angle. en = ethylenediamine; tren = triaminotriethylamine; gly^- = glycinate.

given in Fig. 22. If inner-sphere nitrate complexes are formed the metal–nitrate interactions should appear in the region between about 2.5 and 4 Å. It is obvious that the RDFs in Fig. 22 cannot be used to derive an unambiguous model for the nitrate complexes because of the many overlapping interactions and the resulting nondistinct peaks in the region.

By using the intensity difference curve the light atom interactions can be eliminated and the RDF, including only interactions involving the metal ions, can be calculated. The results, referred to the erbium(III) solutions, are shown in Fig. 23 for three nitrate solutions of different compositions, including the 2.9 *M* solution illustrated in Fig. 22. The intramolecular NO_3^- interactions together with all other nonmetal interactions are now eliminated and the first coordination peak appears as a separate peak. Its shape, however, depends on the composition of the solution, contrary to what was found for perchlorate solutions of similar compositions, and in comparison with these it is significantly broadened. For the 1 *M* solutions the difference is small but it becomes much more pronounced, when the concentration of nitrate ions is in-

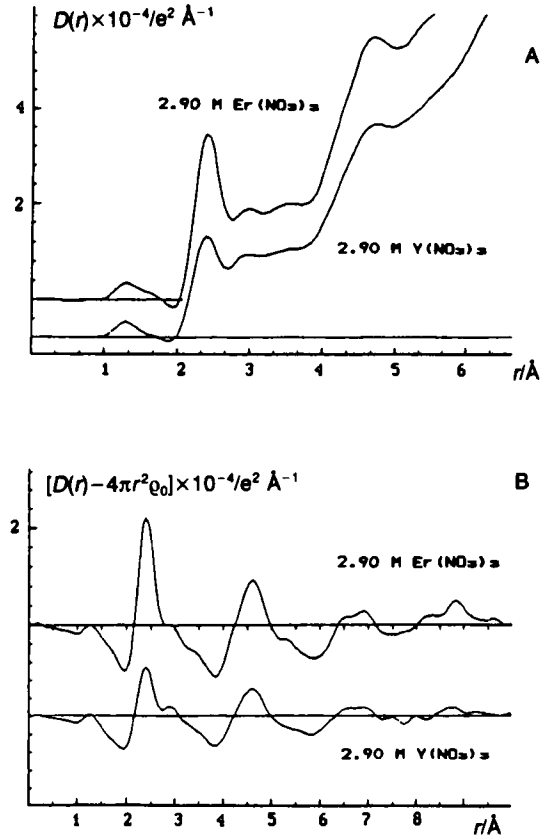

FIG. 22. Radial distribution functions (A) and reduced RDFs (B) for 2.9 *M* isostructural yttrium(III) and erbium(III) nitrate solutions.

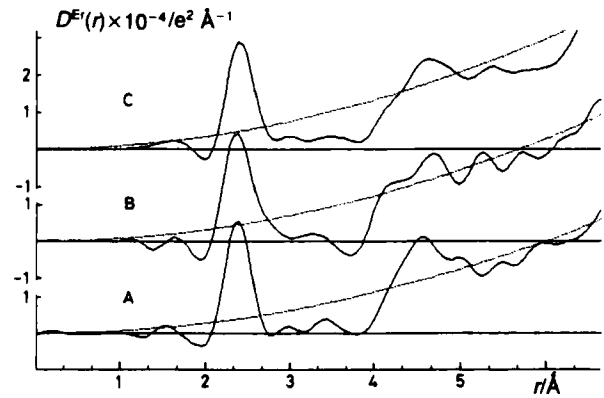

FIG. 23. The RDFs for three erbium(III) nitrate solutions after eliminating nonmetal interactions. (A) 1 *M* $Er(NO_3)_3$; (B) 1 *M* $Er(NO_3)_3$ + 6 *M* $LiNO_3$; and (C) 2.9 *M* $Er(NO_3)_3$.

creased. Although the specific metal–nitrogen interactions are not resolved from neighboring peaks the changes in the first and second coordination spheres in the nitrate solutions, when compared to the perchlorate solutions, can be related to the bonding of a bidentate nitrate ion to erbium(III), as illustrated in Fig. 24. The expected Er—N distance of about 2.8 Å leads to a broadening of the first coordination peak and the shoulder at about 4.1 Å in the second coordination peak

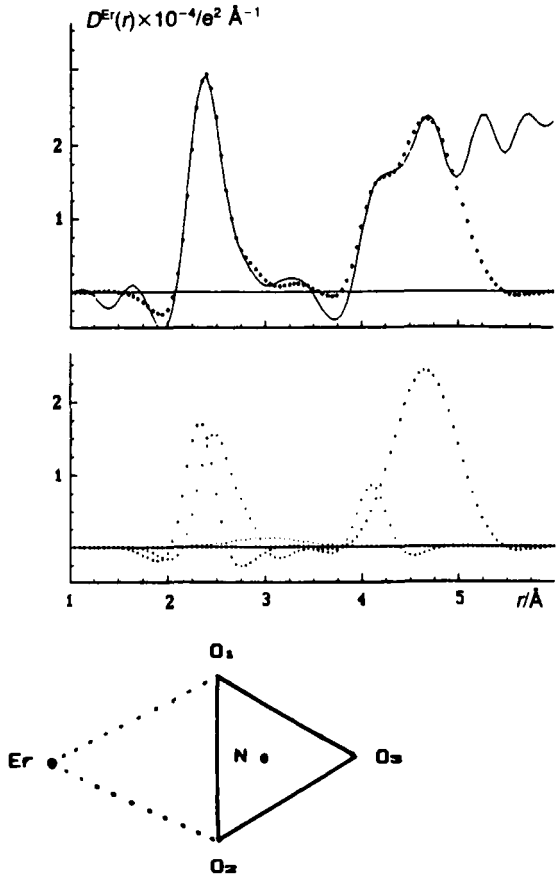

FIG. 24. The RDF for solution B in Fig. 23, after elimination of nonmetal interactions (solid line) is analyzed by comparison with peaks calculated for a bidentate bonding of two nitrate ions to erbium(III). The lower half shows the separate peaks Er—O(H_2O) at 2.32 Å, Er—O(NO_3) and Er—N at 2.45 Å and 2.8 Å, Er—O_3 at 4.1 Å, and Er—H_2O at 4.6 Å. In the upper half of the figure the sum of the individual peaks, indicated by dots, is compared with the experimental RDF.

results from the Er—O distance involving the nonbonded nitrate oxygen, O_3.

A model calculation on the basis of this structure is illustrated in Fig. 24 for one of the solutions. It leads to a symmetric or only slightly asymmetric bidentate bonding of about two nitrate ions to erbium (Fig. 24) with the Er—O(NO_3) bond lengths, 2.45 Å, somewhat longer than the Er—O(H_2O) bonds, 2.32 Å, in the first coordination sphere. The Er^{3+} ion and the nitrate ligand are coplanar as shown by the Er—O_3 distance of 4.1 Å. This bonding of nitrate to the metal ion is very similar to that found in crystals, with the same orientation of the nitrate ion and the same difference between Er—O(H_2O) and Er—O(NO_3) bond lengths (*36*).

The same technique has been used to investigate the bonding of a tetrahedral oxoanion to erbium(III) in aqueous solutions (*33, 34*). Selenate rather than sulfate was chosen because of the higher atomic number and, therefore, the higher scattering power of selenium. Figure 25 shows the RDFs, after elimination of nonmetal interactions, for a 0.8 *M* erbium(III) selenate solution and for a 1 *M* perchlorate solution, both of them normalized to a stoichiometric unit of volume containing one metal atom. The first and the second coordination spheres appear as distinct, well-separated peaks at 2.35 and 4.5 Å. In the selenate solution, however, an additional peak appears at 3.7 Å, which is not present in the perchlorate solution. It can only be explained as an Er—Se distance in an inner-sphere complex, resulting from a monodentate bonding of the SeO_4 group with an Er—Se—O bond angle of about 140°. An analysis of this peak by comparison with theoretical Er—Se peaks shows the complex formation to be weak, however, and only about 0.4 SeO_4 groups are bonded to each Er^{3+} ion in the solution investigated. In crystals of erbium(III) sulfates, which can be expected to have structures very similar to those of the selenates, the sulfate groups usually form bridges between different metal ions, but often have the same type of monodentate bonding with an average Er—O—S angle of approximately the same magnitude as found for the Er—O—Se angle in solution (*34*).

Since the metal–sulfur distance in an inner-sphere sulfate complex appears in a region where a large number of other distances in the solution will also occur, a unique identification and structure determination of sulfate complexes is difficult to make unless difference methods can be used. Definite conclusions cannot generally be made on the basis of an analysis of a single diffraction curve only. Data for several solutions of different compositions are needed and a careful analysis

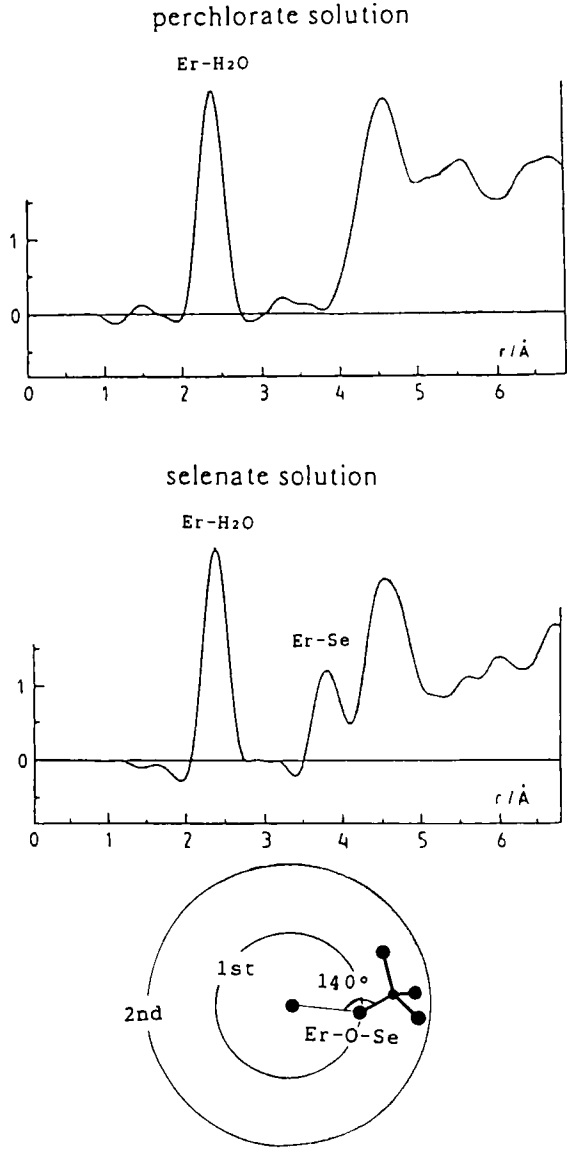

FIG. 25. RDFs for 1 *M* erbium(III) perchlorate and selenate solutions after elimination of nonmetal interactions. The monodentate bonding of SeO_4^{2-} is shown by the Er–Se peak in the RDF for the selenate solution.

is required of both intensity curves and RDFs. Controversies in the literature demonstrate the difficulties involved (*117, 118, 160, 161*).

Complex formation with several other polyatomic ligands have been investigated and results reported in the literature are summarized in Table VI. Some of the ligands, because of their internal structure, are more favorable for structure determinations than others.

The internal structure of a polyatomic ligand is obtained as an additional result in these investigations. Its high concentration and the sharp intramolecular distances often result in dominant contributions to the diffraction curves and make possible a precise determination of its bonding distances. When careful analyses have been made, no significant differences from values found in crystals have been found, however. Therefore, the derived structure for the ligand can serve as an internal check on the quality of the data. Large deviations from values found in crystal structures may be an indication of errors in the data or in the method of analysis.

XII. Nonaqueous Solutions

Although aqueous solutions have been the main object of interest, X-ray diffraction can also be used to study nonaqueous solutions, and to investigate, for example, the influence of a solvent on the structure of a specific complex. A summary of results of structure determinations of complexes in nonaqueous solvents is given in Table VII (*180–199*).

Nonaqueous solutions often have specific characteristics which make them more favorable for structure determinations by X-ray diffraction than aqueous solutions. An illustration is given in Fig. 26, which compares the RDF for a 3 *M* aqueous silver(I) nitrate solution with that for a similar solution in the aprotic solvent dimethylsulfoxide, DMSO. The RDFs are given after subtracting the known intramolecular DMSO and NO_3^- interactions and they are both normalized to a stoichiometric unit of volume containing one Ag atom. The Ag^+ ion is four-coordinated in aqueous solution, but the corresponding Ag—H_2O peak at 2.4 Å is extensively overlapped by H_2O—H_2O hydrogen bonding distances. In DMSO such interactions are absent and here the peak is much better resolved. The first part of the two peaks are identical, however, indicating the Ag—O bonding distances and the coordination number for Ag(I) to be the same in the two solvents, the DMSO molecule being coordinated over oxygen. The DMSO solution also shows a distinct peak at 3.5 Å, corresponding to the Ag—S distance (Fig. 26) in the DMSO solvated Ag^+ ion, and this can be used for an independent determina-

TABLE VII

STRUCTURES OF COMPLEXES IN NONAQUEOUS SOLUTIONS[a]

Cation	Solvent[b]	[C]	Anion	[A]/[C]	Complex	Bond	Ref.
Ag(I)	py	1.1 *M*	ClO_4^-	1	$Ag(py)_4$	—N 2.30(2)	*180*
	py	0.9 *M*	$Sb(C_4H_9)_3$	1.7	1.7(1)	—Sb 2.680(3)	
						—N 2.38(2)	
Ag(I)	melt		I^-	0.2–0.7	AgI_4 p.n.	—I 2.82	*181*
Ag(I)	tht	0.8 *M*	ClO_4^-	1	$Ag(tht)_4$	—S 2.526(7)	*182*
		1.8 *M*	I^-	1	$[AgI(tht)]_4$	—Ag 3.070(11)	
						—I 2.824(4)	
						—S 2.65	
		1.5 *M*	Br^-	1	$[AgBr(tht)]_4$	—Ag 2.866(5)	
						—Br 2.592(3)	
						—S 2.65	
Ag(I)	dmso	3 *M*	NO_3^-	1	$Ag(dmso)_4$	—O 2.42(1)	*183*
						—S 3.49(1)	
	dmso	0.5–1 *M*	I^-	1.5–4	AgI_3	—I 2.775(5)	
					Ag_4I_5	—I 2.86(1)	
						—Ag 2.94	
Cd(II)	dmso	2.5 *M*	I^-	2.0	1.6(2)	—I 2.769(4)	*184*
		1.7 *M*	I^-	3.0	CdI_3	—I 2.773(3)	
		1.3 *M*	I^-	3.8	CdI_4	—I 2.790(3)	
Cd(II)	dmso	0.3 *M*	SCN^-	4.5	2.3	—S 2.634(1)	*185*
Cd(II)	dmf	1.0 *M*	ClO_4^-	2	$Cd(dmf)_6$	—O 2.296(4)	*186*
		1.0 *M*	SCN^-	5–6	$Cd(NCS)_3(SCN)$	—N 2.23(2)	
						—S 2.57(2)	
Cd(II)	dmso	0.7 *M*	ClO_4^-	2	$Cd(dmso)_6$	—O 2.292(3)	*96*
						Cd—O—S 126(1)°	
Co(II)	meth	3.9 m	Cl^-	2	4	—Cl 2.30	*62*
	eth	3.8 m	Cl^-	2	4	—Cl 2.30	
Cu(II)	meth	1.1–3.3	Cl^-	2	2.0–2.1	—O 1.95, 2.44	*187*
						—Cl 2.24	
Cu(II)	dmf	0.6 *M*	ClO_4^-	2	4 + 2	—O 2.03(3), 2.43(5)	*171*
	an + dmf	0.9 *M*	ClO_4^-	2	$Cu(dmf)_4$	—O 2.00(1)	
Hg(II)	dmso	0.9–2.5 *M*	I^-	2–4	HgI_4	—I 2.80(1)	*188*
	dmf	1.0–2.0 *M*	I^-	3–4	HgI_3	—I 2.73(1)	
					HgI_2	—I 2.60(1)	
						I—Hg—I 165°	
Hg(II)	dmso	1.3–4.4 *M*	I^-	1–2	HgI_2	—I 2.625(2)	*189*
						I—Hg—I 159(2)°	
	dmso	0.6–3.2 *M*	Br^-	1–4	$HgBr_4$	—Br 2.636(4)	
					$HgBr_3$	—Br 2.548(4)	
					$HgBr_2$	—Br 2.455(3)	
						Br—Hg—Br 165(3)°	
	dmso	1–1.5 *M*	Cl^-	1–3	$HgCl_3$	—Cl 2.434(4)	
					$HgCl_2$	—Cl 2.350(4)	
	meth	1.5 *M*	Cl^-	2	$HgCl_2$	—Cl 2.308(3)	
Hg(II)	dmso	0.4 *M*	Br^-	4.5	$HgBr_4$	—Br 2.628(3)	*190*
	dmso	0.4 *M*	Cl^-	4.5	$HgCl_4$	—Cl 2.532(2)	

TABLE VII *Continued*

Cation	Solvent[b]	[C]	Anion	[A]/[C]	Complex	Bond	Ref.
Hg(II)	dmso	0.4–0.9 *M*	ClO_4^-	2	$Hg(dmso)_6$	—O 2.393(5) Hg—O—S 120.2(10)°	*96*
Hg(II)	dmso	0.3–0.8 *M*	SCN^-	1–4.6	$Hg(SCN)_2$ $Hg(SCN)_3$ $Hg(SCN)_4$	—S 2.410(2) —S 2.464(3) —S 2.547(4) Hg—S—C 107°	*185*
Hg(II)	py	0.7 *M*	I^-	2.0	$HgI_2(py)_2$	—I 2.665(2) —N 2.43(2) I—Hg—I 143(2)	*191*
	py	0.7 *M*	Br^-	2.0	$HgBr_2(py)_2$	—Br 2.497(2) —N 2.45(2) Br—Hg—Br 151(3)	
	py	0.9 *M*	Cl^-	2.0	$HgCl_2(py)_2$	—Cl 2.375(10) —N 2.47(2)	
Hg(II)	py	1.2 *M*	I^-	1.0	CH_3HgI	—I 2.649(3)	*192*
	py	1.4 *M*	Br^-	1.0	CH_3HgBr	—Br 2.480(3)	
	py	1.2 *M*	Cl^-	1.0	CH_3HgCl	—Cl 2.325(8)	
Hg(II)	tht	0.8 *M*	I^-	2	$HgI_2(tht)_2$	—I 2.670(4) —S 2.72 I—Hg—I 143(2)°	*193*
	tht	0.7 *M*	Br^-	2	$HgBr_2(tht)_2$	—Br 2.535(6) —S 2.62 Br—Hg—Br 132(2)	
La(III)	meth	2.0 m	Cl^-	3.0	$LaCl_3(meth)_5$	—Cl 2.95 —O 2.48	*194*
La(III)	meth	2 m	Cl^-	3.0	0–4	—Cl 2.95 —O 2.48	*195*
Er(III)	dmso	0.9 *M*	NO_3^-	3.0	Er—5.9(3)dmso	—O 2.31(2) —S 3.516(5) Er—O—S 133°	*37*
					Er—1.5 NO_3	—N 2.85(4)	
	dmso	1.0 *M*	Cl^-	3.0	5.2(3) dmso	—O 2.36(3) —S 3.450(5)	
					1.3(1) Cl	Er—O—S 124° —Cl 2.57(2)	
Mg(II)	meth	1.4 *M*	Cl^-	2	$Mg(meth)_6$	—O 2.065(3)	*196*
Mo(II)	eth	0.7–1.5 m	Cl^-	2.3	Mo_6Cl_8	—Mo 2.65	*197*
Tl(III)	CH_2Cl_2	0.8 *M*	I^-	4.0	TlI_4	—I 2.771(3)	*198*
Zn(II)	acet	4.2 m	Br^-	2.0	2	—Br 2.40	*135*
Zn(II)	dmso	0.3 *M*	SCN^-	4.5	$Zn(NCS)_4$	—N 1.93	*185*
Zn(II)	dmso	0.7 *M*	ClO_4^-	2	$Zn(dmso)_6$	—O 2.127(5) —S 3.147(3)	*199*

[a] [C] = concentration of cation. [A]/[C] = ratio between anion and cation concentration. "complex" = The complex formed or the number of coordinated ligands. "bond" = Type of bond and bond length in Å.

[b] py = Pyridine; tht = tetrahydrothiophene; dmso = dimethylsulfoxide; dmf = dimethylformamide; meth = methanol; eth = ethanol; an = acetonitrile; acet = acetone.

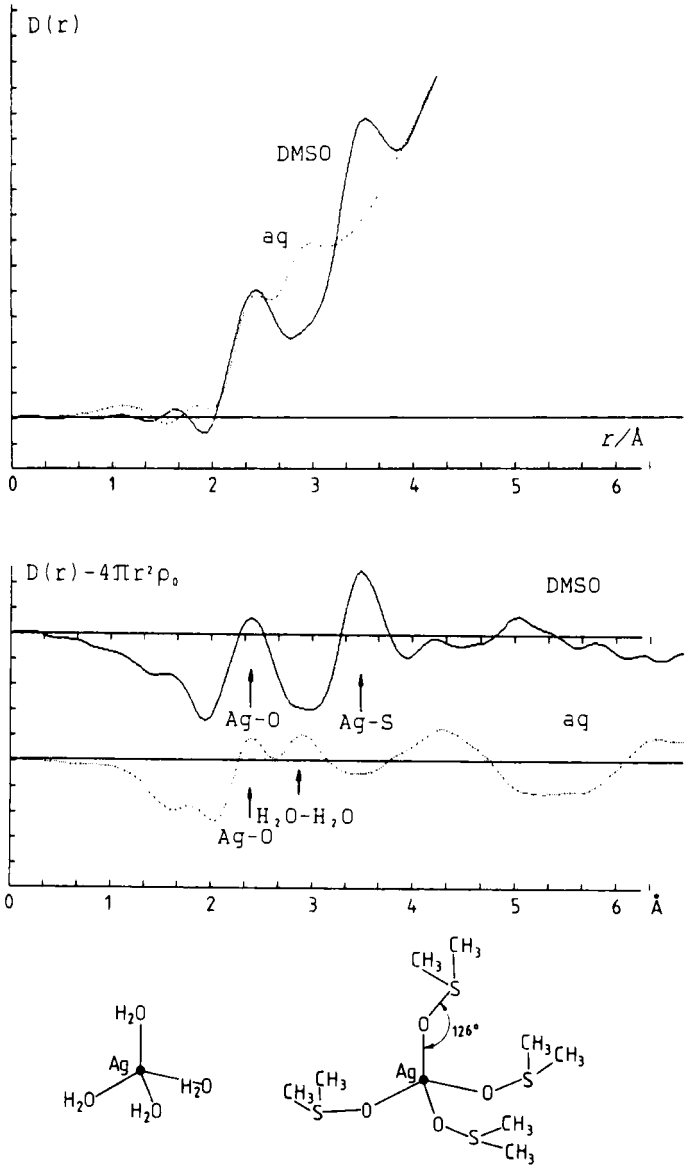

FIG. 26. Comparison between radial distribution functions for 3 *M* silver(I) nitrate in aqueous and in DMSO solutions. Intramolecular interactions of the solvent molecules have been removed. The derived structures for the solvated silver(I) ion in the two solvents are shown.

tion of the coordination number. It also allows a determination of the Ag—O—S bonding angle, 126°, which gives the orientation of the DMSO molecule in the coordination sphere (*183*). Since hydrogen atoms give very weak contributions to the scattering data the corresponding orientation of the solvent molecules in the aqueous solution cannot be determined.

By isostructural substitution, using the Er^{3+}—Y^{3+} pair, the structures of chloride and nitrate complexes of Er^{3+} in DMSO solution have been determined and can be compared with the structures of corresponding complexes in aqueous solution (*37*). The deconvoluted RDFs for 1 *M* erbium(III) nitrate and chloride solutions, calculated from difference curves, are shown in Fig. 27. The structures for the complexes were derived from these RDFs and the final parameter values were obtained by least-squares refinements using the intensity difference curves. The bonding of the ligands and a comparison between experimental values and values calculated for the derived models are shown in Fig. 27.

Chloride ions in aqueous erbium(III) solutions are coordinated in the first sphere only at very high concentrations, while nitrate ions form inner-sphere complexes already at rather low concentrations. In DMSO the complex formation with chloride is much stronger relative to that of nitrate, which probably in part can be ascribed to a relative difference in solvation of Cl^- and NO_3^- in water and in DMSO (*37*). The nitrate ion is bidentately bonded, as was also found in aqueous solution. Er—O(DMSO) bond lengths are significantly shorter than Er—O(NO_3) bonds, as is also observed in the crystalline solvate and in aqueous solution. The average Er—O—S angle is 130°, which is close to values found in crystals. The presence in the RDFs of peaks corresponding to Er—C distances indicate a restricted rotation around the S—O bonds with the trans configuration (Fig. 27) apparently preferred (*37*).

Halide complexes formed by mercury(II) in DMSO solutions have been extensively investigated. The $HgBr_4^{2-}$ and HgI_4^{2-} complexes are regular tetrahedra with bond lengths not significantly different from those found in aqueous solution (Tables III and VII). The $HgBr_3^-$ and HgI_3^- complexes are approximately tetrahedral with a DMSO molecule occupying the fourth corner of the tetrahedron and with X—Hg—X angles slightly larger than expected for a regular tetrahedron. The same structures, with H_2O replacing DMSO, are found in aqueous solution. In many organic solvents the solubility of the HgX_2 complex is much larger than in water, which allows a determination of its structure by X-ray diffraction. It is found to be not quite linear with an X—Hg—X angle in DMSO of about 160°, which deviates significantly

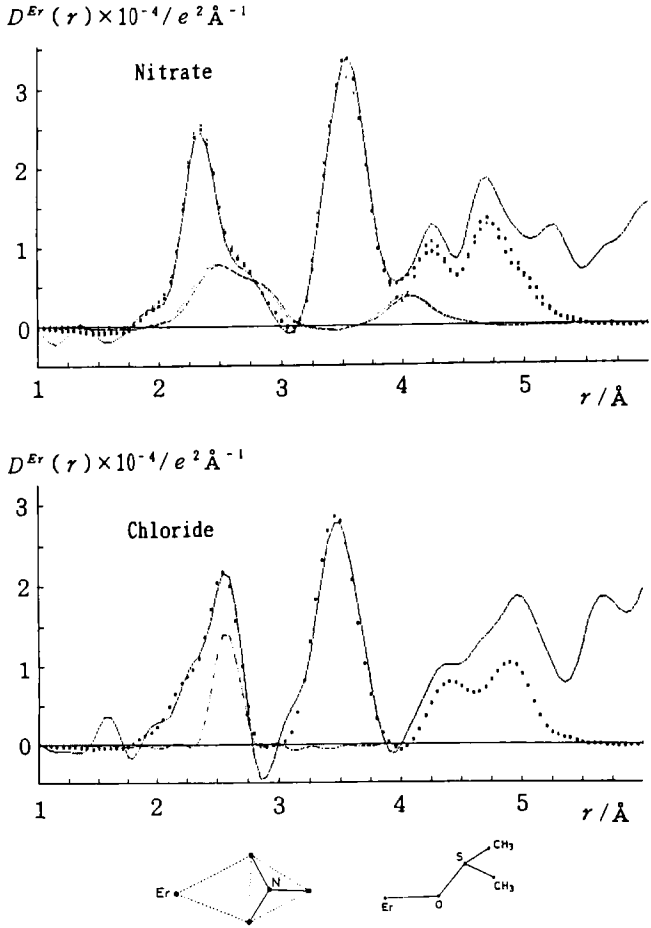

FIG. 27. RDFs for 1 *M* erbium(III) nitrate and chloride solutions in DMSO (solid lines) with nonmetal interactions eliminated. DMSO is coordinated over oxygen with an average Er—O—S angle of abut 130°. Nitrate is coordinated as a bidentate ligand. The Er—Cl distance for chloride in the first coordination sphere is 2.57 Å. Theoretical values calculated for $Er(NO_3)_{1.5}(dmso)_{5.9}$ in the nitrate solution and $ErCl_{1.3}(dmso)_{5.2}$ in the chloride solution are marked by dots. The contributions from the coordinated anions (NO_3^- or Cl^-) are separately shown as dotted lines.

from the linear value of 180° (Table VII). It has been shown by similar investigations in other solvents that this angle is variable and it has been related to the coordination power of the solvent (*191, 193*). Values varying from about 135° in tetrahydrotiophene to about 160° in DMSO have been found (Table VII).

In the absence of complex-forming anions mercury(II) is found to be octahedrally solvated in DMSO with Hg—O bond lengths of 2.39 Å (Table VII), compared to 2.41 Å in the octahedrally hydrated Hg^{2+} ion in aqueous solution (Table III). The values are significantly longer than those found in the corresponding crystal structures, which are 2.34 Å. No such differences are observed for the corresponding cadmium(II) solvates, where the average Cd—O bond length is 2.29 Å. The angles M—O—S are 120° for Hg and 126° for Cd and do not differ significantly from corresponding values in the crystalline solvates (*96*).

XIII. Polynuclear Complexes

Polynuclear complexes, which contain several metal atoms, have structures, which cannot usually be derived from solution X-ray diffraction data alone. However, since the intramolecular metal–metal distances in these complexes are well defined and limited in number, they give distinct contributions to the diffraction data and can often be precisely analyzed in terms of distances, frequencies, and rms variations. When compositions and concentrations of the complexes are known from other measurements, this information can be sufficient for a derivation of the structures. The method has been applied to several hydroxo and oxo complexes and to some halogeno complexes of primarily heavy metal ions.

When hydrolyzed in aqueous solution most metal ions form polynuclear hydrolysis complexes:

$$qM^{z+} + pH_2O \leftrightarrows M_q(OH)_p^{(qz-p)+} + pH^+$$

The composition of these complexes and their stability constants have been determined for a large number of metal ions primarily with the use of emf methods (*200, 201*). The free hydrogen ion concentration and in some cases the free metal ion concentration are determined as functions of the stoichiometric hydrogen ion and metal ion concentrations. From measurements on series of solutions of different concentrations the number of metal atoms in a complex and its charge can be derived, but no information is obtained on the number of water molecules in the complex. Since emf measurements are influenced by changes in activity factors they have usually been done in an inert ionic medium of high concentration (3 *M* $NaClO_4$) and at low metal ion concentrations. The major complexes formed, however, have been found to be stable also in the concentrated solutions needed for X-ray diffraction measurements, and the stability constants determined seem to be

approximately valid. For some systems polynuclear complexes with the same number of metal atoms as those derived for solutions have also been found as discrete units in crystals.

Structure determinations of polynuclear complexes in aqueous solutions are summarized in Table VIII (*202–222*).

The analysis of solution diffraction data for these systems can be illustrated by results for indium(III) in aqueous perchlorate solutions (*211*). The RDFs for two concentrated solutions (≈4 *M*), one slightly acid containing no hydrolysis complexes and one with hydrogen ions removed, each normalized to a stoichiometric unit of volume containing one In atom, are compared in Fig. 28. The major difference between

TABLE VIII

STRUCTURE DETERMINATIONS OF POLYNUCLEAR COMPLEXES IN AQUEOUS SOLUTION

Metal	Conc.	Anion	Complex	Bond length/Å	Ref.
Bi(III)	5.8 *M*	ClO_4^-	$Bi_6(OH)_{12}$	Bi—Bi 3.70	*202*
Bi(III)	4.7 *M*	ClO_4^-	$Bi_6O_4(OH)_4$	Bi—Bi 3.70	*203, 204*
Hf(IV)	0.5–2 m	Cl^-	$Hf_4(OH)_8(H_2O)_{12}$	Hf—Hf 3.57	*205*
	2.0 m	Br^-	$Hf_4(OH)_8(H_2O)_{16}$	Hf—Hf 3.57	
Zr(IV)	2.0 m	Cl^-	$Zr_4(OH)_8(H_2O)_{16}$	Zr—Zr 3.57	
	2.0 m	Br^-	$Zr_4(OH)_8(H_2O)_{16}$	Zr—Zr 3.57	
Zr(IV)	2.1–3.0 *M*	ClO_4^-	$Zr_4(OH)_8(H_2O)_{16}$	Zr—Zr 3.57	*206, 207*
	3.5–5.0 *M*	Cl^-	$Zr_4(OH)_8(H_2O)_{16}$	Zr—Zr 3.57	
	3.1–3.3 *M*	Br^-	$Zr_4(OH)_8(H_2O)_{16}$	Zr—Zr 3.57	
Hf(IV)	1.7 *M*	Cl^-	$Hf_4(OH)_8(H_2O)_{12}$	Hf—Hf 3.57	
Hg(I)	1.1–5.6 *M*	ClO_4^-	$Hg_2(H_2O)_2$	Hg—Hg 2.52(1)	*208*
Hg(II)	3.5–4.6 *M*	ClO_4^-	$Hg_2(OH)(H_2O)_2$ $Hg_3O(H_2O)_3$ $Hg_4O(OH)(H_2O)_3$	Hg—Hg 3.64	*209, 210*
In(III)	4.0–4.8 *M*	NO_3^-	$In_4(OH)_6(H_2O)_{12}$	In—In 3.89	*211*
Mo(VI)	1.6–2.0 *M*	PO_4^{3-}, ClO_4^-	Mo_7O_{24}, $Mo_5P_2O_{23}$		*212*
Mo(VI)	1.6–2.0 *M*	PO_4^{3-}, ClO_4^-	Mo_9PO_{34}		*213*
Mo(VI)	1.6–2.0 *M*	AsO_4^{3-}, ClO_4^-	Mo_9AsO_{34}		*214*
Mo(VI)	2.0 *M*		Mo_7O_{24}, Mo_8O_{26}		*215*
Mo(VI)	1.7–1.8 *M*	AsO_4^{3-}, ClO_4^-	$Mo_6As_2O_{27}$		*216*
Pb(II)	1.9 *M*	ClO_4^-	$Pb_4(OH)_4$	Pb—Pb 3.854(5)	*217*
	1.6 *M*	ClO_4^-	$Pb_6O(OH)_6$		
Rh	0.4–0.9 *M*	NO_3^-	$Rh_2O(NO_3)(H_2O)_8$	Rh—Rh 3.1	*218*
Sn(II)	3 *M*	ClO_4^-	$Sn_3(OH)_4$	Sn—Sn 3.6–4	*122*
Th(IV)	2.0 *M*	NO_3^-	$>Th_2(OH)_2$	Th—Th 3.94	*219*
U(IV)	2.2 *M*	ClO_4^-		U—U 4.00	*130*
U(VI)	3.1 *M*	Cl^-	$(UO_2)_2(OH)_2Cl_2(H_2O)_4$ $(UO_2)_3(OH)_4Cl_3(H_2O)_3$	U—U 3.9	*206, 220*
U(VI)	0.5–0.9 *M*	CO_3^{2-}	$(UO_2)_3(CO_3)_6$	U—U 4.946(5)	*221*
W(VI)	3.7 *M*		$H_4SiW_{12}O_{40}$	W—W 3.36–3.71	*222*

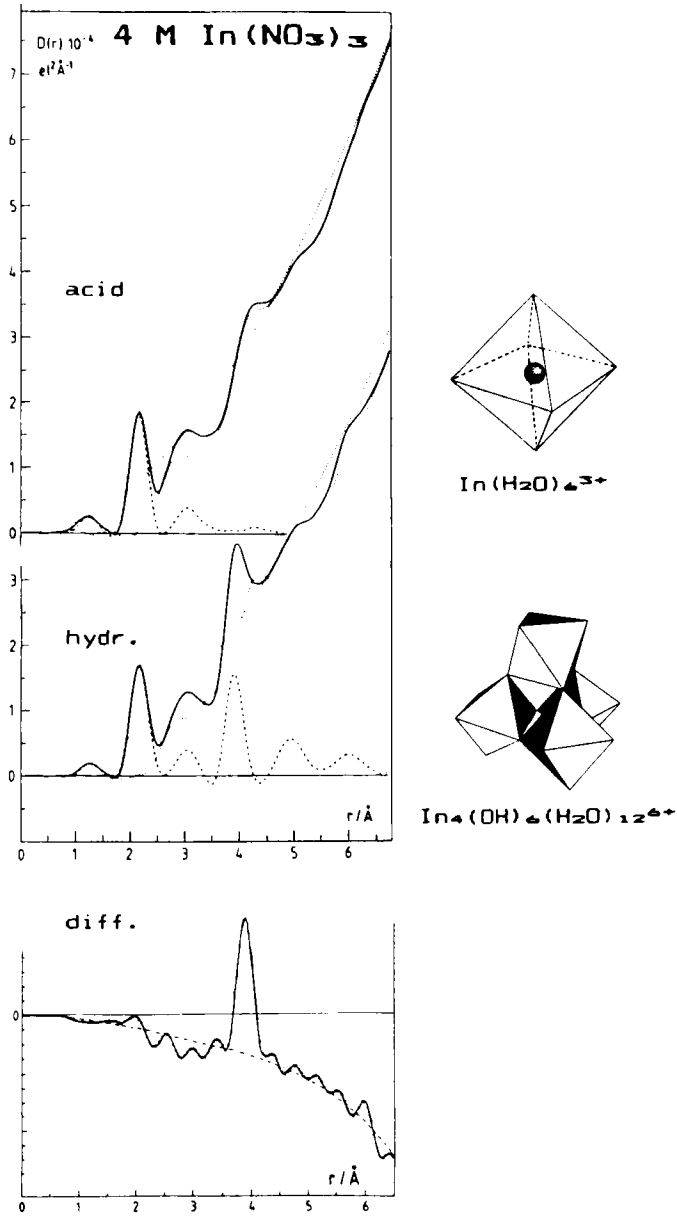

FIG. 28. RDFs for an acid and a hydrolyzed indium(III) nitrate solution and the corresponding difference curve, which shows the sharp In–In interaction at 3.9 Å in the polynuclear hydrolysis complexes. Theoretical peaks, calculated for the models to the right, are shown by dashed lines.

them is a sharp peak, which appears only for the hydrolyzed solution. In the difference between the two RDFs this peak at 4.0 Å remains and appears on a smoothly varying background curve, which has no other distinct features (Fig. 28). The peak is closely reproduced by a theoretical Gaussian In–In peak calculated for a distance of 3.89 Å, with a rms variation of 0.12 Å and a frequency corresponding to 0.65 In—In distances per In atom. A very similar In—In distance, 3.95 Å, is found in crystal structures, where the In atoms are joined by single hydroxo bridges (*223, 224*), suggesting that the same type of bridging occurs in the hydrolysis complexes in solution. Since the RDF indicates no other In—In distances the complexes can only be dinuclear (0.5 In—In distances per In atom) or contain the In atoms arranged at the corners of a regular triangle (1.0 In—In distances per In) or a tetrahedron (1.5 In—In distances per In). Since the analysis of the RDFs shows an average value larger than 0.5 In–In distances per In atom, some of the complexes must contain three or four In atoms.

emf data on solutions of similar compositions have been explained by the formation of tetranuclear complexes, $In_4(OH)_6^{6+}$ (*225*). It seems likely, therefore, that tetranuclear complexes are dominant in the solutions.

An analysis of the RDF for the acid solution shows that the In^{3+} ion is bonded to six water molecules at 2.17 Å (Fig. 28). The same In—H_2O distance is found for octahedrally coordinated In^{3+} in crystal structures (*223, 224*). According to the difference curve this coordination is not changed by the hydrolysis. A possible model for a tetranuclear complex with four octahedrally coordinated In atoms occupying the four corners of a regular tetrahedron and joined by single hydroxo bridges is shown in Fig. 28. It is consistent with the experimental data and seems to be a likely model for the hydrolysis complexes formed in solution, but has not yet been found in crystal structures.

emf measurements on aqueous lead(II) solutions have been interpreted in terms of two dominant complexes (*226*):

$$4Pb^{2+} + 4H_2O \leftrightarrows Pb_4(OH)_4^{4+} + 4H^+$$

$$6Pb^{2+} + 8H_2O \leftrightarrows Pb_6(OH)_8^{4+} + 8H^+$$

The stability constants indicate that solutions can be prepared in each of which one of the complexes is solely dominant (Fig. 29). Diffraction curves for two such solutions, and for an acid solution containing no hydrolysis complexes, give RDFs as shown in Fig. 30 (*217*). The Pb–Pb intramolecular interactions are very distinct and are clearly seen in the two hydrolyzed solutions. For the $Pb_4(OH)_4^{4+}$ solution the single

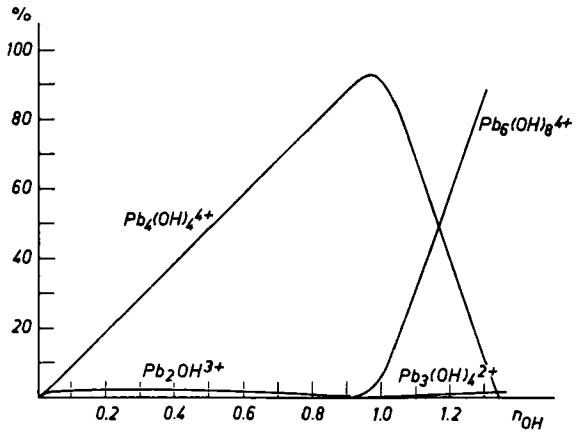

FIG. 29. The percentage of lead, bound in the different hydrolysis complexes, $Ph_q(OH)_p$ in a 2 *M* lead(II) perchlorate solution, as a function of n_{OH}, which is the average number of protons removed from each hydrated lead(II) ion.

Pb–Pb peak at 3.854(5) Å is in close agreement with a theoretical peak calculated for a tetrahedral arrangement of the lead atoms in the complex (Fig. 30).

For the $Pb_6(OH)_8^{4+}$ solution the changed Pb–Pb peak shape at 3.85 Å and two additional Pb–Pb peaks at, 6.4 and 7.1 Å, indicate a more complex structure, which cannot be unambiguously derived from the limited information in the RDF. Crystals can be prepared, however, which contain discrete $Pb_6O(OH)_6^{4+}$ units with the structure shown in Fig. 30 (*227*). Theoretical peaks calculated for the Pb framework in this structure are in complete agreement with the peaks in the RDFs (Fig. 30), which proves that the structure of the complexes are the same in solution and in crystals. Raman spectroscopic measurements are consistent with this interpretation.

The combination of information from different sources thus makes it possible to determine the structure of the complexes in solution even when the information contained in the solution diffraction curves is too limited for a complete and unambiguous structure determination.

Although the metal–oxygen distances in the hydrolysis complexes are usually too weak and too irregular to give distinct features to a diffraction curve they can be observed and can sometimes be used to choose between different conceivable models for the structure. In hydrolyzed bismuth(III) solutions a dominant complex containing six Bi atoms has been shown to occur (*201–204, 226, 228*). The octahedral arrangement of the six Bi atoms can easily be proved from the diffrac-

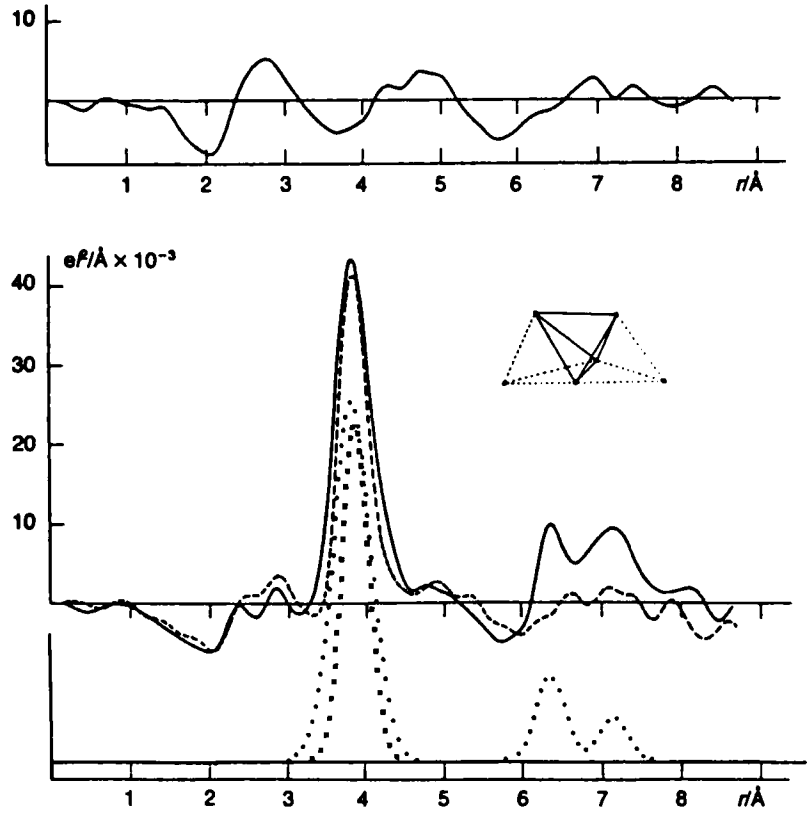

FIG. 30. Reduced distribution functions, $D(r)$-$4\pi r^2\rho_0$, for 1.8 M lead(II) perchlorate solutions. The upper curve is for a slightly acid solution ($n_{OH} = 0$) and the two lower curves for hydrolyzed solutions with $n_{OH} = 0.97$ (dashed line) and 1.33 (solid line). To the right is shown the arrangement of lead atoms in the tetranuclear (solid lines) and the hexanuclear (solid and dashed lines) complexes formed. Theoretical Pb–Pb peaks calculated for these structures (dotted lines) are given for comparison with the observed RDFs.

tion data. The positions of the oxygen atoms in the complex, however, which can reasonably be assumed to be above the centers of the Bi–Bi edges or above the centers of the triangular faces in the octahedron, are not clearly indicated in the RDFs (*201–204, 226*). Discrete $Bi_6O_4(OH)_4^{4+}$ units, where the oxo and hydroxo groups are positioned above the centers of the triangles, have been found in crystals (*203*), however, and it can be shown that theoretical peaks calculated for this model are in significantly better agreement with the observed radial distribution function than are other models for the oxygen positions (*204*).

A different type of bridging occurs in hydrolysis complexes of thorium(IV) (*219*) and uranium(IV) (*130*). Here a distinct peak at 3.94(2) Å in the hydrolyzed solutions can be ascribed to the metal–metal distances in the hydrolysis complexes. Discrete dinuclear complexes with a very similar metal–metal distance, 3.988(2) Å, in which the metal atoms are joined by double hydroxo bridges have been found in crystals of $Th_2(OH_2)(NO_3)_6(H_2O)_8$ (*229*). The same type of bridging, therefore, must occur in solution. When hydrolysis is increased, however, the number of metal–metal distances per metal atom increases beyond a value of 0.5, valid for a dinuclear complex, and larger hydrolysis complexes are obviously formed. These structures are unknown but an extensive X-ray investigation of highly hydrolyzed thorium(IV) solutions has shown that there is probably no close relation between the structures of the hydrolysis complexes in solution and the structure of thorium dioxide, which is the ultimate product of the hydrolysis process (*230*).

Uranium(VI) also forms polynuclear hydrolysis complexes in solution, in which the uranium atoms are joined by double hydroxo or oxo bridges. In chloride solutions the chloride ions can replace some of the bridging hydroxo groups. Depending on the type of bridging the intramolecular U—U distances vary between 3.7 and 4.0 Å. The coordination around the uranium atom is a pentagonal bipyramid with the linear uranyl groups, UO_2^{2+}, perpendicular to the plane through the uranium and the bridging atoms. The structures in solution could be derived by using information from solution diffraction measurements, crystal structure determinations, and equilibrium emf measurements (*206, 220*).

Similar types of bridging between the metal atoms have been found for other metal ions, although complete structure determinations have not always been possible to make. Mercury(II) forms hydrolysis complexes in which three Hg^{2+} ions are joined by an oxo group. Tin(II) forms complexes by similar bridging as found for lead(II) (Table VIII).

Iso and hetero polymolybdates and polytungstates in solution, which form compact structures containing several metal atoms, give distinct contributions to a solution diffraction pattern, but the structures are too complex to allow a complete structure determination from solution X-ray diffraction data alone. Since a large number of them have been found as discrete complexes in crystals, theoretical curves for these known structures can be used for identification of similar complexes in solution. Changes in the diffraction pattern for a solution of a known complex, when the composition of the solution is changed, can then give information on the resulting structural changes in the complex.

At high pH values molybdenum(VI) occurs as tetrahedral MoO_4^{2-}

ions in aqueous solution. On acidification the heptamolybdate ion, $Mo_7O_{24}^{2-}$, well known from crystal structures, is formed. emf data have indicated a transformation of the heptamolybdate into an octamolybdate on further acidification of the solution (Fig. 31). X-ray diffraction data on a series of 2 *M* lithium molybdate solutions of increasing acidities also indicate that a structural change occurs (Fig. 31) (*215*). In order to identify complexes formed the RDFs can be compared with theoretical curves calculated for structures of complexes found in crystals. Theoretical peaks for the known structure of the heptamolybdate ion $Mo_7O_{24}^{6-}$ and for two octamolybdate ions, $Mo_8O_{26}^{4-}$ and $Mo_8O_{28}^{8-}$ are shown in Fig. 32, which also gives the separate contributions from the Mo–Mo, the Mo–O, and the O–O interactions. The characteristic features of the curves are given primarily by Mo–Mo interactions, while the much larger number of O–O interactions gives only a rather smooth background curve. The observed changes in the RDFs (Fig. 31) can be shown to be consistent with a partial transformation into $Mo_8O_{26}^{4-}$ complexes. The features of the curves are sufficiently distinct

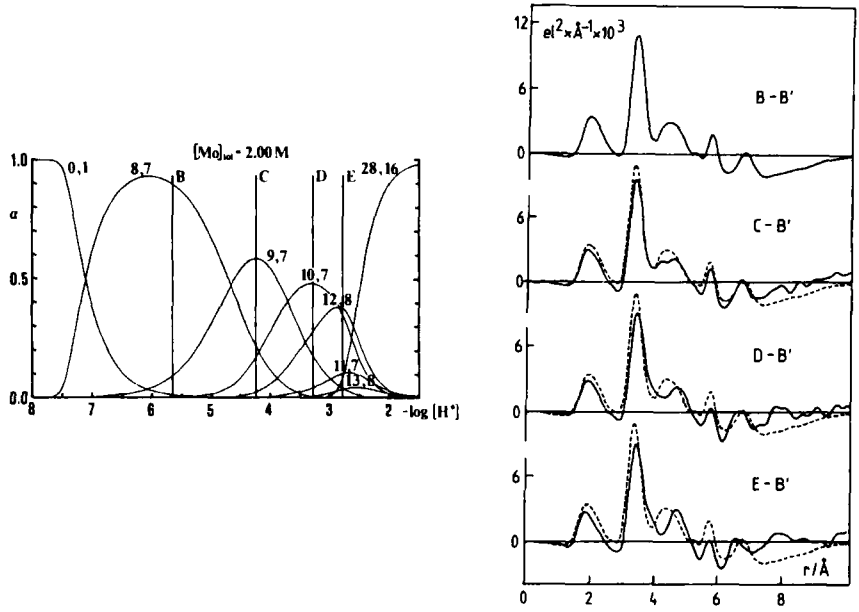

FIG. 31. The fraction of molybdenum bound in different species $H_p(MoO_4)_q$ in a 2.00 *M* molybdate solution as a function of -log[H^+]. Vertical lines indicate compositions of solutions for which X-ray diffraction measurements were made. The corresponding distribution functions are shown to the right. The RDF for the heptamolybdate solution, B, is repeated (dashed lines) in the C–E solutions in order to bring out the changes.

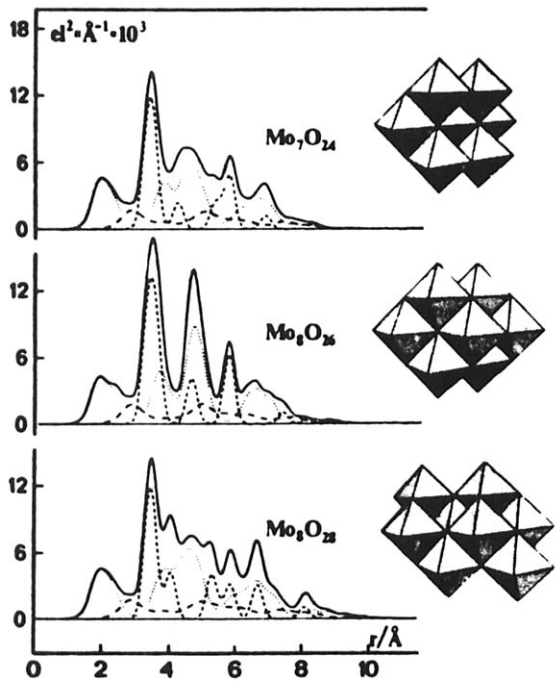

FIG. 32. Peak shapes, calculated from crystal structure parameters for the heptamolybdate ion, $Mo_7O_{24}^{6-}$, and for two octamolybdates $Mo_8O_{26}^{4-}$ and $Mo_8O_{28}^{8-}$. The separate contributions from Mo—Mo distances (short dashes), Mo—O distances (dotted lines), and O—O distances (long dashes) are shown.

to give a unique identification of the complexes and they show the bonding distances to be the same in solution and in crystals.

XIV. Concluding Remarks

X-ray diffraction measurements can give direct structural information on complexes in solution, which cannot be obtained by other methods. Although the complete structure of a solution cannot be derived from the limited information in a single one-dimensional diffraction curve, a separation of the distinct contributions given by intramolecular interactions can often be made. This makes it possible to determine structures of complexes even in solutions with chemically complicated compositions. Comparison of diffraction curves for different solutions can give information on structural changes caused by changes in concentration of a particular atomic species.

For a dominant complex in a solution precise determinations of the intramolecular distances can usually be made. Derivations of coordination numbers and geometries will depend on the specific characteristics of the system investigated. Although solution X-ray diffraction measurements have been primarily concerned with the structures of metal aqua ions, other ligands and nonaqueous solutions often offer more favorable conditions for structure determinations of complexes.

REFERENCES

1. J. E. Enderby, S. Cummings, G. J. Herdman, G. W. Neilson, P. S. Salmon, and N. Skipper, *J. Phys. Chem.* **91,** 5851 (1987).
2. G. W. Neilson, *in* "Water and Aqueous Solutions" (G. W. Neilson and J. E. Enderby, eds.), p. 169. Adam Hilger, London, 1986.
3. J. E. Enderby, *Pure Appl. Chem.* **57,** 1025 (1985).
4. J. E. Enderby, *Contemp. Phys.* **24,** 561 (1983).
5. J. E. Enderby, and G. W. Neilson, *in* "Water: A Comprehensive Treatment" (F. Franks, ed.), Vol. 6, p. 1. Plenum, New York, 1979.
6. G. W. Neilson, and J. E. Enderby, *Adv. Inorg. Chem.* **34,** 195 (1989); *Annu. Rep. Prog. Chem., Sect. C* **76,** 185 (1979).
7. M. Magini, G. Licheri, G. Paschina, G. Piccaluga, and G. Pinna, *in* "X-Ray Diffraction of Ions in Aqueous Solutions: Hydration and Complex Formation (M. Magini, ed.). CRC Press, Boca Raton, FL, 1988.
8. G. Palinkas, and E. Kalman, *in* "Diffraction Studies on Non-Crystalline Substances" (I. Hargittai and W. J. Orville-Thomas, eds.), p. 293. Elsevier, Amsterdam, 1981.
9. G. Palinkas, T. Radnai, and F. Hajdu, *Z. Naturforsch. A* **35,** 107 (1980).
10. R. Caminiti, G. Licheri, G. Piccaluga, G. Pinna, and M. Magini, *Rev. Inorg. Chem.* **1,** 333 (1979).
11. R. Caminiti, G. Licheri, G. Piccaluga, and G. Pinna, *Ann. Chim. (Rome)* **65,** 695 (1975).
12. G. Johansson, *Acta Chem. Scand.* **43,** 307 (1989).
13. G. Johansson, *Pure Appl. Chem.* **60,** 1773 (1988).
14. H. Ohtaki, *Pure Appl. Chem.* **59,** 1143 (1987).
15. H. Ohtaki, *Rev. Inorg. Chem.* **4,** 103 (1982).
16. G. Johansson and M. Sandström, *Chem. Scr.* **4,** 195 (1973).
17. G. Johansson, "Solution Diffraction Data Handling Programs." Stockholm, 1988.
18. M. Maeda, H. Ohtaki, and G. Johansson, *Bull. Chem. Soc. Jpn.* **47,** 2229 (1974).
19. M. Sandström, G. W. Neilson, G. Johansson, and T. Yamaguchi, *J. Phys. C* **18,** L1115 (1985).
20. S. Cummings, J. E. Enderby, and R. A. Howe, *J. Phys. C* **13,** 1 (1980).
21. N. A. Hewish, G. W. Neilson, and J. E. Enderby, *Nature (London)* **297,** 138 (1982).
22. G. W. Neilson, J. R. Newsome, and M. Sandström, *J. Chem. Soc., Faraday Trans.* **77,** 1245 (1981).
23. G. W. Neilson, *J. Phys. C* **15,** L233 (1982).
24. B. K. Annis, R. L. Hahn, and A. H. Narten, *J. Chem. Phys.* **82,** 2086 (1985).
25. C. Cossy, A. C. Barnes, J. E. Enderby, and A. E. Merbach, *J. Chem. Phys.* **90,** 3254 (1989).
26. A. H. Narten, and R. L. Hahn, *Science* **217,** 1249 (1982).

27. A. H. Narten, and R. L. Hahn, *J. Phys. Chem.* **87,** 3193 (1983).
28. A. K. Soper, G. W. Neilson, J. E. Enderby, and R. A. Howe, *J. Phys. C* **10,** 1793 (1977).
29. G. W. Neilson, and J. E. Enderby, *J. Phys. C* **11,** L625 (1978).
30. J. R. Newsome, G. W. Neilson, J. E. Enderby, and M. Sandström, *Chem. Phys. Lett.* **82,** 399 (1981).
31. G. W. Neilson, and J. E. Enderby, *Proc. R. Soc. London, Ser. A* **390,** 353 (1983).
32. W. Bol, G. J. A. Gerrits, and C. L. van Panthaleon van Eck, *J. Appl. Crystallogr.* **3,** 486 (1970).
33. G. Johansson, L. Niinistö, and H. Wakita, *Acta Chem. Scand., Ser. A* **39,** 359 (1985).
34. G. Johansson, and H. Wakita, *Inorg. Chem.* **24,** 3047 (1985).
35. G. Johansson, and H. Yokoyama, *Inorg. Chem.* **29,** 2460 (1990).
36. H. Yokoyama, and G. Johansson, *Acta Chem. Scand.* **44,** 567 (1990).
37. G. Johansson, H. Yokoyama, and H. Ohtaki, *J. Solution Chem.* **20,** 859 (1991).
38. A. Habenschuss, and F. H. Spedding, *J. Chem. Phys.* **70,** 2797 (1979).
39. A. Habenschuss, and F. H. Spedding, *J. Chem. Phys.* **73,** 442 (1980).
40. A. Habenschuss, and F. H. Spedding, *J. Chem. Phys.* **70,** 3758 (1979).
41. M. Maeda, Y. Maegawa, T. Yamaguchi, and H. Ohtaki, *Bull. Chem. Soc. Jpn.* **52,** 2545 (1979).
42. T. Yamaguchi, G. Johansson, B. Holmberg, M. Maeda, and H. Ohtaki, *Acta Chem. Scand., Ser. A* **A38,** 437 (1984).
43. R. O. Nilsson, *Ark. Kemi* **12,** 513 (1958).
44. M. A. Marques, and M. I. DeBarros Marques, *Proc. K. Ned. Akad. Wet., Ser. B: Phys. Sci.* **77,** 286 (1974).
45. W. Bol, and T. Welzen, *Chem. Phys. Lett.* **49,** 189 (1977).
46. R. Caminiti, G. Licheri, G. Piccaluga, G. Pinna, and T. Radnai, *J. Chem. Phys.* **71,** 2473 (1979).
47. R. Caminiti, and T. Radnai, *Z. Naturforsch. A* **35A** 1368 (1980).
48. T. Yamaguchi, H. Ohtaki, E. Spohr, G. Pálinkás, K. Heinzinger, and M. M. Probst, *Z. Naturforsch. A* **41A,** 1175 (1986).
49. G. Licheri, G. Piccaluga, and G. Pinna, *J. Chem. Phys.* **64,** 2437 (1976).
50. R. Caminiti, G. Licheri, G. Piccaluga, and G. Pinna, *Chem. Phys. Lett.* **47,** 275 (1977).
51. R. Caminiti, G. Licheri, G. Paschina, G. Piccaluga, and G. Pinna, *Z. Naturforsch. A* **35A,** 1361 (1980).
52. J. N. Albright, *J. Chem. Phys.* **56,** 3783 (1972).
53. G. Licheri, G. Piccaluga, and G. Pinna, *J. Chem. Phys.* **63,** 4412 (1975).
54. M. M. Probst, T. Radnai, K. Heinzinger, P. Bopp, and B. M. Rode, *J. Phys. Chem.* **89,** 753 (1985).
55. T. Yamaguchi, S. Hayashi, and H. Ohtaki, *Inorg. Chem.* **28,** 2434 (1989).
56. T. Yamaguchi, and H. Ohtaki, *Bull. Chem. Soc. Jpn.* **52,** 1223 (1979).
57. R. Caminiti, and G. Johansson, *Acta Chem. Scand., Ser. A* **A35,** 373 (1981).
58. H. Ohtaki, M. Maeda, and S. Ito, *Bull. Chem. Soc. Jpn.* **47,** 2217 (1974).
59. V. V. Kuznetsov, V. N. Trostin, and G. A. Krestov, *Izv. Vyssh. Uchebn. Zaved., Khim. Khim. Tekhnol.* **25,** 954 (1982).
60. M. Tsurumi, M. Maeda, and H. Ohtaki, *Denki Kagaku* **45,** 367 (1977).
61. G. Paschina, G. Piccaluga, G. Pinna, and M. Magini, *J. Chem. Phys.* **78,** 5745 (1983).
62. D. L. Wertz, and R. F. Kruh, *J. Chem. Phys.* **50,** 4313 (1969).
63. H. Ohtaki, T. Yamaguchi, and M. Maeda, *Bull. Chem. Soc. Jpn.* **49,** 701 (1976).
64. M. Magini, and G. Giubileo, *Gazz. Chim. Ital.* **111,** 449 (1981).

65. M. Magini, *J. Chem. Phys.* **74,** 2523 (1981).
66. H.-G. Lee, Y. Matsumoto, T. Yamaguchi, and H. Ohtaki, *Bull. Chem. Soc. Jpn.* **56,** 443 (1983).
67. G. Paschina, G. Piccaluga, G. Pinna, and M. Magini, *Chem. Phys. Lett.* **98,** 157 (1983).
68. A. Musinu, G. Paschina, G. Piccaluga, and M. Magini, *J. Chem. Phys.* **80,** 2772 (1984).
69. M. Ichihashi, H. Wakita, and I. Masuda, *J. Solution Chem.* **13,** 505 (1984).
70. R. Caminiti, G. Licheri, G. Piccaluga, and G. Pinna, *Chem. Phys.* **19,** 371 (1977).
71. R. Caminiti, G. Licheri, G. Piccaluga, and G. Pinna, *J. Chem. Phys.* **65,** 3134 (1976).
72. M. Magini, *J. Chem. Phys.* **73,** 2499 (1980).
73. R. M. Lawrence, and R. F. Kruh, *J. Chem. Phys.* **47,** 4758 (1967).
74. G. Palinkas, T. Radnai, and F. Hajdu, *Z. Naturforsch. A* **35A,** 107 (1980).
75. Y. Tamura, T. Yamaguchi, I. Okada, and H. Ohtaki, *Z. Naturforsch. A* **42A,** 367 (1987).
76. H. Ohtaki, and M. Maeda, *Bull. Chem. Soc. Jpn.* **47,** 2197 (1974).
77. T. Yamaguchi, and H. Ohtaki, *Bull. Chem. Soc. Jpn.* **52,** 415 (1979).
78. M. Magini, *Inorg. Chem.* **21,** 1535 (1982).
79. A. Musinu, G. Paschina, G. Piccaluga, and M. Magini, *Inorg. Chem.* **22,** 1184 (1983).
80. J. R. Bell, J. L. Tyvoll, and D. L. Wertz, *J. Am. Chem. Soc.* **95,** 1456 (1973).
81. D. L. Wertz, and J. L. Tyvoll, *J. Inorg. Nucl. Chem.* **36,** 3713 (1974).
82. M. Ichihashi, H. Wakita, T. Mibuchi, and I. Masuda, *Bull. Chem. Soc. Jpn.* **55,** 3160 (1982).
83. M. Magini, and R. Caminiti, *J. Inorg. Nucl. Chem.* **39,** 91 (1977).
84. M. Magini, *J. Inorg. Nucl. Chem.* **40,** 43 (1978).
85. G. W. Brady, *J. Chem. Phys.* **29,** 1371 (1958).
86. G. W. Brady, M. B. Robin, and J. Varimbi, *Inorg. Chem.* **3,** 1168 (1964).
87. M. Magini, and T. Radnai, *J. Chem. Phys.* **71,** 4255 (1979).
88. D. L. Wertz, and M. L. Steele, *Inorg. Chem.* **19,** 1652 (1980).
89. M. D. Luter, and D. L. Wertz, *J. Phys. Chem.* **85,** 3542 (1981).
90. M. Magini, *J. Chem. Phys.* **76,** 1111 (1982).
91. C. L. van Panthaleon van Eck, H. B. M. Wolters, and W. J. M. Jaspers, *Recl. Trav. Chim. Pays-Bas* **75,** 802 (1956).
92. M. Sandström, and G. Johansson, *Acta Chem. Scand., Ser. A* **A31,** 132 (1977).
93. M. Sandström, *Acta Chem. Scand., Ser. A* **A31,** 141 (1977).
94. Å. Iverfeldt, and I. Persson, *Inorg. Chim. Acta* **111,** 179 (1986).
95. G. Johansson, *Acta Chem. Scand.* **25,** 2787 (1971).
96. M. Sandström, I. Persson, and S. Ahrland, *Acta Chem. Scand., Ser. A* **A32,** 607 (1978).
97. M. Maeda, and H. Ohtaki, *Bull. Chem. Soc. Jpn.* **50,** 1893 (1977).
98. R. Caminiti, G. Johansson, and I. Toth, *Acta Chem. Scand., Ser. A* **40,** 435 (1986).
99. H. Ohtaki, and M. Maeda, *Kenkyu Hokoku Asahi Garasu Kogyo Gijutsu Shoreikai* **28,** 221 (1976).
100. T. Radnai, G. Palinkas, Gy. I. Szasz, and K. Heinzinger, *Z. Naturforsch. A.* **36A,** 1076 (1981).
101. G. W. Brady, *J. Chem. Phys.* **33,** 1079 (1960).
102. L. S. Smith, and D. L. Wertz, *J. Am. Chem. Soc.* **97,** 2365 (1975).
103. M. L. Steele, and D. L. Wertz, *J. Am. Chem. Soc.* **98,** 4424 (1976).
104. L. S. Smith, and D. L. Wertz, *J. Inorg. Nucl. Chem.* **39,** 95 (1977).
105. M. L. Steele, and D. L. Wertz, *Inorg. Chem.* **16,** 1225 (1977).

106. R. Caminiti, *Chem. Phys. Lett.* **88,** 103 (1982).
107. G. Palinkas, T. Radnai, W. Dietz, Gy. I. Szasz, and K. Heinzinger, *Z. Naturforsch. A* **37A,** 1049 (1982).
108. Y. Tajiri, M. Ichihashi, T. Mibuchi, and H. Wakita, *Bull. Chem. Soc. Jpn.* **59,** 1155 (1986).
109. M. Maeda, and H. Ohtaki, *Bull. Chem. Soc. Jpn.* **48,** 3755 (1975).
110. R. Caminiti, G. Licheri, G. Piccaluga, and G. Pinna, *Rend. Semin. Fac. Sci. Univ. Cagliari* **47,** 19 (1977).
111. R. Caminiti, G. Licheri, G. Paschina, G. Piccaluga, and G. Pinna, *J. Chem. Phys.* **72,** 4522 (1980).
112. R. Caminiti, G. Licheri, G. Piccaluga, and G. Pinna, *Faraday Discuss. Chem. Soc.* **64,** 62 (1978).
113. R. Caminiti, and P. Cucca, *Chem. Phys. Lett.* **89,** 110 (1982).
114. M. Magini, M. deMoraes, G. Licheri, and G. Piccaluga, *J. Chem. Phys.* **83,** 5797 (1985).
115. H. Wakita, M. Ichihashi, T. Mibuchi, and I. Masuda, *Bull. Chem. Soc. Jpn.* **55,** 817 (1982).
116. M. Magini, G. Paschina, and G. Piccaluga, *J. Chem. Phys.* **76,** 1116 (1982).
117. R. Caminiti, *Chem. Phys. Lett.* **88,** 103 (1982).
118. R. Caminiti, *J. Chem. Phys.* **84,** 3336 (1986).
119. M. Maeda, T. Akaishi, and H. Ohtaki, *Bull. Chem. Soc. Jpn.* **48,** 3193 (1975).
120. R. Caminiti, and P. Cucca, *Chem. Phys. Lett.* **108,** 51 (1984).
121. R. Caminiti, D. Atzei, P. Cucca, F. Squintu, and G. Bongiovanni, *Z. Naturforsch. A* **40A** 1319 (1985).
122. G. Johansson, and H. Ohtaki, *Acta Chem. Scand.* **27,** 643 (1973).
123. T. Yamaguchi, O. Lindqvist, T. Claeson, and J. B. Boyce, *Chem. Phys. Lett.* **93,** 528 (1982).
124. R. Caminiti, A. Musinu, G. Paschina, and G. Pinna, *J. Appl. Crystallogr.* **15,** 482 (1982).
125. E. Andersson, O. Lindqvist, and T. Yamaguchi, *Acta Chem. Scand., Ser. A.* **A35,** 591 (1981).
126. G. Johansson, M. Magini, and H. Ohtaki, *J. Solution Chem.* **20,** 775 (1991).
127. J. Glaser, Ph.D. Thesis, Royal Institute of Technology, Stockholm, 1981.
128. J. Glaser, and G. Johansson, *Acta Chem. Scand., Ser. A* **A36,** 125 (1982).
129. J. Glaser, *Acta Chem. Scand., Ser. A* **A36,** 451 (1982).
130. S. Pocev, and G. Johansson, *Acta Chem. Scand.* **27,** 2146 (1973).
131. M. Åberg, D. Ferri, J. Glaser, and I. Grenthe, *Inorg. Chem.* **22,** 3986 (1983).
132. S. P. Dagnall, D. N. Hague, and A. D. C. Towl, *J. Chem. Soc., Faraday Trans. 2* **78,** 2161 (1982).
133. G. Licheri, G. Paschina, G. Piccaluga, and G. Pinna, *Z. Naturforsch. A* **37A,** 1205 (1982).
134. A. Musinu, G. Paschina, G. Piccaluga, and M. Magini, *J. Appl. Crystallogr.* **15,** 621 (1982).
135. D. L. Wertz, R. M. Lawrence, and R. F. Kruh, *J. Chem. Phys.* **43,** 2163 (1965).
136. E. Kalman, I. Serke, G. Pálinkás, G. Johansson, G. Kabisch, M. Maeda, and H. Ohtaki, *Z. Naturforsch. A* **38A,** 225 (1983).
137. P. L. Goggin, G. Johansson, M. Maeda, and H. Wakita, *Acta Chem. Scand., Ser. A* **A38,** 625 (1984).
138. R. F. Kruh, and C. L. Standley, *Inorg. Chem.* **1,** 941 (1962).
139. D. L. Wertz, and J. R. Bell, *J. Inorg. Nucl. Chem.* **35,** 137 (1973).

140. D. L. Wertz, and J. R. Bell, *J. Inorg. Nucl. Chem.* **35,** 861 (1973).
141. T. Yamaguchi, and H. Ohtaki, *Bull. Chem. Soc. Jpn.* **51,** 3227 (1978).
142. T. Yamaguchi, S. Hayashi, and H. Ohtaki, *J. Phys. Chem.* **93,** 2620 (1989).
143. H. Wakita, G. Johansson, M. Sandström, P. L. Goggin, and H. Ohtaki, *J. Solution Chem.* **20,** 643 (1991).
144. J. Glaser, and G. Johansson, *Acta Chem. Scand., Ser. A* **A35,** 639 (1981).
145. G. Johansson, and M. Sandström, *Acta Chem. Scand., Ser. A* **A32,** 109 (1978).
146. G. Johansson, and M. Sandström, *Acta Chem. Scand., Ser. A* **A41,** 113 (1987).
147. M. Sandström, Ph.D. Thesis, Royal Institute of Technology, Stockholm, 1978.
148. G. W. Neilson, and J. E. Enderby, *J. Phys. C* **15,** 2347 (1982).
149. G. W. Neilson, D. Schiöberg, and W. A. P. Luck, *Chem. Phys. Lett.* **122,** 475 (1985).
150. G. Johansson, and R. Caminiti, *Z. Naturforsch. A* **41A,** 1325 (1986).
151. K. Okada, H. Morikawa, F. Marumo, and S. Iwai, *Bull. Tokyo Inst. Techn.* **120,** 7 (1974).
152. K. Matsumoto, A. Kobayashi, and Y. Sasaki, *Bull. Chem. Soc. Jpn.* **48,** 1009 (1975).
153. L. G. Sillen, and A. E. Martell, "Stability Constants of Metal Ion Complexes," Spec. Publ. Nos. 17 and 25. Chemical Society, London, 1964 and 1971; E. Högfeldt, "Stability Constants of Metal Ion Complexes," Part A, Inorganic Ligands, IUPAC Chem. Data Ser., No. 21. Pergamon, Oxford, 1982. Chem. Data Ser., No. 21. Pergamon, Oxford, 1982.
154. R. Holinsky, and B. Brehler, *Acta Crystallogr., Sect. B* **B26,** 1915 (1970).
155. R. D. Rogers, and L. K. Kurihara, *Lanthanide Actinide Res.* **1,** 295 (1986).
156. R. Caminiti, *Z. Naturforsch. A* **36A,** 1062 (1981).
157. R. Caminiti, *Chem. Phys. Lett.* **86,** 217 (1982).
158. M. Magini, *J. Chem. Phys.* **70,** 317 (1979).
159. R. Caminiti, G. Marongiu, and G. Paschina, *Z. Naturforsch. A* **37A,** 581 (1982).
160. G. Licheri, G. Paschina, G. Piccaluga, and G. Pinna, *J. Chem. Phys.* **81,** 6059 (1984).
161. G. Licheri, G. Paschina, G. Piccaluga, and G. Pinna, *J. Chem. Phys.* **85,** 3135 (1986).
162. R. Caminiti, and G. Paschina, *Chem. Phys. Lett.* **82,** 487 (1981).
163. T. Radnai, G. Palinkas, and R. Caminiti, *Z. Naturforsch. A* **37A,** 1247 (1982).
164. R. Caminiti, P. Cucca, and T. Radnai, *J. Phys. Chem.* **88,** 2382 (1984).
165. R. D. Larsen, and G. H. Brown, *J. Phys. Chem.* **68,** 3060 (1964).
166. R. Caminiti, P. Cucca, and A. D'Andrea, *Z. Naturforsch. A* **38A,** 533 (1983).
167. R. Caminiti, P. Cucca, and T. Pintori, *Chem. Phys.* **88,** 155 (1984).
168. R. Caminiti, *J. Chem. Phys.* **77,** 5682 (1982).
169. M. Magini, *Chem. Phys. Lett.* **78,** 106 (1981).
170. R. Caminiti, P. Cucca, M. Monduzzi, G. Saba, and G. Crisponi, *J. Chem. Phys.* **81,** 543 (1984).
171. S.-I. Ishiguro, and H. Ohtaki, *J. Coord. Chem.* **15,** 237 (1987).
172. T. Fujita, T. Yamaguchi, and H. Ohtaki, *Bull. Chem. Soc. Jpn.* **52,** 3539 (1979).
173. T. Fujita, and H. Ohtaki, *Bull. Chem. Soc. Jpn.* **53,** 930 (1980).
174. T. Fujita, and H. Ohtaki, *Bull. Chem. Soc. Jpn.* **55,** 455 (1982).
175. T. Fujita, and H. Ohtaki, *Bull. Chem. Soc. Jpn.* **56,** 3274 (1983).
176. S. P. Dagnall, D. N. Hague, and A. D. C. Towl, *J. Chem. Soc., Faraday Trans. 2* **79,** 1817 (1983).
177. K. Ozutsumi, and H. Ohtaki, *Bull. Chem. Soc. Jpn.* **56,** 3635 (1983).
178. K. Ozutsumi, and H. Ohtaki, *Bull. Chem. Soc. Jpn.* **57,** 2605 (1984).
179. K. Ozutsumi, and H. Ohtaki, *Bull. Chem. Soc. Jpn.* **58,** 1651 (1985).
180. F. Hulten, and I. Persson, *Acta Chem. Scand., Ser. A* **A41,** 87 (1987).
181. B. Holmberg, and G. Johansson, *Acta Chem. Scand., Ser. A* **A37,** 367 (1983).

182. M. Johnson, and I. Persson, *Inorg. Chim. Acta* **130,** 215 (1987).
183. F. Gaizer, and G. Johansson, *Acta Chem. Scand., Ser. A* **A42,** 259 (1988).
184. S. Pocev, R. Triolo, and G. Johansson, *Acta Chem. Scand., Ser. A* **A33,** 179 (1979).
185. I. Persson, Å. Iverfeldt, and S. Ahrland, *Acta Chem. Scand., Ser. A* **A35,** 295 (1981).
186. K. Ozutsumi, T. Takamaku, S. Ichiguro, and H. Ohtaki, *Bull. Chem. Soc. Jpn.* **62,** 1875 (1989).
187. M. Ichihashi, H. Wakita, and I. Maeda, *Bull. Chem. Soc. Jpn.* **56,** 3761 (1983).
188. F. Gaizer, and G. Johansson, *Acta Chem. Scand.* **22,** 3013 (1968).
189. M. Sandström, *Acta Chem. Scand., Ser. A* **A32,** 627 (1978).
190. S. Ahrland, E. Hansson, Å. Iverfeldt, and I. Persson, *Acta Chem. Scand., Ser. A* **A35,** 275 (1981).
191. I. Persson, M. Sandström, P. L. Goggin, and A. Mosset, *J. Chem. Soc., Dalton Trans.* p. 1597 (1985).
192. Å. Iverfeldt, and I. Persson, *Inorg. Chim. Acta* **111,** 171 (1986).
193. M. Sandström, I. Persson, and P. L. Goggin, *J. Chem. Soc., Dalton Trans.* p. 2411 (1987).
194. L. S. Smith, D. C. McCain, and D. L. Wertz, *J. Am. Chem. Soc.* **98,** 5125 (1976).
195. D. L. Wertz, and S. T. Finch, *Inorg. Chem.* **18,** 1590 (1979).
196. T. Radnai, E. Kalman, and K. Pollmer, *Z. Naturforsch. A* **39A,** 464 (1984).
197. C. Brosset, *Ark. Kemi* **43,** 353 (1949).
198. J. Glaser, P. L. Goggin, M. Sandström, and V. Lutsko, *Acta Chem. Scand., Ser. A* **A36,** 55 (1982).
199. I. Persson, *Acta Chem. Scand., Ser. A* **A36,** 7 (1982).
200. L. G. Sillen, *Pure Appl. Chem.* **17,** 55 (1968).
201. C. F. Baes, and R. E. Mesmer, "The Hydrolysis of Cations." Wiley, New York, 1976.
202. H. A. Levy, M. D. Danford, and P. A. Agron, *J. Chem. Phys.* **31,** 1458 (1959).
203. B. Sundvall, Ph.D. Thesis, Royal Institute of Technology, Stockholm, 1979.
204. B. Sundvall, *Acta Chem. Scand., Ser. A* **A34,** 93 (1980).
205. G. M. Muha, and P. A. Vaughan, *J. Chem. Phys.* **33,** 194 (1960).
206. M. Åberg, Ph.D. Thesis, Royal Institute of Technology, Stockholm, 1970.
207. M. Åberg, *Acta Chem. Scand., Ser. B* **B31,** 171 (1977).
208. G. Johansson, *Acta Chem. Scand.* **20,** 553 (1966).
209. G. Johansson, *Acta Chem. Scand.* **25,** 2787 (1971).
210. G. Johansson, *Acta Chem. Scand.* **25,** 2799 (1971).
211. R. Caminiti, G. Johansson, and I. Toth, *Acta Chem. Scand., Ser. A* **A40,** 435 (1986).
212. G. Johansson, L. Pettersson, and N. Ingri, *Acta Chem. Scand.* **28,** 1119 (1974).
213. G. Johansson, L. Pettersson, and N. Ingri, *Acta Chem. Scand., Ser. A* **A32,** 407 (1978).
214. G. Johansson, L. Pettersson, and N. Ingri, *Acta Chem. Scand., Ser. A* **A32,** 681 (1978).
215. G. Johansson, L. Pettersson, and N. Ingri, *Acta Chem. Scand., Ser. A* **A33,** 305 (1979).
216. G. Johansson, L. Pettersson, and N. Ingri, *Acta Chem. Scand., Ser. A* **A35,** 181 (1981).
217. G. Johansson, and Å. Olin, *Acta Chem. Scand.* **22,** 3197 (1968).
218. R. Caminiti, D. Atzei, P. Cucca, A. Anedda, and G. Bongiovanni, *J. Phys. Chem.* **90,** 238 (1986).
219. G. Johansson, *Acta Chem. Scand.* **22,** 399 (1968).
220. M. Åberg, *Acta Chem. Scand.* **24,** 2901 (1970).
221. M. Åberg, D. Ferri, J. Glaser, and I. Grenthe, *Inorg. Chem.* **22,** 3981 (1983).

222. H. A. Levy, P. A. Agron, and M. D. Danford, *J. Chem. Phys.* **30,** 1486 (1959).
223. G. Johansson, *Acta Chem. Scand.* **15,** 1437 (1961).
224. K. Schubert, and A. Seitz, *Z. Anorg. Chem.* **256,** 226 (1948).
225. G. Biedermann, and D. Ferri, *Acta Chem. Scand., Ser. A* **A36,** 611 (1982).
226. Å. Olin, *Sven. Kem. Tidskr.* **73,** 482 (1961).
227. T. G. Spiro, D. H. Templeton, and A. Zalkin, *Inorg. Chem.* **8,** 856 (1969).
228. Å. Olin, *Acta Chem. Scand.* **11,** 1445 (1957).
229. G. Johansson, *Acta Chem. Scand.* **22,** 389 (1968).
230. M. Magini, A. Cabrini, G. Scibona, G. Johansson, and M. Sandström, *Acta Chem. Scand., Ser. A* **A30,** 437 (1976).